

POLITECNICO DI MILANO

Faculty of Industrial Engineering

Master of Science in
Mechanical Engineering



Modeling of CP titanium annealing process with a single or dual
beam laser source

Supervisor: Prof. Barbara PREVITALI

Co- Supervisor: Eng. Stefano ZARINI

Master of Science Thesis by:

Hossein ABEDI

Matr.779362

Academic Year 2013 - 2014.

Acknowledgment

First of all, I wanted to thank Prof. Barbara Previtali who gives me this opportunity to work on this subject, and helped me to find the right way with their constant guidance. During the work I always felt her positive energy and this made me determined. Stefano Zarini was who I always attracted with his perseverance and creativity. He helped me a lot from the very first day of the work, treated me with patience, and supported me in both words and actions. I also would thank Eng. Carlo Biffi who introduced me to the subject.

I want to thank all equipment and instruments I worked with during the work, they gave meaning to my life, I know they hear me.

Then I would like to appreciate what my friends did for me through past two years. They helped me to know myself more, which is not easily obtain.

At last but not the least, my cordial gratitude goes to the most precious thing I have, to my family.

*I dedicate this thesis to my mother
for her sacrifice, encouragement, and endless love.*

Contents

Abstract	XIV
Sommario	XV
Chapter 1 Introduction.....	1
PART 1 Definition of the laser annealing process	
Chapter 2 Contest, problems and objectives.....	6
2.1 Laser heat treatment process description.....	6
2.2 Titanium laser heat treatment.....	9
2.3 Modeling of laser heat treatments process.....	13
2.4 Objective.....	21
PART 2 Equipment and material description	
Chapter 3 Software for modeling.....	24
Chapter 4 Experimental equipment and methods.....	26
4.1 Monitoring.....	26
4.1.1 Thermocouples.....	28
4.1.2 Process.....	29
4.2 Sample preparation and analyzing instruments.....	35
4.2.1 Rolling machine.....	35
4.2.2 Micrograph observation equipment.....	35
4.2.3 Microhardness measurements.....	38
Chapter 5 Workpiece definition.....	41
Chapter 6 Base Material Titanium (CP Ti1).....	42
6.1 Commercially pure Titanium.....	43

PART 3 Single source modeling and calibration

Chapter 7	Calibration procedure.....	48
7.1	Calibration strategy	52
Chapter 8	Experimental analysis	54
8.1	Design of experiment	54
8.1.1	Fixed process parameters	54
8.2	Experimental execution.....	55
8.3	Experimental Results.....	56
8.3.1	Temperature Profiles.....	56
Chapter 9	Numerical analysis	64
9.1	Preprocessing.....	65
9.1.1	Geometry.....	65
9.1.2	Material	65
9.1.3	Heat Source	66
9.1.4	Boundary condition:.....	70
9.1.5	Mesh.....	72
9.2	Processing.....	75
9.3	Post Processing:.....	76
9.3.1	Calibration parameters effect	76
Chapter 10	Comparison	78
10.1	Experimental average and numerical comparison	78
Chapter 11	Conclusion	83

PART 4 One laser source productivity optimization

Chapter 12	One Laser Source Optimization.....	86
12.1	Productivity definition	86
12.2	One source optimizing method.....	89
12.2.1	Optimization Strategy	91
12.2.2	Assumption	92
12.3	Annealing temperature identification	92

12.3.1	Experimental Analysis	92
12.3.2	Numerical analysis	95
12.3.3	Results	97
12.3.4	Conclusion	98
12.4	Optimized solution.....	99
12.4.1	Study design	99
12.4.2	Isotherms productivity measurements.....	101
12.4.3	Results	102
12.4.4	Proposed Parameters	103
12.5	Experimental validation.....	104
12.5.1	Design of experimental validation	104
12.5.2	Execution of experimental validation	105
12.5.3	Results	105
12.6	Comparison.....	111
12.7	Conclusion	114

PART 5 Dual side by side laser sources productivity optimization

Chapter 13	Two laser sources	117
13.1	Two sources concept.....	117
13.2	Optimization strategy.....	118
13.3	Boundary limit of process parameters	119
13.4	Productivity evaluation	120
13.4.1	Laser track speed and laser power definition	120
13.4.2	Results	120
13.5	Conclusion	123

PART 6 Single source and dual laser sources productivity comparison

Chapter 14	Single and dual sources comparison	126
14.1	Comparison with Equal process parameters	126
14.2	Optimal process parameters comparison	127

14.3	Conclusion	127
	Future Developments.....	128
	Appendix A Trajectory of heat source MATLAB code	129
	Appendix B Heat source generation MATLAB code	135
	References.....	137

List of figures

Figure 1-1 Titanium and its alloys applications; sport, aviation, medical and lifestyle products	1
Figure 1-2 Efficient solution to deal with laser titanium heat treatment problem.	2
Figure 2-1 Laser annealing.....	6
Figure 2-2 Annealing steps	7
Figure 2-3 Typical Laser Annealing temperature profile	7
Figure 2-4 Different Laser Beam Positions	20
Figure 3-1 COMSOL desktop, general view	24
Figure 4-1 Power weld results.....	26
Figure 4-2 Thermocouple welding to the sample	27
Figure 4-3 Controller unit and sample connection.....	27
Figure 4-4 Measuring chain	27
Figure 4-5 Schematic presentation of micro thermocouple welding circuit	29
Figure 4-6 Laser Source	30
Figure 4-7 ABB robot, IRB 2400.....	31
Figure 4-8 Working area of ABB robot,IRB 2400	31
Figure 4-9 Bimo laser head, HIGHYAG laser technology, Laser delivery schematic.....	32
Figure 4-10 Laser head schematic.....	33
Figure 4-11 Laser annealing system set up	34
Figure 4-12 Cold rolling machine	35
Figure 4-13 Mounting machine.....	36
Figure 4-14 Planar grinding machine.....	36
Figure 4-15 (A) Fine polishing machine, (B) Ultrasonic polishing machine	37
Figure 4-16 Macroscopic observation.....	37
Figure 4-17 Microstructure image acquisition system.....	38
Figure 4-18 The indenter head in Vickers test	39
Figure 4-19 Microhardness tester.....	40
Figure 5-1 Workpiece dimensions[mm]	41
Figure 6-1 Properties of pure elemental titanium at room temperature	43
Figure 7-1 Absorption coefficient for metals and non metals for different wavelengths.....	49
Figure 7-2 Absorption does not depend on the material characteristics and wavelength	49
Figure 7-3 Laser track movement and laser trajectory, dimension [mm]	52
Figure 7-4 welding thermocouples in the favorite position, all dimensions in [mm]	53
Figure 7-5 Temperature profile comparison technique.....	53
Figure 8-1 laser head and workpiece position.....	55

Figure 8-2 Experimental Temperature profile at the centerline related to laser pass	57
Figure 8-3 Experimental temperature profile at distance 5[mm] from the centerline	58
Figure 8-4 Experimental temperature profile at distance 10 [mm] from the centerline	58
Figure 8-5 Experimental temperature profile at distance 15 [mm] from the centerline	59
Figure 8-6 Experimental temperature profile at distance 20[mm] from the centerline	59
Figure 8-7 Average of experimental temperature profiles at centerline	60
Figure 8-8 Average of experimental temperature profiles at distance 5[mm] from the centerline	60
Figure 8-9 Average of experimental temperature profiles at distance 10[mm] from the centerline	61
Figure 8-10 Average of experimental temperature profiles at distance 15[mm] from the centerline	61
Figure 8-11 Average of experimental temperature profiles at distance 20[mm] from the centerline	62
Figure 8-12 Maximum temperature respect to different distances from centerline	62
Figure 9-1 Modeled geometry of the workpiece	65
Figure 9-2 Thermal Conductivity CP Ti1	66
Figure 9-3 Specific heat capacity CP Ti1	66
Figure 9-4 Delivery source	67
Figure 9-5 Fiber delivery	68
Figure 9-6 Gaussian distribution	69
Figure 9-7 Heat Source and Gaussian distribution	70
Figure 9-8 Constant natural convection for all the surfaces	71
Figure 9-9 External upside and downside natural convection	71
Figure 9-10 radiation for all surfaces	72
Figure 9-11 Mesh preciseness decision to have a independent mesh	73
Figure 9-12 maximum temperature at centerline and no. of element for each mesh decision	73
Figure 9-13 duration of simulation and no. of element for each mesh decision	74
Figure 9-14 Part mesh	74
Figure 9-15 Effect of absorpction coefficient	76
Figure 9-16 Effect of hconvective	77
Figure 9-17 Effect of emissivity	77
Figure 10-1 getting close to the correct parameters	78
Figure 10-2 Experimental and numerical comparison at centerline	79
Figure 10-3 Experimental and numerical comparison at 5[mm] far from centerline	

.....	80
Figure 10-4 Experimental and numerical comparison at 10[mm] far from centerline.....	80
Figure 10-5 Experimental and numerical comparison at 15[mm] far from centerline.....	81
Figure 10-6 Experimental and numerical comparison at 20[mm] far from centerline.....	81
Figure 10-7 Experimental and numerical maximum temperature comparison...	82
Figure 12-1 Studied cross section.....	86
Figure 12-2 Length, Angle of annealed area.....	87
Figure 12-3 Melted.....	88
Figure 12-4 Not annealed.....	88
Figure 12-5 Not fully penetrated.....	88
Figure 12-6 Low angel annealing.....	88
Figure 12-7 Accepted annealing.....	88
Figure 12-8 Study area, skim of numerical and experimental overlapping.....	91
Figure 12-9 Variable Process Parameters.....	93
Figure 12-10 Ton-off interval plot.....	98
Figure 12-11 Area used to define process parameters and the expansion area...	99
Figure 12-12 First iteration in order to define the study area.....	100
Figure 12-13 Study area.....	100
Figure 12-14 Productivity measurement for accepted annealing.....	101
Figure 12-15 Annealing status according to the numerical isotherms.....	102
Figure 12-16 Length and Angle measurement of numerical isotherms.....	102
Figure 12-17 Prod. Calculation for accepted numerical isotherms.....	103
Figure 12-18 Chosen process parameters in order to experimental validation.	105
Figure 12-19 Length Comparison.....	112
Figure 12-20 Angle Comparison.....	112
Figure 12-21 Productivity Comparison.....	112
Figure 12-22 Percentage error, Length and Productivity.....	113
Figure 12-23 Percentage error, Angle.....	113
Figure 12-24 Ton-off decision and the optimized parameters.....	114
Figure 13-1 Favorite density profile and possible evolution.....	117
Figure 13-2 Analysis area, parameters effect investigation.....	118
Figure 13-3 Distance definition between two sources.....	118
Figure 13-4 Annealing status and productivity for distance=2.16[mm].....	121
Figure 13-5 Annealing status and productivity for distance=2.28[mm].....	121
Figure 13-6 Annealing status and productivity for distance=2.40[mm].....	122
Figure 13-7 Annealing status and productivity for distance=2.52[mm].....	122
Figure 13-8 Annealing status and productivity for distance=2.64[mm].....	123

List of tables

Table 3-1 Some features of COMSOL Multi-physics version 4.2a.....	25
Table 4-1 Characteristics of K type thermocouple	28
Table 4-2 Parameters to weld thermocouples	28
Table 4-3 Characteristics of the laser source, IPG YLR-1000 1Kw	30
Table 4-4 Some specification of robotic arm.....	31
Table 4-5 Laser head datasheet	33
Table 4-6 Kroll composition as micro-etchant.....	37
Table 4-7 Technical specification of microscope and its lens	38
Table 4-8 Microhardness tester specification	39
Table 6-1 Description of commercial titanium alloys [52].....	44
Table 6-2 General characteristics of CP Ti1 [52]	45
Table 7-1 Optical emissivity values reported for titanium and titanium alloys ..	50
Table 8-1 fixed and variable process parameters.....	54
Table 8-2 Temperature profile measurement test design.....	57
Table 9-1 Number of divisions, elements and nodes for the selected mesh	74
Table 9-2 Processing parameters	75
Table 9-3 Calibration parameter range	76
Table 10-1 process parameters.....	79
12-1 Reported annealing temperatures for titanium and its alloys	90
Table 12-2 Parameters behavior Assumption	92
Table 12-3 A sample of micrographs for each process parameter combination.	94
Table 12-4 Detailed summery of measurement for variable process parameters	95
Table 12-5 Numerical isotherms for each process parameter combination.....	96
Table 12-6 An example of numerical isotherms and experimental micrographs overlapping.....	97
Table 12-7 Ton-off decision.....	98
Table 12-8 Length Angle and Prod. For accepted numerical isotherms.....	103
Table 12-9 Proposed process parameters.....	104
Table 12-10 Chosen process parameters in order to experimental validation ..	104
Table 12-11 Sample 1 macro observation (melting status).....	106
Table 12-12 Sample 2 hardness test and micro observation (low angle status)	106
Table 12-13 Sample 3 hardness tests and micro observation (Accepted annealing)	107
Table 12-14 Sample 4 hardness tests and micro observation (Accepted annealing)	108
Table 12-15 Sample 5 hardness tests and micro observation (Accepted annealing)	109
Table 12-16 Sample 6 hardness tests and micro observation (Accepted annealing)	110

Table 12-17 Length Angle and Prod. for experimental validation	111
Table 12-18 Optimized and validated process parameters	114
Table 13-1 distance range	119
Table 13-2 distance division	119
Table 13-3 Study area	120
Table 13-4 Optimum distance and process parameters.....	123
Table 13-5 Two laser sources optimum productivity	123
Table 14-1 productivity comparison single and dual laser sources (P=300, V=7[mm/s]).....	126
Table 14-2 Optimized productivity and process parameters for single and dual sources.....	127

Abstract

In recent years, commercially pure titanium grade 1, is finding application in a wide range of fields because its advanced high strength, good formability, and reduced density. Nevertheless, the deformation proprieties of titanium can be increased through the use of specific heat treatment.

A laser beam can be used as a flexible heat treatment tool. Because of the complexity of this process, numerical simulation becomes vital for reducing experiments costs. Various set of process parameter which guaranties different level of effectiveness of the process can be identified. In the industrial environment, the choice among these parameters is a trade-off between quality assurance and productivity maximization. In order to identify the best choice of process parameters, a 3D transient numerical model has built up in COMSOL multi-physics to simulate laser annealing process of the Commercially pure Titanium (CP Ti1). Firstly, a model calibration through temperature measurement via thermocouple is performed. Punctual temperature profile comparison between simulation and experiments is used as method to calibrate the model. Secondly, quantitative productivity information are extrapolated from the FEM model using different process parameters identifying the maximum productivity point. Further experiment are carried out to validate the increase in productivity in the optimal point.

Finally, the productivity of a single beam source is compared with a different solution where two adjacent sources are used to obtain a favorable temperature distribution inside the work piece aimed at further increase the laser annealing productivity.

KEY WORDS : numerical heat treatment modeling, temperature field calibration, fiber laser stress relief, productivity optimization, adjacent heat sources.

Sommario

Negli ultimi anni, il titanio commercialmente puro grado 1 sta trovando un largo impiego in differenti ambiti di applicazione a cause delle ottime caratteristiche meccaniche, di deformabilità e leggerezza che lo costituiscono. Tuttavia l'incremento delle sue proprietà di deformazione plastica possono essere incrementate ulteriormente tramite l'utilizzo di un trattamento termico.

Il laser per via delle sue caratteristiche può essere utilizzato come strumento per effettuare il trattamento termico. Tuttavia, a causa della complessità del fenomeno la simulazione numerica può essere un ottimo strumento di supporto per ridurre il costo degli esperimenti. Differenti combinazioni di parametri di processo possono portare al corretto conseguimento dell'incremento di proprietà di deformazione del materiale. In ambito industriale, la scelta tra questi differenti set di parametri è dettata da un bilancio tra efficacia del processo e produttività

Al fine di identificare i migliori parametri di processo finalizzati a massimizzare la produttività del processo, si è creato un modello agli elementi finiti tramite l'utilizzo di COMSOL. In prima battuta, il modello è calibrato paragonando i risultati derivanti dalle simulazioni con degli esperimenti dove la temperatura viene misurata utilizzando delle termocoppie. Successivamente, tramite l'utilizzo del modello agli elementi finiti proposto, si valuta la produttività del processo al fine di massimizzare la produttività. Tali parametri di processo sono validati tramite una successiva campagna sperimentale.

In fine, la produttività del modello proposto viene paragonata con una soluzione dove è previsto prevede l'utilizzo di due sorgenti gaussiane affiancate per ottenere un campo termico favorevole all'incremento di produttività all'interno del materiale trattato.

PAROLE CHIAVE: simulazione del scambio termico, calibrazione del campo di temperatura, addolcimento laser, ottimizzazione della produttività, sorgenti laser adiacenti.

Chapter 1 Introduction

Titanium alloys have been successfully applied for a vast variety of applications due to its properties such as low density and high formability. Moreover, exploit titanium as a sheet metal type is a widespread issue in industry. Figure 1-1 shows some applications of titanium and its alloys.

To use these characteristic it is important to be able to heat treat and anneal this material. Moreover, it should be noticed that productivity of heat treatment is important. Improving productivity is at the top of nearly every manufacturer's list but making it happen can be a tough challenge, increasing the productivity is a rare win-win deal.



Figure 1-1 Titanium and its alloys applications; sport, aviation, medical and lifestyle products

Laser beams, owing to their high coherence and directionality, are widely used in surface modification of many kinds of metals.

The advantages of laser processed material over other material processing technology are highly localized and low-in-total heat input, which minimizes the distortion of the work piece, high density and concentrated energetic beam, as the only needed tool that produces very high local heating and cooling rates of materials, higher production rates, greater flexibility, and automatic controllability

in industrial applications.

While in laser types, high power fiber lasers are a new developed laser, which has attracted a great deal of attentions in the industrial fields, due to its multiple advantages. The fiber lasers are very compact, robust and excel in terms of performance, power scalability, reliability, efficiency and operating lifetimes. These lasers are highly efficient, reducing electrical requirements and also providing better beam quality than the conventional solid-stage lasers in addition to the longersystem's lifetime.

So, laser titanium treatments is becoming a high interest for the industries since it is a new process to reduce the costs of production chains, but still the experimental works such as setting up and tuning activities increases the costs of process, and supposes a high obstacle for introducing laser titanium treatments in a large scale. By using process models it is possible minimize the time invested in the previous tuning, avoiding unproductive time on the machine.

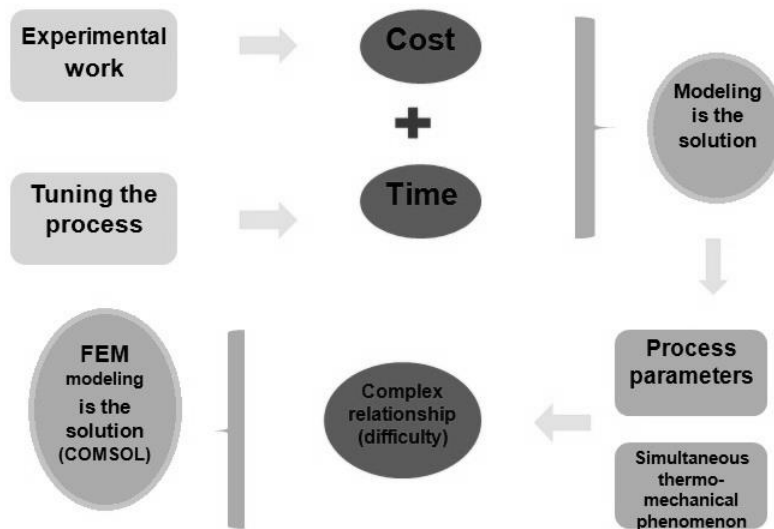


Figure 1-2 Efficient solution to deal with laser titanium heat treatment problem.

Furthermore, complex relationships exist among the process parameters and the simultaneous thermo-mechanical phenomenon which generally occur during the laser beam interaction with the materials (heat transfer, deformation mechanics, mass transfer, fluid flow, may be also phase transformations). This is the reason why the design of a laser titanium treatment components may be difficult. The finite element method(FEM) can provide important preliminary information about the thermal and mechanical stresses induced by thermal cycles giving this opportunity to predict the exact final favorite goal. COMSOL multi-physics is a suitable software due to its powerful feature in order to model most kind of

physical phenomenon Figure1-2 depicts the highlighted issues and the way to handle the problem. When the model is approached, it is applicable to improve the favorite goal, as the importance of productivity is known for anybody, so the model will be used in order to optimize the process parameters to have the optimum productivity.

This thesis work is going to be like discussing the laser annealing process definition in part 1, introducing modeling and experimental equipment in part 2, modeling and calibration of the single laser source annealing in part 3, optimizing the process parameters in order to have optimum possible productivity in part 4, improve the model to have the double laser sources in side by side position in part 5 and finally productivity comparison of single and double laser sources in part 6.

Part 1

Definition of the laser annealing process

Chapter 2 Contest, problems and objectives

The laser has some unique properties for surface heating. The electromagnetic radiation of a laser beam is absorbed within the first few atomic layers for opaque materials, such as metals.

The applied energy can be placed precisely on the surface only where it is needed. Thus, it is a true surface heater and a unique tool for surface engineering. Surface treatment is a subject of considerable interest at present because it seems to offer the chance to save strategic materials or to allow improved components with idealized surfaces and bulk properties. Figure 2-1 presents a typical annealing process.



Figure 2-1 Laser annealing

2.1 Laser heat treatment process description

Laser beam can be adopted in order to perform a heat treatment, due to a imposed and controlled thermal cycle (heating and cooling).

The goal of the heat treatment is the modifications of the surface properties of the material. Heat treatment is performed by means of thermal cycle which is imposed on metals or metal alloys in order to obtain a specific structure and specific final properties. These treatments perform on a material in a solid state and in a controlled environment.

Generally the essential parts, which can define a heat treatment, are (Figure 2-2):

- heating phase: heating the workpiece until a certain temperature.
- maintaining phase: maintaining at a certain temperature.
- cooling phase: cool the heated surface from this temperature to room

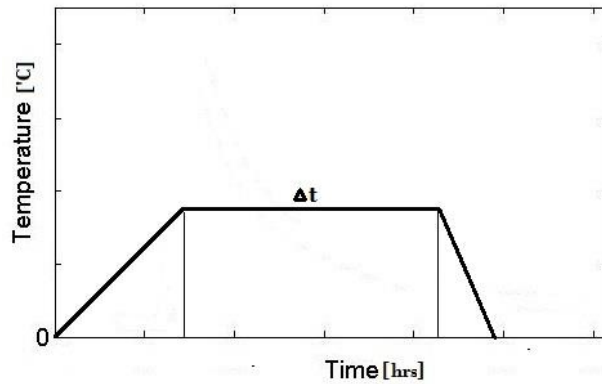


Figure 2-2 Annealing steps

Because only a narrow surface can be heated by means of a laser beam and the movement of laser is typically consider fast, in case of laser annealing there is no maintaining phase. The typical annealing temperature profile for laser treatment would be like Figure 2-3.

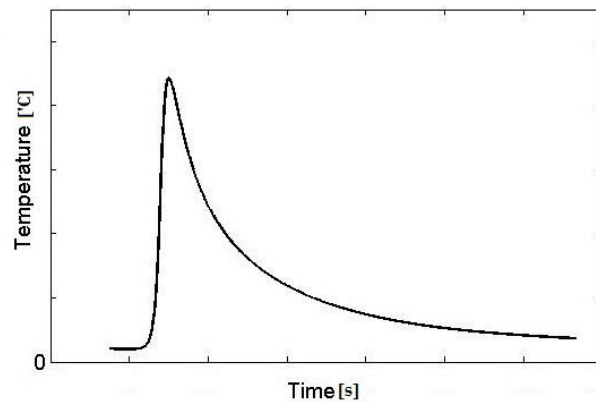


Figure 2-3 Typical Laser Annealing temperature profile

Several types of laser can be used in order to heat treatment:

- Diode lasers: they are particularly suitable for surface heat treatment because of their because the related wavelength is $\lambda = 0.8 - 0.95 \mu\text{m}$ which ensures a good absorption coefficient, rectangular laser spot with uniform distribution of irradiance.
- Continues wave mode NY:Yag lasers: this type of laser are also suitable for laser surface heat treatment but the efficiency are less than diode lasers because this kind of lasers are pumped by diode laser.

- CO₂ lasers: previously surface heat treatments were performed by this type of lasers then their uses limited because of low absorption coefficient in the medium infrared field for metallic materials.
- Fiber lasers: this type of lasers are also very suitable for surface laser heat treatment and not studied widely yet. No drawbacks related to efficiency or low absorption coefficient for this laser type. Fiber laser due to its advantages such as compact size, high optical quality, high source and delivery flexibility and high overall power efficiency can be a very good choice in order to use for heat treatment.

In order to understand the annealing process and modeling laser annealing it is necessary to have a general idea about the different type of material annealing.

There are different general types of annealing which presented below, it should take into the consideration that there would be also different categorization related to a specific material:

- Normalization:
Normalization is an annealing process applied to ferrous alloys to give the material a uniform fine grained structure and make it less brittle. Material is soaked for a short period at special temperature and then allowed to cool in air. Smaller grains form that produce a tougher, more ductile material. Normalizing improves machinability of a component and provides dimensional stability if subjected to further heat treatment processes.
- Process annealing:
Process annealing, also called intermediate annealing, subcritical annealing, or in-process annealing, is a heat treatment cycle that restores some of the ductility to a product during the process of cold working, so it can be worked further without breaking further heat treatment cycles. The temperature range for process annealing ranges from 260 °C (500 °F) to 760 °C (1400 °F), depending on the alloy in question.
- Full anneal:
A full anneal typically results in the second most ductile state a metal can assume for metal alloy. It creates a new uniform microstructure with good dynamic properties. The details of the process depend on the type of metal and the precise alloy involved. In any case the result is a more ductile material but a lower yield strength and a lower tensile strength. Often the material to be machined is annealed, and then subject to further heat treatment to achieve the final desired properties.

- Short cycle anneal:
Short cycle annealing is used for turning normal ferrite into malleable ferrite. It consists of heating, cooling, and then heating again from 4 to 8 hours.

2.2 Titanium laser heat treatment

As it mentioned titanium and titanium alloys have been widely for aerospace technology and surgical implants because of their high Corrosion resistance, excellent biocompatibility, good oxidation resistance, strength–weight ratio and low mass-to volume ratio. However, the commercially pure titanium (CP-Ti) used possesses low mechanical strength, low surface hardness and poor [1]. Consequently, an increased interest has been shown to modify the surface microstructure and composition with the addition of alloying elements to improve these properties.

Wear resistance laser beams are widely used for heat treatment and surface modification [1, 2].

Titanium heat treating is the industrial process of applying extremely high temperatures to titanium so that the metal becomes more workable for manufacturing purposes [3].

Generally titanium and titanium alloys are heat treated in order to:

- Reduce residual stresses developed during fabrication (stress relieving)
- Produce an optimum combination of ductility, machinability, and dimensional
- and structural stability (annealing)
- Increase strength (solution treating and aging)
- Optimize special properties such as fracture toughness, fatigue strength, and high-temperature creep strength

Various types of annealing treatments (single, duplex, (beta), and recrystallization annealing, for example), and solution treating and aging treatments, are imposed to achieve selected mechanical properties. Stress relieving and annealing may be employed to prevent preferential chemical attack in some corrosive environments, to prevent distortion (a stabilization treatment) and to condition the metal for subsequent forming and fabricating operations.

Stress Relieving

Titanium and titanium alloys can be stress relieved without adversely affecting strength or ductility.

Stress-relieving treatments decrease the undesirable residual stresses that result from first, non-uniform hot forging or deformation from cold forming and straightening, second, asymmetric machining of plate or forgings, and, third, welding and cooling of castings. The removal of such stresses helps maintain shape stability and eliminates unfavorable conditions, such as the loss of compressive yield strength commonly known as the Bauschinger effect.

Annealing

The annealing of titanium and titanium alloys serves primarily to increase fracture toughness, ductility at room temperature, dimensional and thermal stability, and creep resistance. Many titanium alloys are placed in service in the annealed state. Because improvement in one or more properties is generally obtained at the expense of some other property, the annealing cycle should be selected according to the objective of the treatment [4].

Annealing is used to fully soften the material and remove all residual stresses. Annealing of wrought products at typical temperatures (below the beta transus) results in a fully recrystallized equiaxed alpha structure. Precise control of grain size (and mechanical properties) can be achieved by adjusting the anneal temperature [5].

Common annealing treatments are:

- Mill annealing
- Duplex annealing
- Recrystallization annealing
- Beta annealing

Mill annealing is a general-purpose treatment given to all mill products. It is not a full anneal and may leave traces of cold or warm working in the microstructures of heavily worked products, particularly sheet.

Duplex annealing alters the shapes, sizes, and distributions of phases to those required for improved creep resistance or fracture toughness.

Recrystallization annealing and β annealing are used to improve fracture toughness. In recrystallization annealing, the alloy is heated into the upper end of the α - β range, held for a time, and then cooled very slowly. In recent years,

recrystallization annealing has replaced β annealing for fracture critical airframe components.

β (Beta) Annealing Like recrystallization annealing, β annealing improves fracture toughness. Beta annealing is done at temperatures above the β transus of the alloy being annealed. To prevent excessive grain growth, the temperature for β annealing should be only slightly higher than the β transus. Annealing times are dependent on section thickness and should be sufficient for complete transformation. Time at temperature after transformation should be held to a minimum to control β grain growth. Larger sections should be fan cooled or water quenched to prevent the formation of a phase at the β grain boundaries.

Straightening, sizing, and flattening of titanium alloys are often necessary in order to meet dimensional requirements. The straightening of bar to close tolerances and the flattening of sheet present major problems for titanium producers and fabricators.

Unlike aluminum alloys, titanium alloys are not easily straightened when cold because the high yield strength and modulus of elasticity of these alloys result in significant springback. Therefore, titanium alloys are straightened primarily by creep straightening and/or hot straightening (hand or die), with the former being considerably more prevalent than the latter [4].

Titanium and its alloys have a high affinity for gases including oxygen, nitrogen and hydrogen. When CP Ti is heated in air, oxygen absorption results in the formation of an extremely hard, brittle, oxygen-stabilized alpha phase layer known as alpha case.

Intermediate and final annealing of CP Ti is often performed in a vacuum or inert gas atmosphere to avoid alpha case formation and the associated material loss. Vacuum annealing can also be used to remove excess hydrogen pickup, a process known as vacuum degassing. Parts to be vacuum heat treated must be thoroughly cleaned [5].

Solution Treating and Aging

A wide range of strength levels can be obtained in α - β or β alloys by solution treating and aging. With the exception of the unique Ti-2.5Cu alloy (which relies on strengthening from the classic age-hardening reaction of Ti₂Cu precipitation similar to the formation of Guinier-Preston zones in aluminum alloys), the origin of heat-treating responses of titanium alloys lies in the instability of the high-temperature β phase at lower temperatures.

Heating an α - β alloy to the solution-treating temperature produces a higher ratio of β phase. This partitioning of phases is maintained by quenching, on subsequent aging, decomposition of the unstable β phase occurs, providing high strength. Commercial β alloys generally supplied in the solution-treated condition, and need

only to be aged.

After being cleaned, titanium components should be loaded into fixtures or racks that will permit free access to the heating and quenching media. Thick and thin components of the same alloy may be solution treated together, but the time at temperature is determined by the thickest section [4].

Contamination is a crucial issue in titanium heat treating. Fabrication shops often have separate areas for titanium since this metal is especially prone to contamination from air, moisture, dust, and grease. Other high-performance metals, such as stainless steel and nickel-base alloys, do not require as strict attention to cleanliness as they are not as sensitive as titanium to contamination while being formed or welded.

It is important to note that pure elemental titanium is rarely used in modern manufacturing as it is a rather soft metal on its own. Titanium alloys, mixtures of titanium with other metals, allow for maximum hardening properties. Each particular titanium alloy will respond differently to the heat treatment process, however [3].

The application of titanium alloys under severe wear and friction conditions is highly restricted due to their poor tribological properties such as high friction coefficient and low hardness. On the other hand, although titanium and its alloys are commonly used as a medical implants for many years, they are bioinert materials and occasionally failure because of the corrosion-fatigue which titanium implants suffered in body fluids. In addition, it is dangerous for Ti-6Al-4V to stay in the human body for a long time, because the element aluminum has strong neurotoxicity and vanadium is a strong cytotoxin. So, heat treatment of titanium and its alloys is a promising work in enlarging their application scope.

Laser beams, owing to their high coherence and directionality, are widely used in surface modification of many kinds of metals. Thus, the disadvantages of titanium alloys can be compensated for by laser surface modification treatment on the workpieces where they suffer in operation, or by laser cladding a layer of bioceramic coatings on the surface of titanium alloy substrates to meet the requirement for implantation in human body [6].

Laser processing of materials has been developing for more than 20 years since the 1970s when laser technology started to boom. The advantages of laser processed material over other material processing technology are highly localized and low-in-total heat input, which minimizes the distortion of the work piece, high density and concentrated energetic beam, as the only needed tool that produces very high local heating and cooling rates of materials, higher production rates, greater flexibility, and automatic controllability in industrial applications. Since, many mathematical and computational models for laser applications have also been developed recently [7].

Micro structural feature of titanium alloys, which is one of the important factors to control mechanical properties, is sensitively affected by heating temperature,

holding time and cooling rate of the substrates. Laser parameters have to be optimized in order to reduce defects and to optimize microstructure [8]. Morphology of the layers created and nature of the phases formed mostly depend on the laser beam overlapping, the nature of surrounding gas [9] and the intensity of laser beam [1].

2.3 Modeling of laser heat treatments process

Engineering analysis of mechanical systems have been addressed by deriving differential equations relating the variables of through basic physical principles such as equilibrium, conservation of energy, conservation of mass, the laws of thermodynamics, Maxwell's equations and Newton's laws of motion. However, once formulated, solving the resulting mathematical models is often impossible, especially when the resulting models are nonlinear partial differential equations. Only very simple problems of regular geometry such as a rectangular of a circle with the simplest boundary conditions were tractable.

The basic concept in the physical interpretation of the FEM is the subdivision of the mathematical model into disjoint (non-overlapping) components of simple geometry called finite elements or elements for short. The response of each element is expressed in terms of a finite number of degrees of freedom characterized as the value of an unknown function, or functions, at a set of nodal points.

The response of the mathematical model is then considered to be approximated by that of the discrete model obtained by connecting or assembling the collection of all elements.

Numerical process simulations gain more and more importance both for industrial applications and for scientific purposes. In science these simulations enable for thorough process understanding as it is possible to separate different process or material parameters in their influence on the processing result. They also enable for a look inside the work piece also on very short time scales and thus allow the analysis of processes that can not or only hardly be observed by experimental means. In industrial production simulations serve as a tool for planning of single production steps or even of whole process chains. Furthermore, simulations are important for the development of production means like new machining tools.

Contrary to other technologies, like e.g. forming, simulations for laser material processing are not yet state of the art especially in industrial production. This is due to the complexity of laser processes where a variety of different physical phenomenon are coupled with each other. To reduce this complexity in state of the art models most of these phenomena are regarded as decoupled or they are

even neglected dependent on the process that is to be simulated.

Thus these models are only capable to analyze certain effects of the processing like e.g. thermal distortion or residual stresses [10].

Laser heating analysis gives insight into the physical process that takes place during the laser heating pulse. Depending on the laser pulse intensity, the heating process can be classified as non conduction-limited or conduction-limited heating. In conduction limited heating substrate material remains in the solid phase while phase change (melting and evaporation) occurs in the non conduction-limited heating. As the substrate material is heated, its temperature rises to elevated temperatures, which, in turn, results in thermal expansion of the substrate material. Consequently, depending on the thermal strain developed, stress levels well in excess of elastic limit of the substrate material can result.

Moreover, since the process is transient, the stress wave generated propagates into the substrate. Generally the thermal stress is generated in the solid substrate, since substrate material in the liquid phase expands freely during the heating process. Consequently, regardless of the type of heating process, thermal stress develops only in the solid phase of the substrate material. Since analytical solutions to the heating and thermal stress problems provide useful information to reduce the experimental time and cost, analytical investigations into the heating problem are fruitful[11].

There are several analytical and numerical studies related to:

- Laser heating of solid substrates
- Thermal stresses due to the laser irradiation on substrate
- Heat transfer and fluid flow during laser heating

Considerable research studies were carried out to explore the laser heating of solid substrates. Ready [12] introduced the analytical solution for the temperature rise inside a substrate due to a step input pulse. Laser heating of a two-layer system was formulated by Al-Adawi et al. [13] using a Laplace transformation method. The analytical solution for temperature rise inside a solid substrate due to a pulse varying exponentially in time was obtained by Yilbas [14]. He demonstrated that the pulse parameters had a significant effect on the temperature rise inside the substrate. Yilbas [15] introduced a closed form solution for a laser pulse varying exponentially in time. He indicated that the thermal integration at the surface was almost possible as the pulsing frequency was increased to 1 kHz. Yilbas and Shuja [16] studied the conduction-limited heating process due to a laser heating pulse. They introduced a dimensionless equilibrium temperature inside the substrate. Yilbas and Kalyon [17] obtained a closed form solution for temperature rise inside a solid substrate due to a pulse varying exponentially in time and with *convective* boundary condition at the surface. They indicated that for a set

of laser pulse parameters, temperature at the surface attains its maximum for heat transfer coefficients less than $10^7 [\frac{W}{m^2k}]$. The actual laser pulse has time-dependent power intensity distribution and the temporal variation of the laser pulse can not be ignored in the analysis. Consequently, laser pulse profile needs to be incorporated in the mathematical analysis.

Considerable numbers of research studies were carried out on thermal stresses due to laser irradiation on substrates. A numerical study of fracture initiation in aluminum oxide ceramics during laser cutting was carried out by Li and Sheng [18]. They indicated that the fracture initiation resulted from high-energy density cutting conditions. The thermal stress development in a solid due to a laser heating process was studied by Wang et al.[19].

They analyzed the complex coupling action between temperature, phase transformation, and stresses during elastic-plastic deformation. Elastic displacement of the surface due to a laser heating pulse was studied by Yilbas et al.[11]. They indicated that in the heating cycle, the rate of temperature rise and the rate of thermal expansion were similar. Yilbas and co-workers [20] investigated the thermal stresses induced in the surface region of the substrate due to the laser heating pulse. They indicated that high stress levels resulted in the surface region of the substrate.

The role of heat-transfer phenomena in annealing, surface treatment and welding is crucial for obtaining high quality surfaces by eliminating defects, such as undercutting, non-uniform surface profile, and cavities, which are attributed to changes in fluid flow and heat transfer[21].

Numerical and analytical models to simulate heat transfer and fluid flow during steady and transient fusion welding were developed during the last two decades. Calculations were obtained for both moving [22]and stationary heat sources and for laser beam as well as arc welding [23]. In an arc weld pool, flow driven by both surface tension and electromagnetic fields play an important role. However, in laser welding, only surface tension driven flow is significant [24]. These models were used to calculate weld pool geometry by calculating temperature fields during the welding of titanium alloys [25]. Pulsed lasers are used as the energy source for cutting, welding, rapid manufacturing, machining and ablation, melting, alloying [26], cladding, and surface hardening of the materials [27]. The understanding of the laser irradiation of materials involves numerous phenomena namely heat transfer, absorption, distortion, variation of the thermophysical properties, and phase transformation. Until now, a model that considers all these phenomena has not existed because of the multidisciplinary nature of the problem spanning thermal, chemical, and mechanical fields [21].

In order to model laser heat treatment phenomena it is usual to have some uncertain parameters like absorption coefficient for this reason calibration method

is used.

Another important issue in laser heat treatment process is the beam intensity distribution. More specific information about calibration and beam intensity profile will be discussed.

- Calibration
- Beam shaping

Role of calibration

In many fields of science and engineering, mathematical models are used to represent complex processes. Commonly, quantities simulated by the mathematical model are more readily measured than are model input values, and model calibration is used to construct a model and estimate model input values. In model calibration, various parts of the model, including the value of model input values, are changed so that the measured values (often called observations) are matched by equivalent simulated values, and, hopefully, the resulting model accurately represents important aspects of the actual system.

The model inputs that need to be estimated are often distributed spatially and (or) temporally, so that the number of parameter values could be infinite. The number of observations, however, is generally limited and able to support the estimation of relatively few model input values. Addressing this discrepancy is one of the greatest challenges faced by modelers in many fields. Generally a set of assumptions are introduced that allows a limited number of values to be estimated, and these values are used to define selected model inputs throughout the spatial domain or time of interest.

Formal methods have been developed that attempt to estimate parameter values given some mathematically described process and a set of relevant observations. These methods are called inverse models, and they generally are limited to the estimation of parameters as defined above for some processes, the inverse problem is linear, in that the observed quantities are linear functions of the parameters [28].

Main reasons to use the calibration methods:

- Models are approximations of reality; they can not precisely represent natural systems
- There is no single, accepted statistic or test that determines whether or not a model is valid
- Both graphical comparisons and statistical tests are required in model calibration and validation
- Models can not be expected to be more accurate than the errors (confidence intervals) in the input and observed data.

Although numerical models have contributed to understand the underlying mechanisms of different physical phenomenon, there are certain input model parameters that can not be easily determined. Thus, the model predictions do not always agree with experimental results, therefore, model calibration is a logical approach to make modeling more complete.

Many studies with different subjects has used this approach, A. De and T. DebRoy developed a smart model for the estimation of effective thermal conductivity and effective viscosity in weld pool. Experimental data on weld penetration and width for six conduction mode laser welds were used. The computed weld dimensions were found to be sensitive to both the effective thermal conductivity and effective viscosity. It is found that the effective thermal conductivity and effective viscosity depended on the heat input. The optimum values of both effective thermal conductivity and effective viscosity were independent of their initial guessed values. However, their initial choice affected the volume of numerical calculations. The accuracy of the estimated values is verified using the numerical heat transfer and fluid flow model and the experimental data. [29], S. Rouquette, J. Guo, P. Le Masson estimate a heat source in a longitudinal section during an electron beam welding. The aim of work was the parameter identification of the Gaussian source term representative of the dissipated heat flux in the liquid zone from measured temperatures in the solid zone. They have analyzed the feasibility of the estimation for a source term $S(x, z, t)$ in a transversal section. The direct thermo-metallurgical problem is presented in a two-dimensional longitudinal section (x, y) for a quasi-steady state. Here, they solve only a linear case. The sample is divided in the axial direction z in few sections. At each section, a source term is defined with a part of the beam and creates a vaporized zone and a fused zone. The goal of the work was the rebuilding of the complete source term with the estimations at each section [30], instead S. Pereyra*, G.A. Lombera, G. Frontini, S.A. Urquiza apply sensitivity analysis and parameter estimation to test heat transfer and material flow models. A forward-difference approximation was used to compute the sensitivity of the solution with respect to the unknown model parameters. The numerical models were developed by the finite element method (FEM). The way in which the unknown model parameters independently affect the results and the importance of the location of reference points that take part in the objective function were determined [31].

In modeling of laser cladding, also using a calibration method is a typical way to make the model more precise. There are a lot of process parameters that control laser material deposition and calibration seems an inevitable part of this process, Zhiqiang Fan, Kaushik Phatak and Frank Liou use simulation and experiments to investigate the effect of the process input parameters: laser power, powder mass flow rate, and scanning speed on the output parameters. Numerical simulations

and experiments are conducted using a factorial design. The results are statistically analyzed to determine the significant factors and their interactions. The simulation results are compared to experimental results [32]. M. Picasso, C.F. Marsden, A. Frenk, and M. Rappaz approach a model which takes into account the main phenomena occurring during the laser-cladding process. For a given laser power, beam radius, powder jet geometry, and clad height, this model evaluates two other processing parameters, namely, the laser-beam velocity and the powder feed rate. It considers the interactions between the powder particles, the laser beam, and the molten pool. The laser power reaching the surface of the workpiece is estimated and, assuming this power is used to remelt the substrate with the clad having been predeposited, the melt-pool shape is computed using a three-dimensional (3-D) analytical model, which produces immediate results, even on personal computers [33].

Calibration methods also a common method to deal with hydrodynamic models, Ming-Hsi Hsu and Albert Y. Kuo applied numerical hydrodynamic model to the Tanshui River system in Taiwan, most hydrodynamic models, friction and turbulent diffusion/dispersion coefficients are the important calibration parameters affecting the calculation of surface elevation, velocity and salinity distribution. They present a rational approach to calibrate and verify a hydrodynamic model of partially stratified estuaries. The calibration procedures and verification requirements are demonstrated with the application of a vertical (laterally averaged) two-dimensional model to a branched estuarine river system. The friction coefficient is calibrated and verified with model simulation of barotropic flow, and the turbulent diffusion and dispersion coefficients are calibrated through comparison of salinity distributions. The overall model verification is suggested to be achieved with comparisons of Eulerian residual circulation and salinity distribution [34], K.W. Chau use calibration for numerical modeling of flow and water quality The study trans-forms expert knowledge in model manipulation into a knowledge base, which is then integrated with numerical modeling. A prototype expert system for model manipulation for flow and water quality was developed. Expertise in model manipulation, including the knowledge as to what is the correct manipulation direction and how to enhance manipulation effectiveness, are incorporated into the prototype system. It is shown that, through the successful development of this prototype system, expert system technology can be integrated into numerical modeling systems [35].

Calibration methods has used in different kind of industries like coal or even sound industries. Essie Esterhuizen, Chris Mark, Michael M. Murphy, model the large-scale response of coal measure rocks due to mining. Numerical models, provided the main characteristics of the coal pillars, the overburden, and the gob are captured in the models the calibration process described had the objective to obtain good agreement between model results and pillar strength, surface subsidence, and in seam stress distributions. The models of individual pillars were calibrated

against strong roof and floor case histories in which the pillar strength is governed by failure and yielding of the coal within the pillar and the strong surrounding strata had a limited impact on pillar strength. Subsidence matching assisted in verifying that the large-scale rock mass parameters and the gob compaction characteristics are realistic. Further calibration was carried out against stress measurements in coal pillars and in the unmined coal abutments [36].

Hans cappon, Member IEEE, and Karel J. Keesman, made a numerical calibration and validation procedure applied to 2-d FE models of an empty and filled acoustic separator, while preserving known physical and geometrical properties. The model of an empty separator was first calibrated to estimate the unknown system parameters then, with all parameters fixed, validated with measurements on a water-filled model. The accuracy and the sensitivity of the model indicate that system optimization can be done numerically to a large extent [37].

Role of beam shaping

Till now, the emphasis was on the modeling and calibration, while beam shaping and modifying is the important idea to use in the calibrated model for increasing the productivity.

It is a novel issue to modifying the beam intensity profile , one possible solution to make it is optically .There are several classes of random beams [38-46].the recently introduced Rectangular Multi-Gaussian Schell-Model (RMGSM)beam [47] is the first one to be generated by a source with arbitrary spatial intensity distribution while forming far-field intensity distribution with rectangular symmetry.

Moreover, the obtained far-field rectangular intensity pattern can have adjustable edge sharpness and is shape-invariant throughout the far zone.

O. Korotkova and E. shchepakina approach the expression for the cross-spectral density function of beams generated by a novel class of RMGSM sources and propagating in free space and in atmospheric turbulence. The beams of this class are shown to gradually acquire a rectangular intensity profile towards the far zone [47].

It is possible to have more than one laser head in order to improve the goal or have the favorite intensity profile .It is possible to put the two laser heads in the side by side position as it shown it Figure 2-4 so it is possible to manipulate the density profile. Till know there are not many studies that put the two laser heads in a side by side position but there are some studies that put the two laser heads in the tandem position as it shown in Figure 2-4. For example, J. Xie performed a detailed investigation to quantify the benefits of dual beam laser processing and to understand the mechanism for improving weld quality. A 6-kW CO₂ laser beam

was split into two equal-power beams and the dual beams were located in tandem (one beam follows another) during welding. Experimental results indicated the dual-beam laser could significantly improve weld quality. For steel, surface quality was improved with fewer surface defects such as undercut, surface roughness, spatter, and under fill. Weld hardness and centerline cracking susceptibility were also reduced. In aluminum, quality improvements were in the form of smooth weld surfaces and fewer weld defects such as porosity, surface holes, and undercut.

Dual laser beams arranged in tandem have been reported to provide benefits over conventional single-beam laser welding such as improved weld quality. The study is focused on the tandem dual-beam laser welding process and its impact on weld quality.

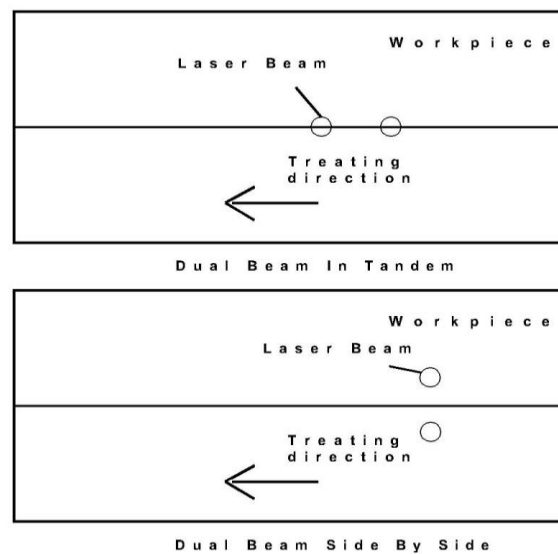


Figure 2-4 Different Laser Beam Positions

Dual-beam laser processing was also reported to help reduce porosity and prevent cracking in laser welding of aluminum alloys. Porosity in weld metal could be significantly reduced when the leading laser beam was focused at the workpiece surface and the trailing beam was defocused at 2 mm above the workpiece [48, 49].

As far as author knowledge no studies have been done to build up specific beam intensity profile to shape the temperature profile inside the material aimed improving productivity.

2.4 Objective

Given the state of the art a lack of scientific research in modeling laser annealing of titanium aimed to improve the productivity is found. Consequently, the objective of this thesis is to investigate the laser annealing of titanium and modeling the phenomena with single and dual laser sources in order to optimize the productivity.

Annealing of titanium with laser has chosen the proper way to investigate and improve the mechanical properties of the titanium. As it mentioned before, the cost of experimental work is a big obstacle, therefore, finite element modeling have chosen the most suitable approach to model the laser annealing of titanium. Considering the fact that productivity in the both senses of saving time and money is an important issue, the model can be used to enhance this aim. Furthermore, having double side by side laser sources in order to modify the laser beam density profile having the favorite temperature distribution can be another solution to increase the productivity.

In this thesis, process parameter productivity optimization of a single beam laser heat treatment is investigated through FEM simulation and further validated. In a second phase, modelling of temperature distribution of the two adjacent beam is simulated as well as its productivity. The two solutions are thus compared to identify which is the best one.

Part 2

Equipment and material
description

Chapter 3 Software for modeling

In order to simulate the annealing process it is important to be equipped with a program that can simulate the physical phenomenon specially heat transfer. COMSOL multi-physics is widely used from both companies and research centers to approach this problem . There are several programs in order to simulate annealing process such as SYSWELD and ABAQUES but COMSOL due to the high degree of flexibility and interface of communication with several programs such as MATLAB, AUTOCAD, CATIA is the most appropriate program to deal with the problem.

COMSOL Multi-physics brings an unprecedented level of clarity to the simulation work by giving both an organized model overview and a streamlined model-building process. The COMSOL user interface reduces clutter and redundant tasks, so the attention can be focused on the substance of the design studies resulting in increased productivity. The COMSOL desktop helps to organize your simulation by presenting a clear overview of your model at any point. It uses functional form, structure, and aesthetics as the means to achieve simplicity for modeling complex realities. For instance, task-specific tools appear on the desktop right when you need them; showing only what is currently possible, which removes uncertainty from model building and brings order to your simulations. Figure 3-1 shows the general view of COMSOL desktop.

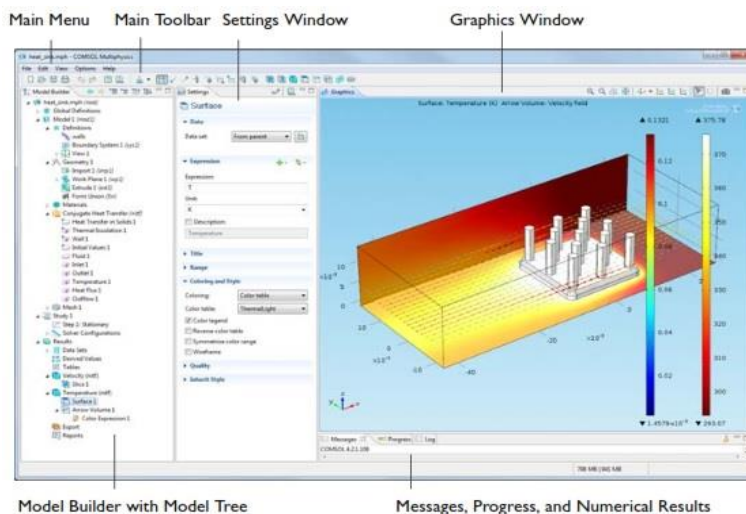


Figure 3-1 COMSOL desktop, general view

The desktop is made up of several windows, which may or may not be displayed depending on the need. These windows include the Model Builder, Settings, Graphics, Messages, Progress, Help, and others. Table 3-1 shows some features of COMSOL Multi-physics version 4.2 a, and its compatibility with other programs.

Programming Language		
FILE FORMAT	READ	WRITE
MATLAB®: Model M-File (.m)	Yes	Yes
MATLAB®: Function (.m)	Yes	No
Java: Model Java File (.java)	Yes	Yes
C: Function Yes No	Yes	No
Mesh		
FILE FORMAT	READ	WRITE
NASTRAN Bulk Data (.nas, .bdf, .nastran, .dat)	Yes	No
VRML, v1 (.vrm1, .vrl)	Yes	No
Interpolation Data Formats		
FILE FORMAT	READ	WRITE
Spreadsheet	Yes	Yes
Grid	Yes	No
Sectionwise	Yes	Yes

Table 3-1 Some features of COMSOL Multi-physics version 4.2a

The software is going to use in order to measure the temperature profiles and isotherms.

Chapter 4 Experimental equipment and methods

During the experiments several devices have been used. They include devices and equipment used for annealing, samples preparation, sample observation and mechanical tests.

4.1 Monitoring

Monitoring is necessary to be aware of the state of a system and obtain the results in order to analyze. The approaches and equipment used in order to monitoring the system are explained below:

Two wires which constitute thermocouple are welded together in order to obtain a small joint (Figure 4-1). This joint has to be as small as possible (to measure temperature in a single point) and as strong as possible (to resist to the high temperature of the process).

Welding process of two materials is done thanks to a machine called “power-weld” (laser welding). This machine uses a single laser shot to heat two wires and weld them (Figure 4-1).



Figure 4-1 Power weld results

Once joint is obtained, it has to be weld onto the sample Figure 4-2. This process is done using a “capacitive welding”.

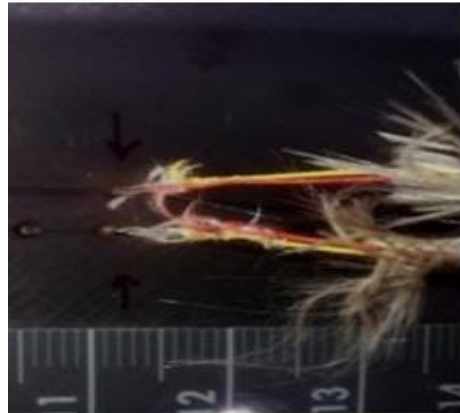


Figure 4-2 Thermocouple welding to the sample

Other extremity of thermocouple is connected to the controller unit (figure4-3), samples are put below the annealing head and controller unit is connected with the computer which record the temperature history. Figure 4-4 shows the measurement chain.



Figure 4-3 Controller unit and sample connection



Figure 4-4 Measuring chain

4.1.1 Thermocouples

Since the experimental temperature profiles in favorite positions of the workpiece is needed, temperature monitoring is essential. To do so, it has decided to exploit thermocouple type K.

Type K microthermocouple is suitable to be employed in a range of temperatures considering some conditions such as life expectancy and environmental situation. Table 4-1 presents permissible temperature ranges and appearance of K type microthermocouple [50].

The micro-K thermocouples has small hot junction diameter about 0.3 mm, and as a consequence by a very short its time constant is also sufficiently short which guarantees proper capturing of rapid heating and cooling cycles [51].

Thermocouple type K				
Item	Temp range (°C)	Standard tolerance (°C)	Time constant (sec)	Sheathing color
Value	0 - 1260	$\geq \pm 2,2$ °C or $\pm 0,75\%$	$2,23 \times 10^{-3}$	red and yellow

Table 4-1 Characteristics of K type thermocouple

Table 4-2 reperent the parameters used in mircothermocouple welding.

Item	Dimension	Value/description
Wavelength	nm	1070
max pulse power	KW	1

Table 4-2 Parameters to weld thermocouples

Having a globular point on the tip of micro thermocouple, it is possible to join the tip on the back of material(CP Ti1) sheet using a static welding circuit composed of 12 serially connected batteries, connecting cables, and voltage and current adjuster. Schematic presentation of micro thermocouple welding against titanium sheet is presented in Figure 4-5.

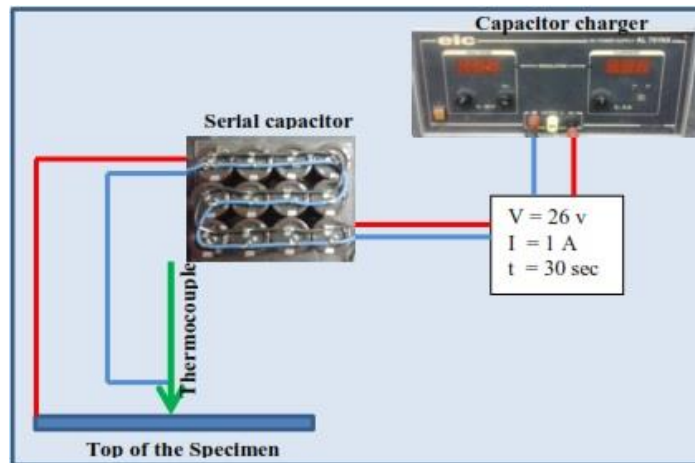


Figure 4-5 Schematic presentation of micro thermocouple welding circuit

4.1.2 Process

Following what reported before, the laser annealing process which is the core of the experimental part is done with combination of laser source, robot arm, laser head in order to deliver and focus the laser on the substrate.

4.1.2.1 Laser source

IPG's low-order-mode kilowatt-class fiber lasers range in power from 1kWatts to 50kWatts, operating in CW or modulated modes up to 20 kHz with wall-plug efficiencies of greater than 25%. The dynamic operating range of these devices is available from 10 percent to 105% of full power with no change in beam divergence or beam profile throughout the entire range. This allows a previously unheard-of capability: a single laser can be utilized for both high-power and low-power applications and for both welding and precision cutting.

The divergence specifications from these lasers are superior by orders of magnitude over any other laser operating at these power levels. This permits the use of long focal-length processing lenses for vastly improved depth-of-field. The units can be supplied with fiber lengths to 200 meters, different fiber diameters and variety of multi-port beam switches, beam couplers. Termination optics, scanners, etc.



Figure 4-6 Laser Source

The laser source used for annealing in this work is YLR-1000 a 1KW Fiber Laser. Table 4-3 represents some characteristics of the source, the source also is shown in Figure 4-6 operational modes are continuous and quasi continuous wave with random polarization. The typical emission line Weight and BPP (beam parameter product) are 3 nm and 2.0 mm*mrad with the maximum values as 6 nm and 2.5 mm*mrad. YLR-1000 is using Ytterbium for doping the active medium in optical fiber to reach the output power of around 1000 Watts.

Optical Properties		
Nominal Output Power	W	1000
BPP after Feeding Fiber	mm*mrad	<2.0'
BPP after Processing Fiber	mm*mrad	<4
Feeding Fiber Core Diameter	um	50
General Parameters		
Max. Cooling Water Consumption (250C)	m3/h	0.6
Cooling Water Temperature Range	°C	20-25
Dimensions	cm	86x120x81
Weight	kg	250
Ambient Temperature	°C	10-50

Table 4-3 Characteristics of the laser source, IPG YLR-1000 1Kw

4.1.2.2 Robot Arm

The laser head is being hold and moved by the robot. Which is a 6-axis anthropomorphic robot manufactured by ABB. The IRB 2400 is used for welding throughout the experiment.

The IRB 2400 with M94A control is an excellent multi-purpose robot. With a 10kg capacity and excellent accuracy the IRB 2400 can be set up for gluing, welding, burring pick and place and etc. In Figures 4-7, 4-8 it is possible to observe ABB robot arm and its working area.



Figure 4-7 ABB robot, IRB 2400

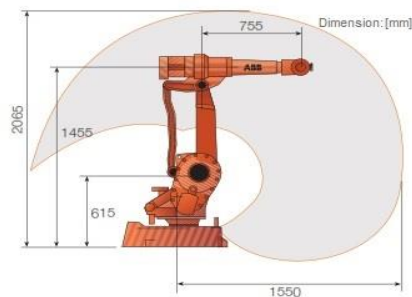


Figure 4-8 Working area of ABB robot,IRB 2400

Most popular industrial robot IRB 2400 comprises a complete family of application optimized robots that maximize the efficiency of the arc welding process and tending applications. Table 4-4 present the some robot features.

Features	
Control	S4 - M94A
Position repeatability (RP)	0.03 mm
Path repeatability	0.11-0.15 mm
Reach	1.55 m

Table 4-4 Some specification of robotic arm

4.1.2.3 Laser delivery and Focusing

The laser beam is delivered to the laser focusing system by means of optical fiber which has the diameter equal to $50\mu\text{m}$. The optical fiber is connected directly from the laser source to the laser head, as the focusing system. The laser head used for the experiment is BIMO Laser Processing Head, a product of HIGHYAG laser technologies. This focusing head has the magnification equal to 2.0 for the collimation and 1.0 for the focusing.

The laser head, delivery schematic and the Schematic of laser head is represented in Figures 4-9, 4-10 respectively also the datasheet is shown in Table 4-5.



Figure 4-9 Bimo laser head, HIGHYAG laser technology, Laser delivery schematic

The laser beam is guided in a flexible system with matched components from the beam source to the workpiece. The individual components (from the beam launching unit at the laser via the laser light cable to the focus head at the workpiece) are matched in a manner that ensures almost loss-free beam transmission.

The features in overview:

- Corrected optical systems for avoiding aberations.
- Reproducible plug-in connections ensure that individual parts of the system can be replaced without a need for re-adjustment.
- Minimum power and beam quality losses.

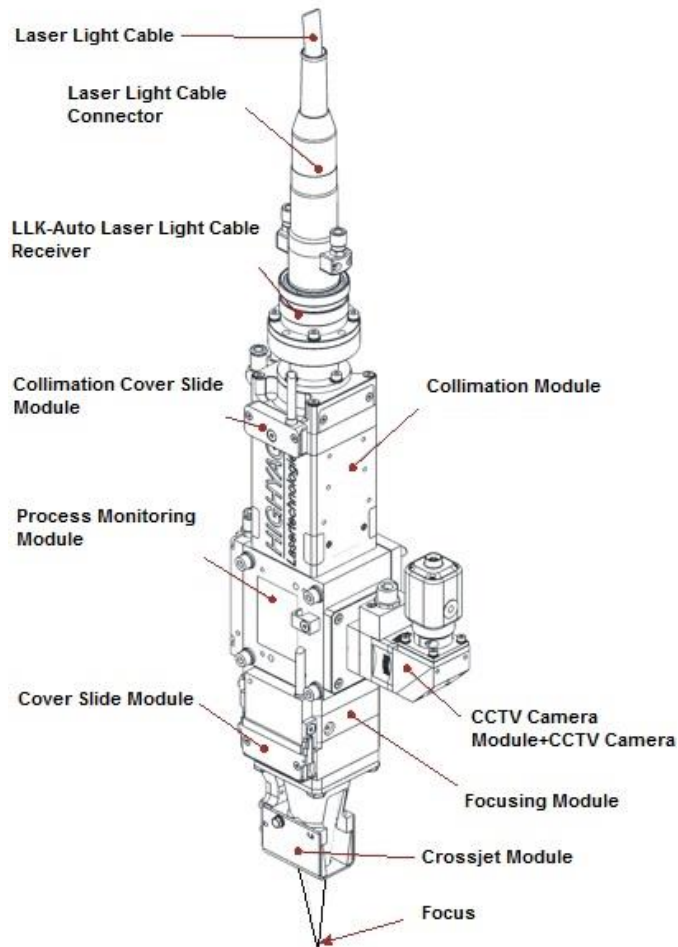


Figure 4-10 Laser head schematic

Laser Processing Head			
Collimation length	$f_c=100$ [mm]	NA=0.175	$\lambda=1025-1080$ nm
Focal length	$f_f=200$ [mm]		$\lambda=1025-1080$ nm

Table 4-5 Laser head datasheet

4.1.2.4 Assembled Laser Components

There are a lot of components join together to do any kind of laser processing, as it mentioned before main parts are laser source, laser delivery, laser head and the clamping parts. Figure 4-11 shows a full presentation of the laser components.



Figure 4-11 Laser annealing system set up

4.2 Sample preparation and analyzing instruments

First annealed samples must be prepared, they must be mounted in a resin bed, polished, and finally etched. Furthermore, to be able to investigate annealing, it is necessary to impose a minimum level of cold work to the material, which will be done using a cold rolling machine. Critical points, characteristics, and safety consideration of the mentioned equipment are going to be pointed out.

4.2.1 Rolling machine

Deformation of sheets of CP Ti1 is done through rolling process at ambient temperature. As it was discussed earlier in part I, it is desired to have smaller strain rate, so rotation speed of cylinders of roller are kept as small as possible. As a result, a more uniform material in terms of grain configuration and hardness deviation will be obtained. It also needs to be mentioned that thickness reduction is done in several steps with small increasing load. After each step, thickness is measured at different zones of strip by caliper. The deformation percentage is considered 50%. Figure 4-12 shows the mentioned rolling machine.



Figure 4-12 Cold rolling machine

4.2.2 Micrograph observation equipment

In order to examine the underlain structure of a material, the specimen needs to pass a series of preparation procedure. Primarily, it is cut using a rotating disk cutting machine. Then they are attached together by clips, and will be mounted in a resin (phenol powder) bed at specific temperature profile. In order to have

adequate adhesion, the specimen must be carefully degreased prior to mounting. (Figure 4-13)



Figure 4-13 Mounting machine

Planar grinding have done in this stage, Grinding paper is used to carry out the planar grinding. In this case it has been performed in 6 steps, on 320, 400, 600, 800, 1200 and 2500 grains size. It is compulsory to start with the paper of biggest grain size and finish with the finest one. Water should be used in all of these steps to avoid thermal residual stress. Each step took about 5 minutes. The slower rotational speed and a uniform pressing of specimen toward rotating disk will lead to a better quality of surface.

This step is done with planar polishing machine (Figure 4-14).



Figure 4-14 Planar grinding machine

Following planar grinding, polishing have performed with fine polishing machine (Figure 4-15A). It consists in 3 steps: $6\mu\text{m}$, $3\mu\text{m}$ and $1\mu\text{m}$ using diamond abrasives in aerosol on “TEXMET” cloths. “DP-Blue” is used for cooling and lubrication. Using ultrasonic polishing machine (Figure 4-15B) and air drying between each step in order to completely remove the abrasive grains is essential. The last step of polishing is to polish the samples on “TEXMET” cloths Impregnated with

Silicon (35%)+Kroll(5%)+Water(60%) composition. This composition is harmful for human body, so, having gloves is essential.



Figure 4-15 (A) Fine polishing machine, (B) Ultrasonic polishing machine

After having a polished surface it is time to etched the sample. The etchant is selected to be Kroll according to literature, which is a general-purposed etchant used for titanium and its alloys. The composition of Kroll is presented in Table 4-6.

Agent	HF	HNO ₃	H ₂ O
Amount (mL)	1.5	4	94

Table 4-6 Kroll composition as micro-etchant

A ball of cotton has soaked in kroll and gently have sweep the whole surface of sample repeatedly for 10 to 12 second. Then water washing and air drying. It is easily get burnt the titanium samples if it is exposed to Kroll even 5 seconds more than required time. In case of over etching polishing with diamond solution and silicon should be repeated. Kroll is highly harmful for human body so etching should be done under hood and with gloves.

The sample now is prepared to observe, first a macro examination have done. Macro examination is a method of examination of large regions of the specimen surface or fractured section with the naked eye or under low magnification. During the examination, any defects on the sample may be assessed, as slag, porosity or melted regions (Figure 4-16).



Figure 4-16 Macroscopic observation

Then a micro examination have done. Optical microscope has used to take photo of the favorite area Table 4-7 presents technical characteristics of exploited microscope for image acquisition (Figure 4-17).

Item	Dimension	Value
Microscope manufacturer	...	Leitz
Lenz manufacturer	...	Carl Zeiss
Range of integration time	μs	10 up to 2000
Pixel size	μm^2	2.2 x 2.2
Sensor size	mm^2	5.7 x 4.28
Digitization	bits/pixel	3 x 8
Housing (WxDxH)	mm^3	65 x 65x 63
Power supply	V , Hz	00-240 , 50/60

Table 4-7 Technical specification of microscope and its lens



Figure 4-17 Microstructure image acquisition system

4.2.3 Microhardness measurements

Hardness is the property of a material that enables it to resist plastic deformation, usually by penetration. This indenter is pressed into the surface of the sample using a specific force. Either the depth or size of the indent is measured to determinate the hardness value.

Hardness measurements are widely used for the quality control of materials because they are quick and considered to be non-destructive tests when the marks

or indentations produced by the test are in low stress areas. In this thesis work Vickers hardness test has been used.

Vickers hardness is a measure of the hardness of a material, calculated from the Size of an impression produced under load by a pyramid-shaped diamond indenter. This indenter is a square-based pyramid with an angle of 136° between opposite faces, Figure 4-18.

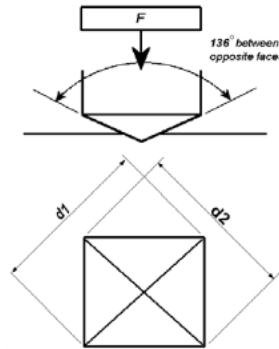


Figure 4-18 The indenter head in Vickers test

The two diagonals of the indentation left in the surface of the material after removal of the load are measured using a microscope and their average calculated. The area of the surface of the indentation is calculated. The Vickers hardness is the value obtained by dividing the kg load by the square mm area of indentation. Load time is around 5 to 30 seconds. To cover all testing requirements the Vickers test has two different force ranges, Micro (10g. to 1000g) and Macro (1kg to 100kg). Moreover, general specifications of used microhardness machine in this project is stated in Table 4-8. (Figure 4-19)

Item	Dim.	Value/Description
Manufacturer	...	Metkon
Model	...	MH3
test load range	Gr	10 - 3000
Dwell time range	Sec	5 - 99
Min. measuring unit	μm	0,1
Dimension	mm^3	190 x 430 x 520
Weigth	Kg	42

Table 4-8 Microhardness tester specification



Figure 4-19 Microhardness tester

Summary of response variables

The analyzing and temperature monitoring facilities have used in order to measure favorite response variables which are:

- 1- Hardness profiles
- 2- Micrographs
- 3- Temperature profiles

Chapter 5 Workpiece definition

The workpiece is a rectangular plate of CP Ti grade 1, the original thickness of the plate was 1.5[mm], the plates has deformed 50% to have some energy inside and result in better annealing, so the obtained thickness is 0.75[mm], Figure 5-1 is the draw of the workpiece.

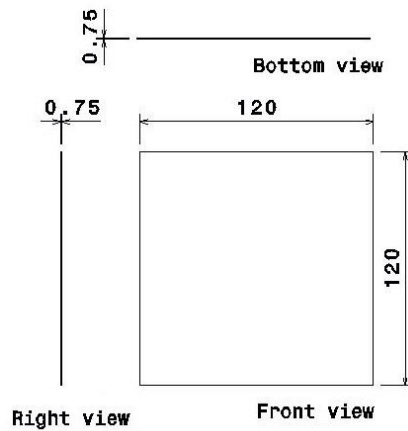


Figure 5-1 Workpiece dimensions[mm]

Chapter 6 Base Material Titanium (CP Ti1)

Titanium has recognized as an element for at least 200 years. Nowadays it is one of the most important metals in the industry. Titanium alloys are common, readily available engineered metals that compete directly with stainless and specialty steels, copper alloys, nickel based alloys and composites [52].

The element was first discovered in England by Gregor in 1790, although it did not receive its name until Klaproth named it after the mythological first sons of the earth, the Titans, in 1795 [53].

Titanium is a metal which has only achieved direct engineering usage, as distinct from some minor applications as a strengthening alloy in other metals, since the Second World War [54]. Chemically, titanium is one of the transition elements in group IV and period 4 of Mendeleef's periodic table. It has an atomic number of 22 and an atomic weight of 47.9 [55]. Figure 6-1 shows the properties of pure elemental titanium at the room temperature.

the elemental form, titanium has a high melting point (1668 8 °C) and possesses a hexagonal closely packed crystal structure (hcp) α up to a temperature of 882.5 8°C. Titanium transforms into a body centered cubic structure (bcc) β above this temperature. Titanium alloys may be classified as α , near α , $\alpha + \beta$, metastable β , or stable β depending upon the room temperature microstructure. The properties of the materials depend on the composition, relative proportions of the α and β phases, thermal treatment, and thermo-mechanical processing conditions. The β alloys also offer the unique characteristic of low elastic modulus and superior corrosion resistance [53].

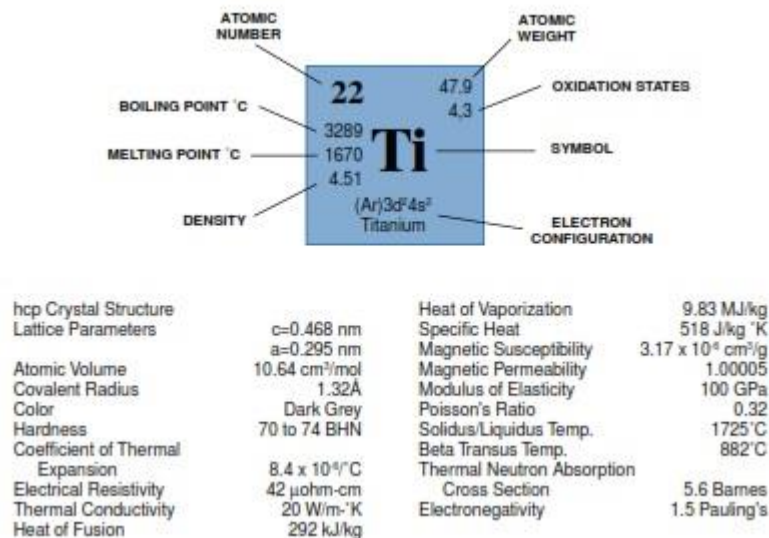


Figure 6-1 Properties of pure elemental titanium at room temperature

Titanium emerged as a “wonder” metal that makes sense as the material of choice for a wide variety of applications [56].

Today, titanium and its alloys are highly used for aerospace, industrial and consumer applications. Moreover, titanium is used in several applications such as missiles, spacecraft, chemical and petrochemical production, hydrocarbon production and processing, power generation, desalination, nuclear waste storage, pollution control, ore leaching and metal recovery, offshore, marine deep sea applications, navy ship components, armor plate applications, anodes, automotive components, food and pharmaceutical processing, recreation and sports equipment, medical implants and surgical devices as well as many other areas [52]. Titanium alloys are capable of being fabricated into all conventional mill products and into near net shapes for components using conventional metal-processing equipment. These alloys are quite strong at typical hot working temperatures so high load capacity processing equipment is required [57].

6.1 Commercially pure Titanium

Usually Titanium is classified in two main categories: commercially pure titanium (CP Ti) and titanium alloys having such additives as aluminum (Al) and vanadium (V) [58].

To clarify more, titanium alloys are classified as α , $\alpha + \beta$, and β alloys, with further subdivision into near α and metastable β alloys. This is schematically outlined in a three dimensional phase diagram, which is composed of two phases diagrams with an α and a β stabilizing element respectively. According to this scheme, the α alloys comprise CP Ti and alloys exclusively alloyed with α stabilizing and

neutral element. If minor fractions of β stabilizing elements are added, they are referred to as near α alloy. The $\alpha + \beta$ alloys is the most widely used alloy group [52].

Unalloyed Commercially Pure Titanium is represented by four distinct grades, specifically 1, 2, 3 and 4. CP Titanium is ordered in relation to the corrosion resistance, formability (ductility) and strength requirements of a specific application. As it can be seen in Table 6-1 CP Titanium ranges from grade 1, which has the highest corrosion resistance, formability and lowest strength, to grade 4, which offers the highest strength and moderate formability [59].

Alloy Composition [Common Name]	Alloy Description	Available Product Forms
Ti Grade 1	Lower strength, softest, unalloyed Ti grade with highest ductility, cold formability, impact toughness, with excellent resistance to mildly reducing to highly oxidizing media with or without chlorides and high weldability.	Ingot/Bloom, Bar, Billet, Plate, Strip, Welded Tubing, Welded Pipe, Wire
Ti Grade 2	Moderate strength unalloyed Ti with excellent weldability, cold formability, and fabricability; “workhorse” and “garden variety” Ti grade for industrial service with excellent resistance to mildly reducing to highly oxidizing media with or without chlorides. Approved for sour service use under the NACE MR-01-75 Standard.	Ingot/Bloom, Bar, Billet, Plate, Strip, Welded Tubing, Welded Pipe, Seamless Tubing, Wire, Foil
Ti Grade 3	Slightly stronger version of grade 2 titanium with similar corrosion resistance with good weldability, reasonable cold formability and ductility.	Ingot/Bloom, Bar, Billet, Plate, Strip, Welded Tubing, Welded Pipe
Ti Grade 4	Much stronger, high interstitial version of grades 2 and 3 Ti with reasonable weldability and reduced ductility and cold-formability.	Ingot/Bloom, Bar, Billet, Plate, Strip

Table 6-1 Description of commercial titanium alloys [52]

Commercially pure titanium is manufactured generally by a process comprising ingot forging or slabbing, hot rolling, annealing, pickling, cold rolling, and final annealing [60]. This thesis work is focused on CP Ti1.

General characteristics of CP Ti1 is depicted in Table 6-2.

ASTM GRADE (UNS NO.)	GRADE 1 (R50250)			
Chemical Composition	0.08C; 0.03N; 0.18O; 0.20Fe; 0.015H			
(Max. values unless range is shown)				
TENSILE PROPERTIES	Guar.R.T. Min.	Typical Elevated Temperature Properties		
		93°C	204°C	315°C
Ultimate Strength [MPa]	241	262	200	159
Yield Strength, 0.2% offset [MPa]	172	138	97	83
Elongation in 51 mm (%)	24	40	38	48
Reduction in Area - Bar, Billet & Forging only (%)	30			
Other Mechanical properties				
Charpy V-Notch Impact @ R.T. Joules	95-162			
Bend Radius	Under 1.78 mm thick	1.5* Thickness		
	1.78 mm and over	2.0* Thickness		
Welded Bend Radius	1.5_2.0* Thickness			
Nominal Hardness HRB	70			
PHYSICAL PROPERTIES				
Nominal Beta Transus °C	890			
Density g/cm ³	4.51			
Melting point .Approximation °C	1670			
Thermal conductivity W/m*°C	20.8			
Specific Heat J/Kg*°C	520			

Table 6-2 General characteristics of CP Ti1 [52]

Part 3

Single source modeling and
calibration

Chapter 7 Calibration procedure

In order to explain why calibration is needed, the role of involved uncertain parameters are described.

- Absorption coefficient (CP Ti1)
- Emissivity coefficient (CP Ti1)
- Convective coefficient

Absorption

In physics, absorption of electromagnetic radiation is the way in which the energy of a photon is taken up by matter, typically the electrons of an atom. Thus, the electromagnetic energy is transformed into internal energy of the absorber.

The value of the absorption coefficient will vary with the same effects that affect the reflectivity.

For opaque materials: $\text{Reflectivity} = 1 - \text{absorptivity}$

For transparent materials: $\text{Reflectivity} = 1 - (\text{transmissivity} + \text{absorptivity})$

In metals the radiation is predominantly absorbed by free electrons in an “electron gas”. These free electrons are free to oscillate and re-radiate without disturbing the solid atomic structure. Thus, the reflectivity of metals is very high in the waveband from the visible to the DC, for example very long wavelengths. As a wave front arrives at a surface, then all the free electrons in the surface vibrate in phase, generating an electric field 180° out of phase with the incoming beam. The sum of this field will be a beam whose angle of reflection equals the angle of incidence. This “electron gas” within the metal structure means that the radiation is unable to penetrate metals to any significant depth, only one to two atomic diameters. Metals are thus opaque and they appear shiny [61].

Absorptivity and reflectivity depend on the following features:

- Emission wavelength
- Incident angle
- Material type
- Material state (solid, liquid, gas)
- Surface roughness

In this thesis work all the above parameters are constant except the material state that sometimes there is the possibility to reach near melting which increase the absorption, Figure 7-2 depicts the importance of material state for the absorption. Two main categories can be considered:

Metallic material and non metallic materials, Figure 7-1 shows the absorption coefficient for these two groups considering different emission wavelengths

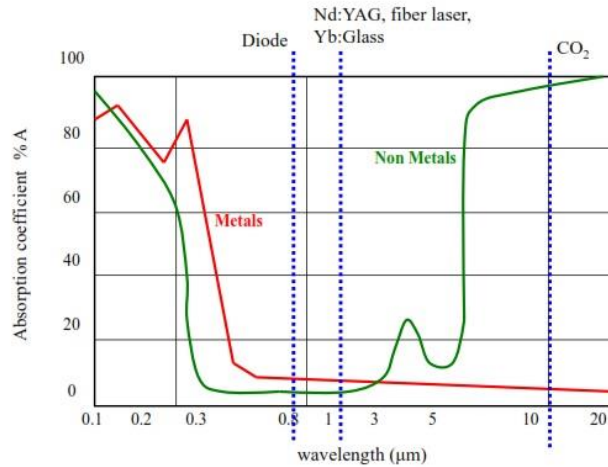


Figure 7-1 Absorption coefficient for metals and non metals for different wavelengths

Absorption does not depend on the material characteristics and wavelength while there is melting or vaporization condition, Figure 7-2 shows this concept.

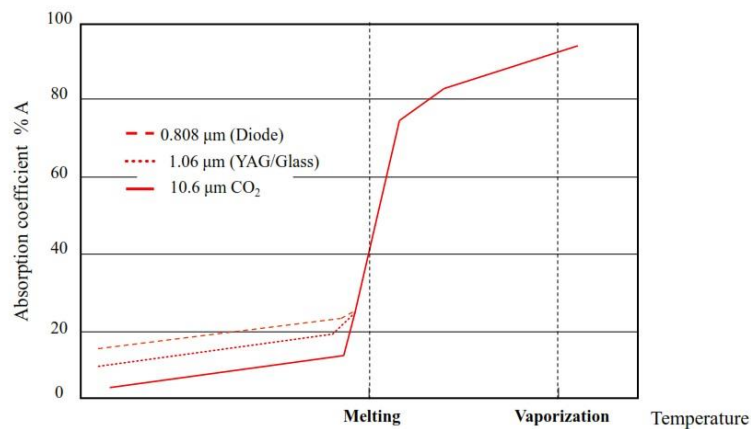


Figure 7-2 Absorption does not depend on the material characteristics and wavelength

There are not many studies about the absorption coefficient of titanium and commercially pure titanium, for the Titanium grade 1 and annealed it is about 0.44 in visible light according to [62].

Emissivity

One of the important parameters in heat transfer is emissivity. All objects at temperatures above absolute zero emit thermal radiation. However, for any particular wavelength and temperature the amount of thermal radiation emitted depends on the emissivity of the object's surface. Emissivity is defined as the ratio of the energy radiated from a material's surface to that radiated from a blackbody (a perfect emitter) at the same temperature and wavelength and under the same viewing conditions. It is a dimensionless number between 0 (for a perfect reflector) and 1 (for a perfect emitter).

Table 7-1 lists emissivity values reported for titanium and titanium alloys:

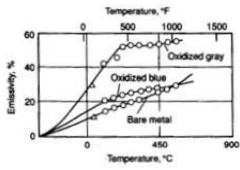
Material	Emissivity value	Condition	Reference
Pure titanium	0.63	Un oxidized; 650 nm	[63]
Titanium	0.19	polished	[64]
Titanium ASTM grade 1 annealed	0.3	Hi purity Ti at 710 °C	[62]
Titanium Alloy C110M	0.08-.19	Polished	[65]
Titanium Alloy C110M	0.51-0.61	Oxidized at 538 °C	[65]
Titanium Alloy Ti-95A	0.35-0.48	Oxidized at 538 °C	[65]
Titanium Anodized onto SS	0.96-0.82		[65]
Titanium grade 7	0.63		[66]
Unalloyed titanium		Oxidized gray, Oxidized blue, Bare metal	[67]

Table 7-1 Optical emissivity values reported for titanium and titanium alloys

The emissivity of a surface depends not only on the material but also on the nature of the surface. For example, a clean and polished metal surface will have a low emissivity, whereas a roughened and oxidized metal surface will have a high emissivity. The emissivity also depends on the temperature of the surface as well as wavelength and angle.

Knowledge of surface emissivity is important both for accurate non-contact temperature measurement and for heat transfer calculations. Radiation thermometers detect the thermal radiation emitted by a surface. They are generally calibrated using blackbody reference sources that have an emissivity as close to 1 as makes no practical difference. When viewing 'real' more reflective surfaces, with a lower emissivity, less radiation will be received by the thermometer than from a blackbody at the same temperature and so the surface will appear colder than it is unless the thermometer reading is adjusted to take into account the material surface emissivity. Unfortunately, because the emissivity of a material surface depends on many chemical and physical properties it is often difficult to estimate. It must either be measured or modified in some ways, for example by coating the surface with high emissivity black paint to provide a known emissivity value [68].

Convective coefficient

The $h_{\text{convective}}$ also can have a huge range of variation depending to the working area and the process. This parameter also is considered as a calibration parameter.

As it mentioned absorption coefficient and emissivity for the CP Ti1 are two parameters related to laser interaction with material and heat transfer that have not a fixed value reported. According to the state of art calibration is the method to deal with these uncertain parameters, so, there should be a strategy in order to apply the calibration method and find the value of emissivity, absorption and the convective coefficient which is presented in the next section.

7.1 Calibration strategy

In order to overcome the problem originated from the uncertainty of heat transfer parameters, calibration is requested.

The following strategy has been used to calibrate the model:

The laser track has designed to have linear movement over a CP Ti1 sheet (Figure7-3).

The length of laser track should be chosen in a way to assure almost steady state condition in the middle of the laser track. The laser track has designed to have 90[mm] length.

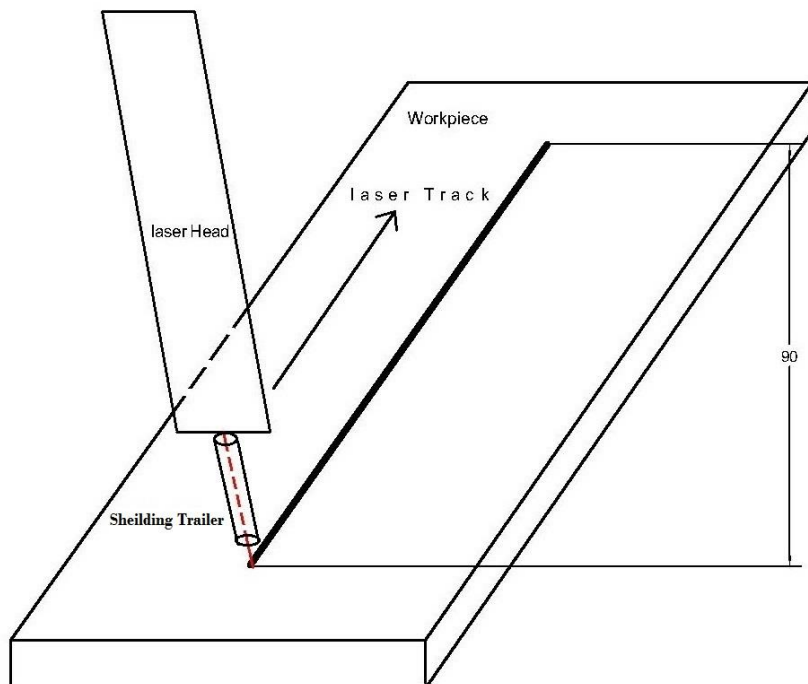


Figure 7-3 Laser track movement and laser trajectory, dimension [mm]

The strategy is that to build up a numerical model first then try to calibrate the model through calibration parameters which are the emissivity, absorption and $h_{convective}$ coefficient to fit the experimental temperature profiles measured in favorite positions (Figure7-4).

Temperature profile measurement is in the middle of the laser track, since almost steady state condition is dominating there, and temperature measurement will be done there. (Figure7-4)

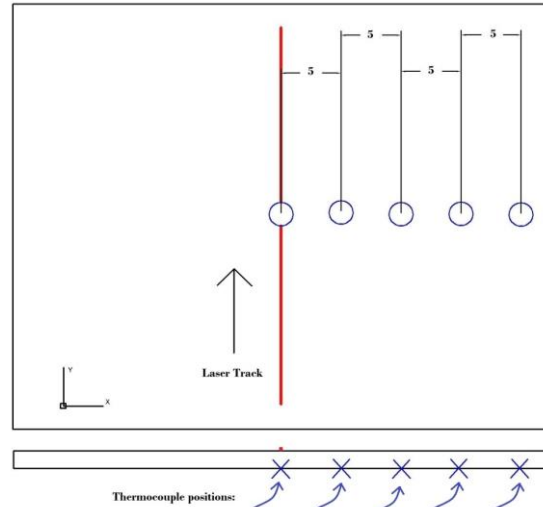


Figure 7-4 welding thermocouples in the favorite position, all dimensions in [mm]

The experimental and numerical temperature profile are compared according to flowchart presented in Figure 7-5.

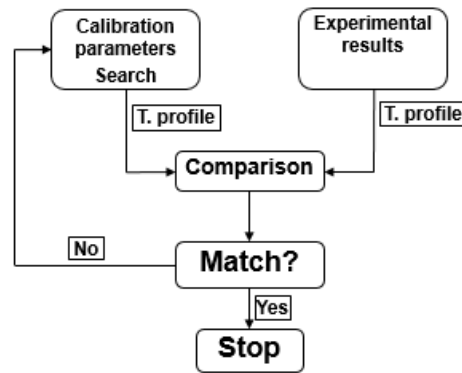


Figure 7-5 Temperature profile comparison technique

It is logical to start from the farthest experimental point, since there we have smaller temperature gradient and it is quite easier to find the right combination of calibration parameters, of course, the results will be tested for all the measured temperature profiles.

Since there are three parameters to deal with, the approach selected is to study the effect of these parameters first then different sets of calibration parameters will be considered trying to get closer and closer to find the best one. In each step all the numerical and experimental temperature profiles has compared with each other.

Chapter 8 Experimental analysis

Following the calibration strategy the experimental parts have designed and execute and finally the results have gathered.

8.1 Design of experiment

The goal of experiments is to compare and calibrate the model with the numerical modeling. The first step is to define a process parameters working with.

8.1.1 Fixed process parameters

According to the [69] a set of process parameters have selected to ensure a successful annealing of CP Ti1. Table 8-1 present the selected process parameters.

Parameters	Value
Shielding gas	Argon
Shielding gas flow	20-30 [NI/min]
Collimation length	100[mm]
Focusing length	200 [mm]
Fiber diameter	50[mm]
Defocalization	-50[mm]
Spot diameter	3.4 [mm]
Laser beam angle	10°
Density mode	Gaussian
Laser Power[P]	200[W]
Laser track speed[V]	3[mm/s]

Table 8-1 fixed and variable process parameters

The shielding gas used in the annealing of CP Ti 1 is argon which has mounted laterally, the flow rate is 20-25 NI/min (NI/min is the flow in l/min measured at some reference point but converted to standard or normal air conditions 1.01325 bar absolute, 0°C and 0% Relative Humidity) have the optimum protection. The spot diameter dimension is 3.4 [mm] on focus point. Defocalization is -50 [mm], the reason is to be able anneal larger area, while the spot is stable. The density profile have the Gaussian distribution.

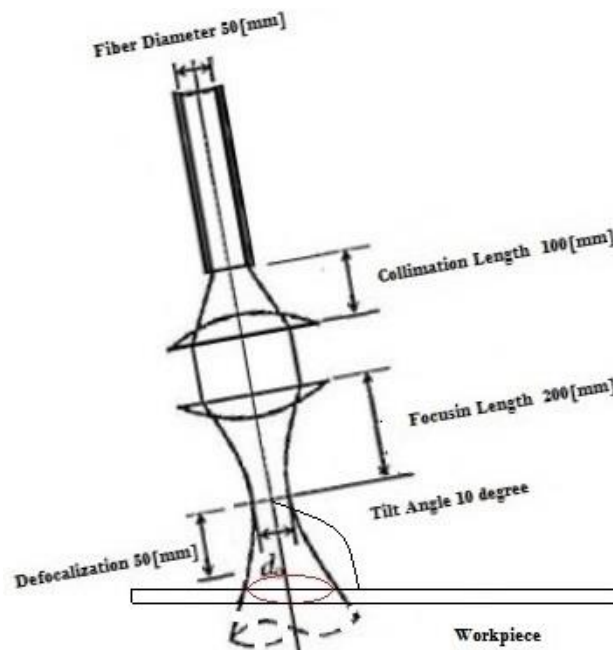


Figure 8-1 laser head and workpiece position

The laser head has tilted about 10 degrees, to prevent any kind of reflection originates from collision with the surface of the specimen. The laser reflection back to the laser head transfers from optical delivery fiber to the laser source and can cause damages to the fiber laser source. Figure 8-1 is the schematic of workpiece and the laser beam position.

8.2 Experimental execution

The experiments have done with the instruments described in section 4 and according to the process parameters which ensures a successful annealing described in section 8.1.1.

Here is the detailed sequence of the execution steps:

- Preparing the sample:
 1. Rolling plates for 50% deformation
 2. Cutting deformed plates into defined dimension
 3. Cleaning the workpieces

- Laser annealing the workpieces:
 1. Welding the Thermocouples
 2. Connecting Thermocouples
 3. Clamping the part
 4. Setting up the robotic arm
 5. Setting up the laser head
 6. Setting up the shielding trailer
 7. Defining the laser pass with controller
 8. Opening shielding gas valve
 9. Test Run
 10. Collecting data

The total number of 12 experiments and temperature profile measurements for each specific distance from the centerline have performed. Two subsequent experiments have done with the same thermocouples.

8.3 Experimental Results

This section is dedicated to all measured temperature profiles gathered experimentally.

8.3.1 Temperature Profiles

As it mention in section 8.2 two subsequent experiments have done with same thermocouples. During these experiments some thermocouples either failed or had problem (see Table 8-2).

This is due to the fact that capacitive welding of thermocouples are affect by a numerous parameters:

- Dust presence: it attenuates bonding among thermocouple and sample;
- Oxide presence in the sample: it attenuates bonding among thermocouple and sample;
- Thermocouple joint dimension and purity: it is difficult to control it using the power weld consequently contact surface area changes;
- Clamps position;
- Welding point;

Furthermore, the difficulty to place the thermocouples in exact distance specially for the further ones and the high temperature gradient during the annealing increase the chance of thermocouples failures. Failure have happened in the second usage of thermocouples more, also the results shows more instability, so the temperature profiles recorded with the second thermocouple usage are not considered.

Distance from the centerline[mm]	No. of total designed measurement tests	No. of successful first usage of thermocouple	No. of successful second usage of thermocouple
0	12	6	4
5	12	8	6
10	12	4	3
15	12	4	3
20	12	2	2

Table 8-2 Temperature profile measurement test design

Figures 8-2, 8-3, 8-4, 8-5, 8-6 depict the temperature profile for the distances 0, 5, 10, 15, 20 [mm] far from laser track respectively:

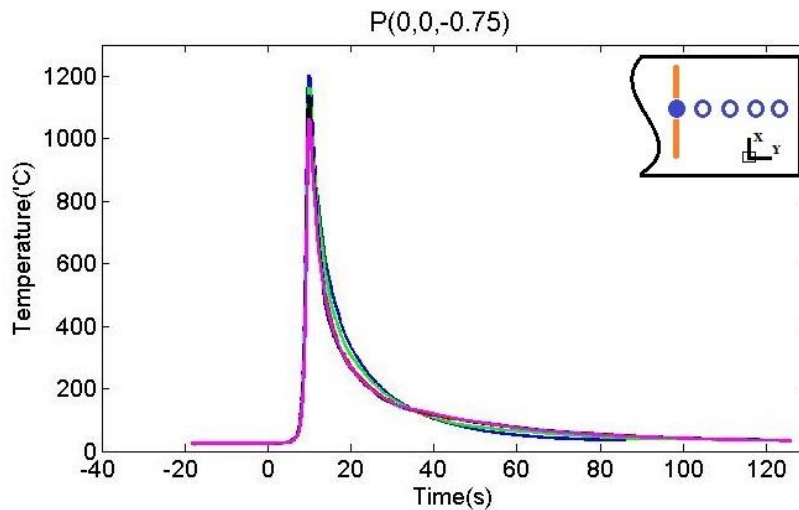


Figure 8-2 Experimental Temperature profile at the centerline related to laser pass

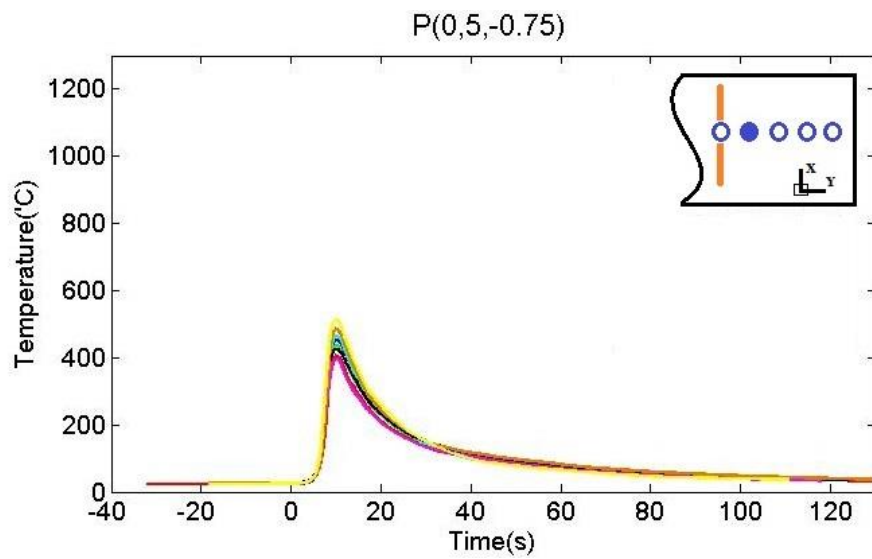


Figure 8-3 Experimental temperature profile at distance 5[mm] from the centerline

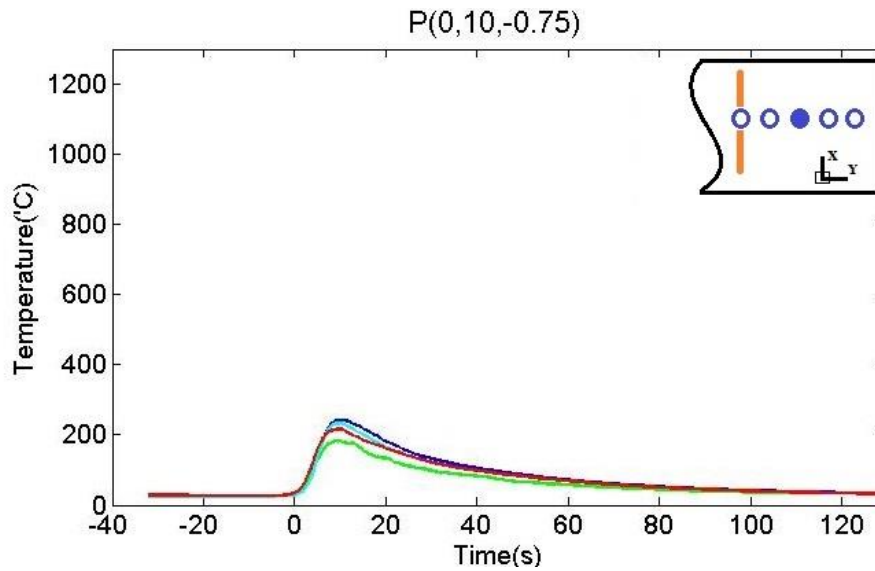


Figure 8-4 Experimental temperature profile at distance 10 [mm] from the centerline

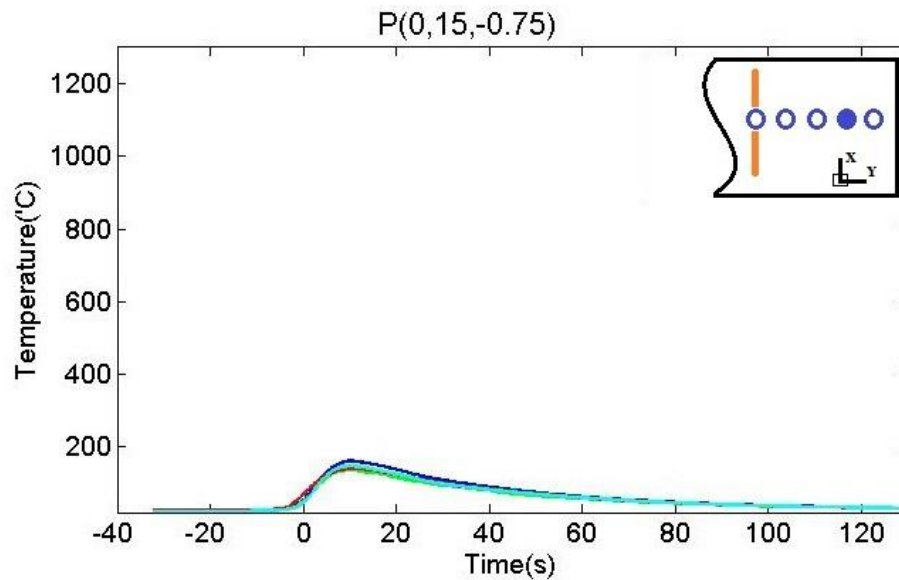


Figure 8-5 Experimental temperature profile at distance 15 [mm] from the centerline

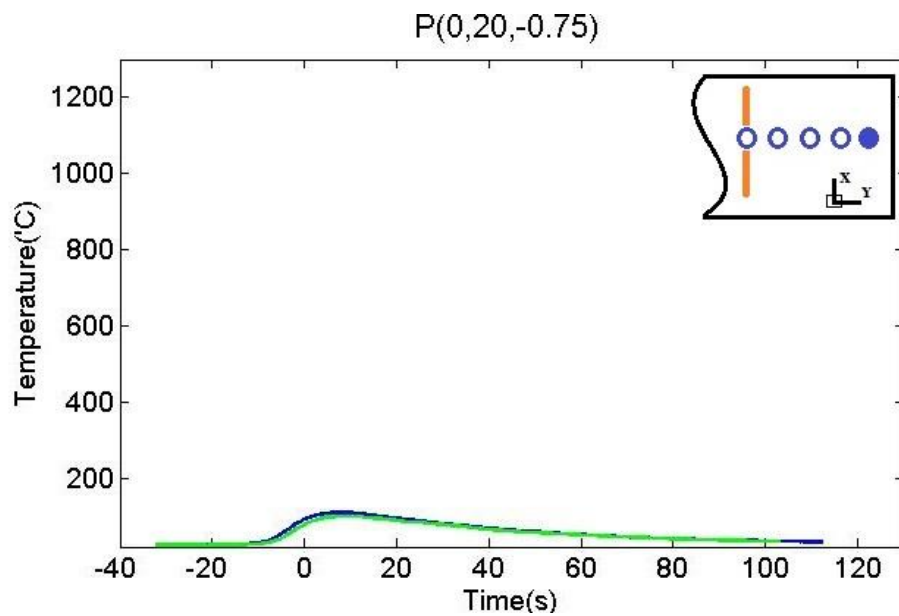


Figure 8-6 Experimental temperature profile at distance 20[mm] from the centerline

Since a comparison between experimental and numerical temperature profiles is needed to calibrate the model the average of successful experimental temperature profile are calculated and presented in Figures 8-7, 8-8, 8-9, 8-10, 8-11.

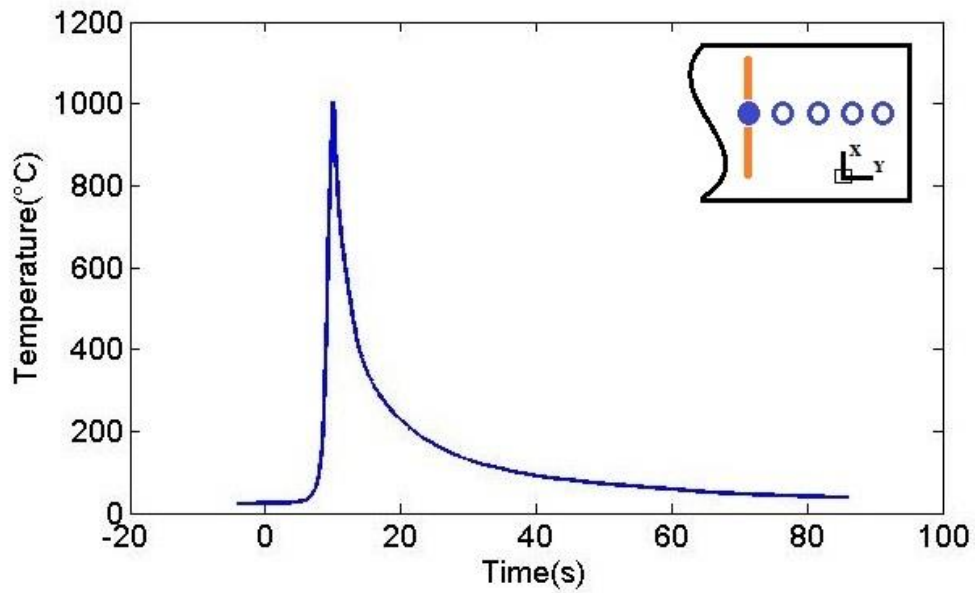


Figure 8-7 Average of experimental temperature profiles at centerline

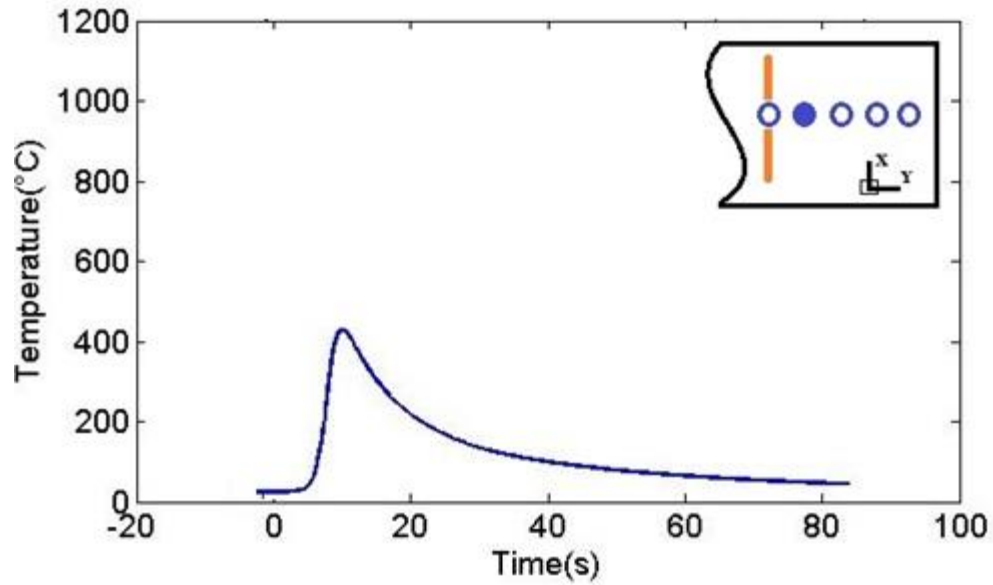


Figure 8-8 Average of experimental temperature profiles at distance 5[mm] from the centerline

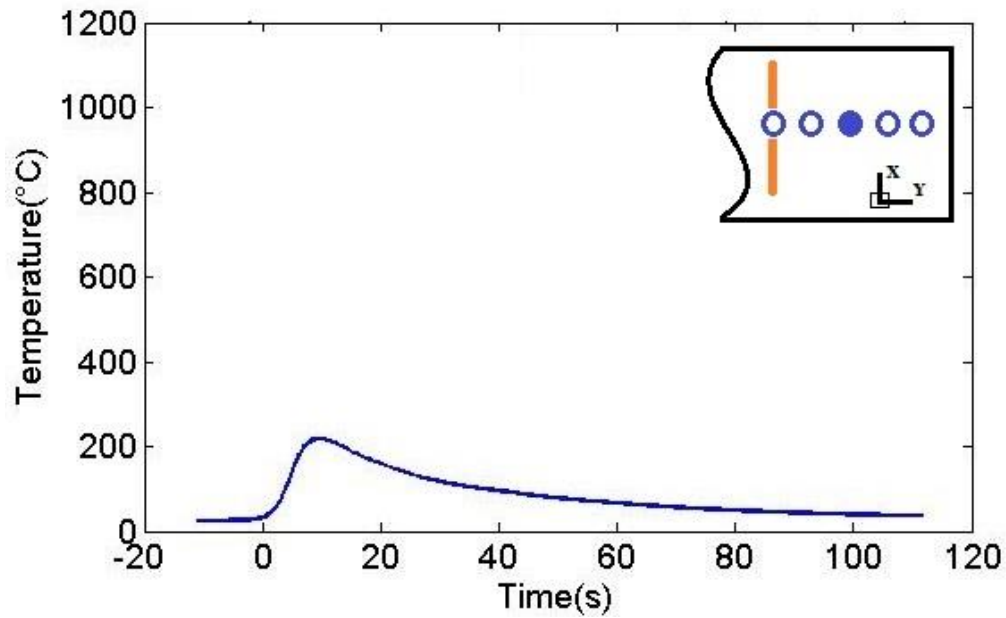


Figure 8-9 Average of experimental temperature profiles at distance 10[mm] from the centerline

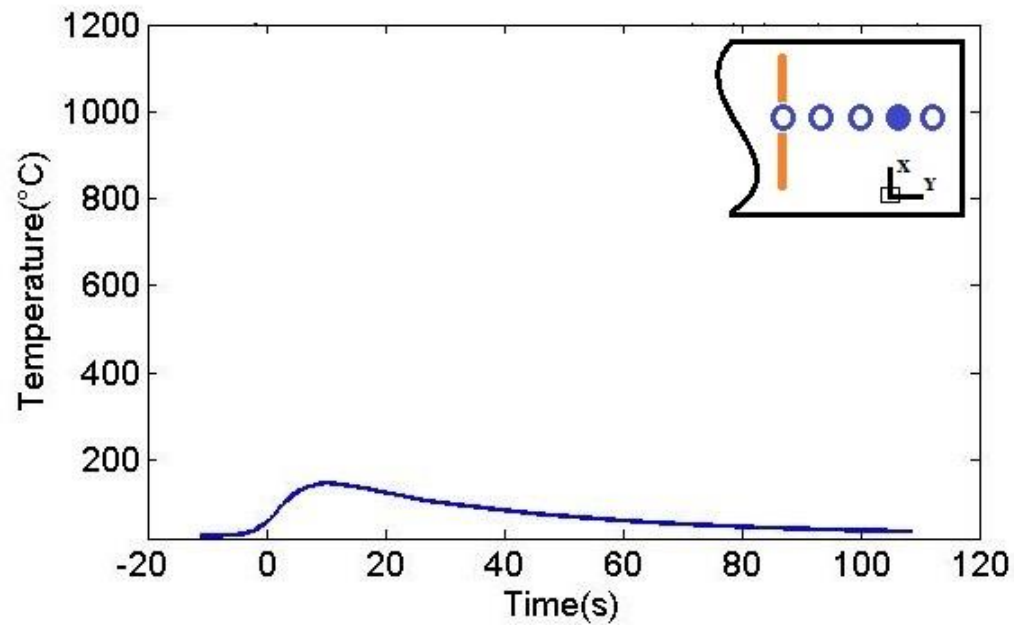


Figure 8-10 Average of experimental temperature profiles at distance 15[mm] from the centerline

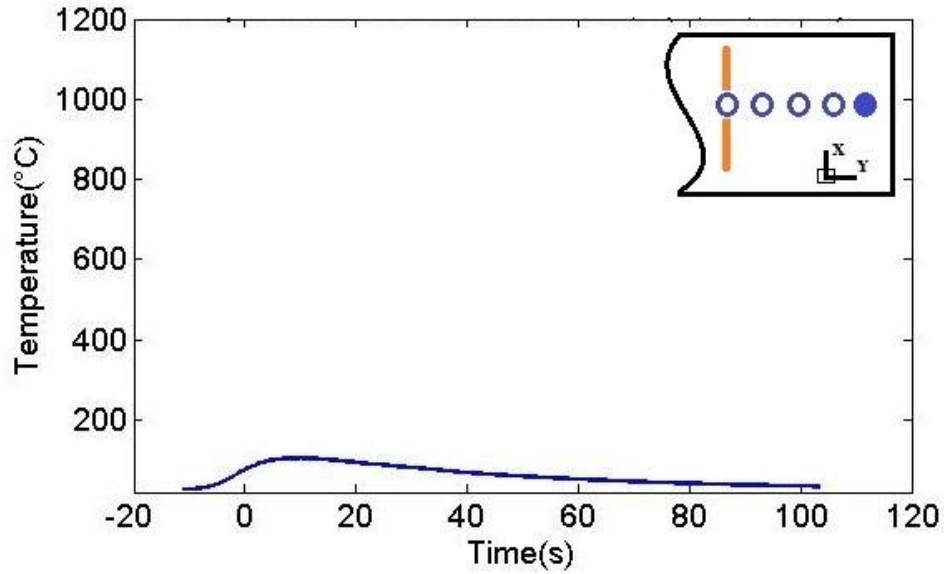


Figure 8-11 Average of experimental temperature profiles at distance 20[mm] from the centerline

Maximum temperature is a vital characteristic that can affect the tribological characteristics of material a lot. Figure 8-12 shows a peak of temperature for any specific distance from laser pass.

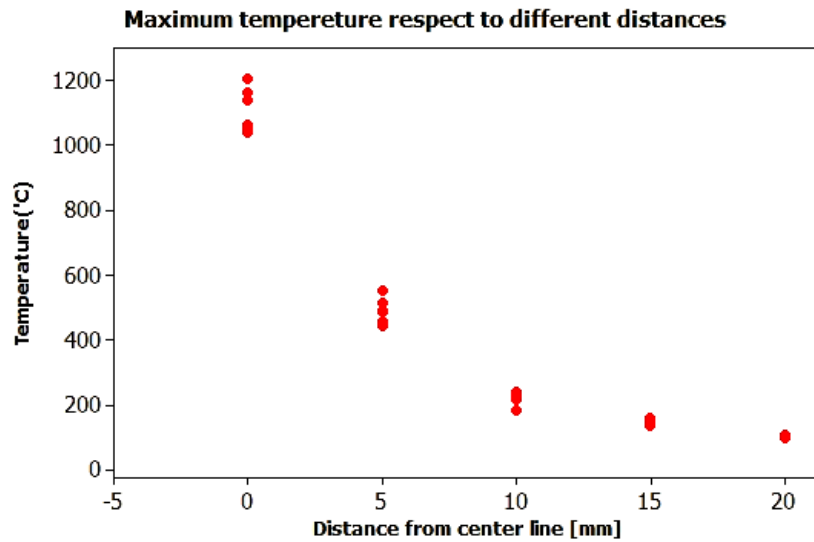


Figure 8-12 Maximum temperature respect to different distances from centerline

The difficulty in welding the thermocouples exactly in their positions leads to have some errors. The errors are not important for the areas far from the centerline but they are very important for the areas at or near the centerline. The temperature gradient at or near the centerline are so high and a small error in thermocouple location can lead to have a great different in maximum temperature. It can be seen in Figure 8-12 that the variation of maximum temperature is higher when the measurement is nearer to the centerline, so, attention must be pay for identification of the maximum temperature at the centerline.

Chapter 9 Numerical analysis

Engineering analysis of mechanical systems have been addressed by deriving differential equations relating the variables of through basic physical principles such as equilibrium, conservation of energy, conservation of mass, the laws of thermodynamics, Maxwell's equations and Newton's laws of motion. However, once formulated, solving the resulting mathematical models is often impossible, especially when the resulting models are nonlinear partial differential equations. Only very simple problems of regular geometry such as a rectangular of a circle with the simplest boundary conditions were tractable.

The finite element method (FEM) is the dominant discretization technique in structural mechanics. The basic concept in the physical interpretation of the FEM is the subdivision of the mathematical model into disjoint (non-overlapping) components of simple geometry called finite elements or elements for short. The response of each element is expressed in terms of a finite number of degrees of freedom characterized as the value of an unknown function, or functions, at a set of nodal points.

This approach has a great flexibility to model complex geometries, can handle general boundary conditions, variable material properties can be handled, clear structure and versatility helps to construct general purpose software for applications, Has a solid theoretical foundation which gives added reliability and makes it possible to mathematically analyze and estimate the error in the approximate solution.

As it previously mentioned (section 3), COMSOL multi-physics has used in order to model the physical parameters, this program is a finite element evaluator and solver for various physics and engineering applications, especially coupled phenomenon, or multi-physics.

COMSOL multi-physics also offers an extensive interface to MATLAB and its toolboxes for a large variety of programming, preprocessing and post-processing possibilities.

9.1 Preprocessing

Several physical parameters should fulfill in order to build up the model and use the merits of FEM:

1. Geometry
2. Mesh
3. Materials
4. Heat Source
5. Boundary conditions

9.1.1 Geometry

The geometry is the simple plate, the dimensions are explained in chapter 5. Figure 9-1 depicts the built geometry in COMSOL multi-physics.

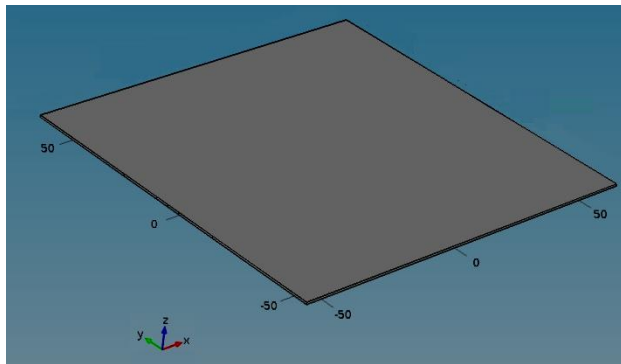


Figure 9-1 Modeled geometry of the workpiece

9.1.2 Material

Being laser annealing a thermal process, it is possible to say that variations of these elements causes a variation of the thermal field and consequently material properties identification is a fundamental issue.

As it mentioned before CP Ti1 is the material used in this thesis work. Thermo-physical properties of the material are temperature dependent. Thermal conductivity(K), specific heat capacity at constant pressure are presented in Figures 9-2, 9-3 and the density(ρ) does not change a lot with temperature variation (it is about $4400[Kg/m^3]$).

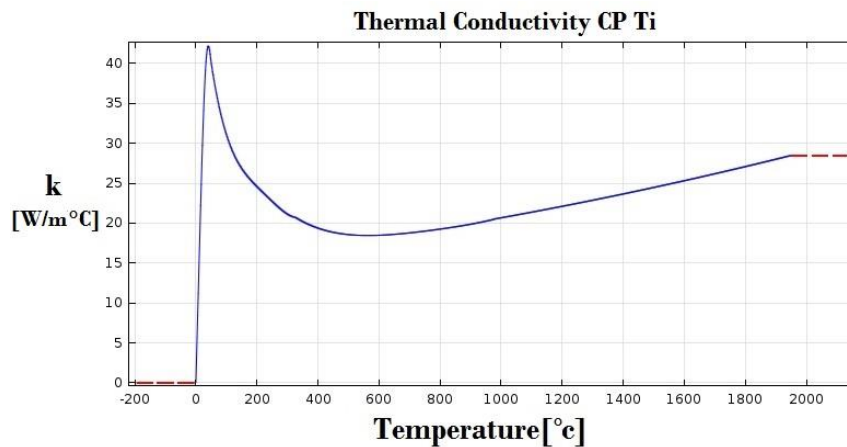


Figure 9-2 Thermal Conductivity CP Ti1

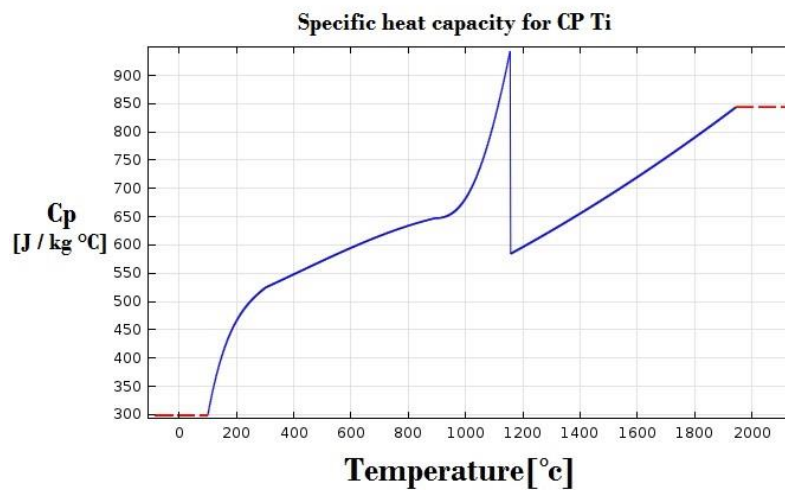


Figure 9-3 Specific heat capacity CP Ti1

9.1.3 Heat Source

To model the heat source two MATLAB codes have done, one of them to model the movement of the heat source and the other is to model the heat source distribution which is a gaussian one. Later these codes have used in COMSOL multi-physics which is compatible with MATLAB.

Here are the steps to model the heat source:

- Heat source Movement
- Heat source parameter definition
- Link the heat source movement and the its parameter to eachother

Heat source movement:

A MATLAB file has approached with three output, first the motion in X direction and the motion in Y direction and last a function that make the heat source equal to zero, all of these elements are function of time (Appendix A).

Heat source parameter definition:

A MATLAB code has approached to model the shape beam, the beam delivery is fiber and the intensity distribution is the Gaussian one.

For the typical delivery system the divergence angle is calculated like below (Figure 9-4) :

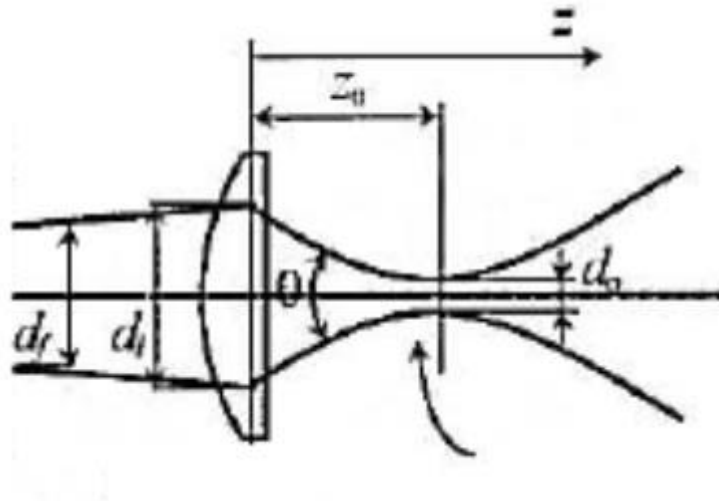


Figure 9-4 Delivery source

With the assumption of $\sin(\theta) = \theta$;

$$d^2 = d_0^2 + (z - z_0)^2 \theta^2$$

and the divergence angle is

$$\theta = 2 \tan^{-1} \left(\frac{1}{2} \frac{dl}{z_0} \right)$$

Where dl is the laser beam diameter on the mean plain of the focusing lens. Under the hypothesis of small angles of the laser beam in exit of the laser source:

$$dl = df$$

after the approximation: $z_0 = f$,

$$\theta = 2 \tan^{-1} \left(\frac{1}{2} \frac{d_l}{z_0} \right) = \frac{d_f}{f}$$

For a beam, limited in diffraction:

$$d_0 \theta = k \lambda$$

where the k is a beam quality (for Gaussian distribution $k=1$), and λ is the wavelength.

For the delivery with fiber (Figure 9-5):

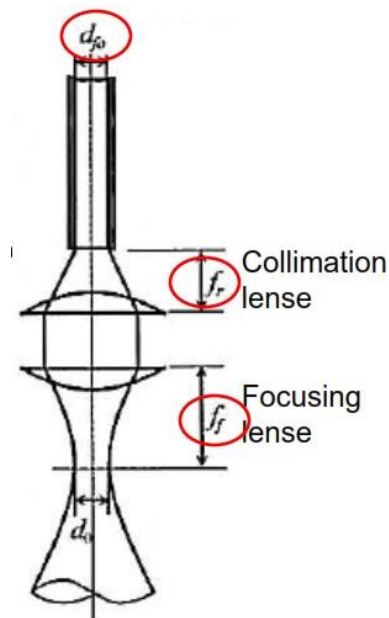


Figure 9-5 Fiber delivery

$$d_0 = \frac{F_f}{f_r} d_f$$

In order to calculate the intensity we know that power density is only a medium value evaluated on the whole section on the laser beam. However the power density distribution change in each point of the section.

The distribution of the power density is strictly affected by the geometry and the dimension of the resonator. According to the mirrors geometry is possible to obtain a distribution that is highly focused in the middle instead of quite uniform.

A distribution that is vary important in lasers is the Gaussian distribution (see figure 9-6) where the power density distribution is defined by the equation:

$$I(r, \theta) = I_0 e^{-\left(\frac{r}{r_0}\right)^2}$$

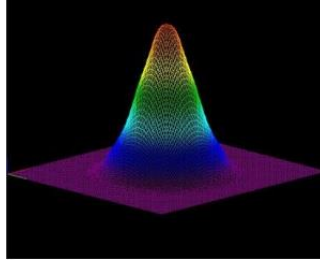


Figure 9-6 Gaussian distribution

Where I_0 is the power density on the beam axis and r_0 is a distribution parameter correlated to the beam radius.

Power density distribution changes in a continuous way inside the beam section and it's difficult to define a diameter. The standard UNI EN ISO 11146 define an equation to evaluate the diameter of a laser beam:

$$d = \sqrt{2} \sigma$$

where σ is the second moment of power density distribution function defined by the equation:

$$\sigma^2 = \frac{\int_0^{+\infty} \int_0^{2\pi} r^2 I(r, \theta) r dr d\theta}{\int_0^{+\infty} \int_0^{2\pi} I(r, \theta) r dr d\theta}$$

This works in case of circular spot geometries, in case of Gaussian distribution σ is equal to:

$$\sigma^2 = \frac{\pi r_0^4 I_0}{(\pi r_0^2 I_0)} = r_0^2$$

So, $r_0 = \frac{d}{2\sqrt{2}}$;

Finally, the equation to define a heat source is presented below:

$$I \left[\frac{W}{m^2} \right] = I_0 A e^{-\left[\frac{r}{r_0}\right]^2}$$

Where:

I_0 : intensity on the beam axis [W/m^2]

r_0 : distribution parameter correlated to the beam radius

r : radius of spot

A : The absorption coefficient of CP Ti1

Figure 9-7 shows the heat source and its movement and the density profile

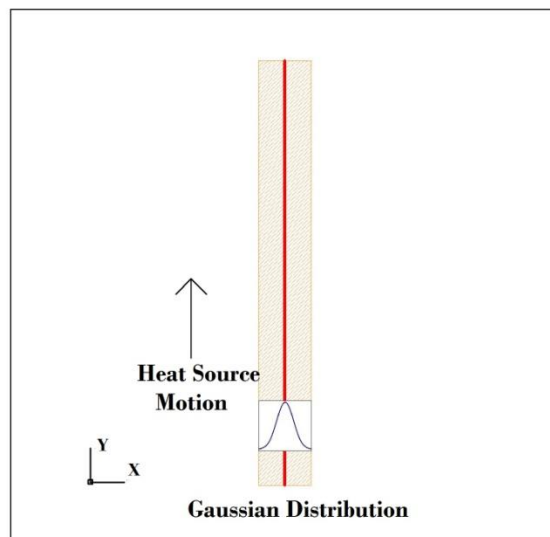


Figure 9-7 Heat Source and Gaussian distribution

The detailed MATLAB code for the calculation of the laser source generation is presented in Appendix B.

9.1.4 Boundary condition:

The model should have a good perception of what is happen in reality, following this the boundary conditions can described as:

- Convection;
- Radiation;
- Initial condition;

Convection:

There are two convection parts, natural one and forced convection which originated from the shielding gas stream.

Constant Natural convection in air is assumed with a coefficient called $h_{convective}$ [$\frac{W}{m^2K}$], for all the surfaces.

Instead of the forced convection part, an extra external natural convection has assumed for the upper surface and the lower surface separately which has proposed by COMSOL multi-physics. Figure 9-8, 9-9 shows the convection applied to the model.

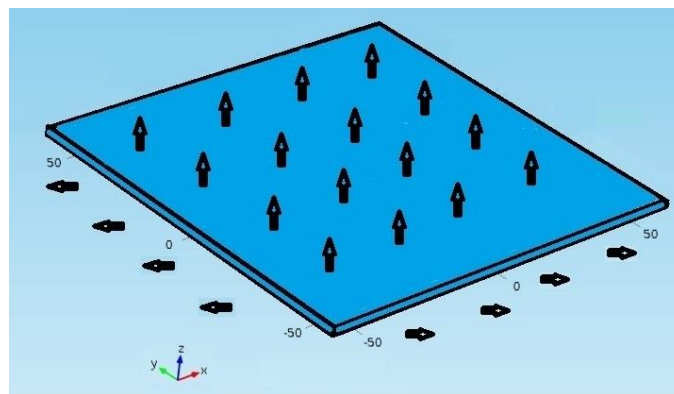


Figure 9-8 Constant natural convection for all the surfaces

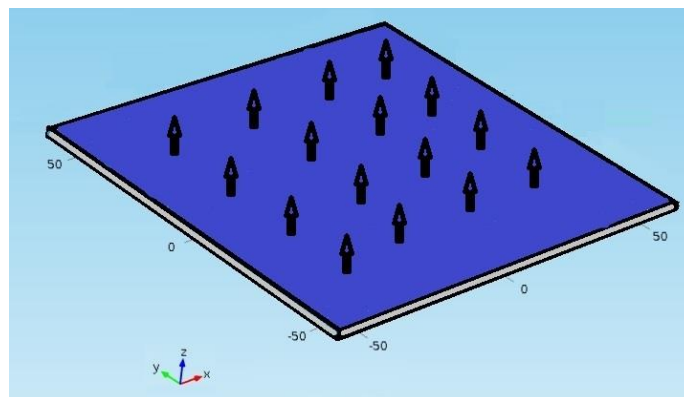


Figure 9-9 External upside and downside natural convection

Radiation:

Heat transfer through radiation takes place in form of electromagnetic waves mainly in the infrared region. Radiation emitted by a body is a consequence of thermal agitation of its composing molecules. Radiation problem depends of the fourth power of the temperature.

Figure 9-10 shows the radiation applied for all surfaces.

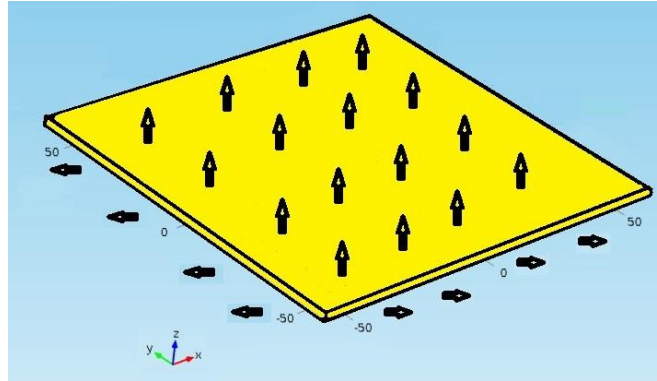


Figure 9-10 radiation for all surfaces

Here the heat loss through the radiation is the center of attention, so while a hot object is radiating energy to its cooler surroundings the net radiation heat loss rate can be expressed as:

$$q = \varepsilon\sigma(T_h + T_c)(T_h^2 + T_c^2)$$

Where:

q : net radiation heat loss rate $[\frac{W}{m^2K}]$

ε : radioactive property of surface called emissivity

σ : Stefan-Boltzmann constant $[\frac{W}{m^2K^4}] (5.67e^{-8})$

T_h : hot body absolute temperature [k]

T_c : cold surroundings absolute temperature[k]

The temperature for the initial condition is considered a room temperature which is 293.25 K .

9.1.5 Mesh

The mesh should be independent in all the three directions related to thickness, width, length and also independent with respect to time increment. In this way the quality of mesh is acceptable and the model is trustable.

The approach have chosen to achieve this favor is to have a fine and proportional mesh at critical areas with higher temperature gradient which are at the centerline and less preciseness for farther distances. Whole part have split into different smaller parts. Figure 9-11 shows the mesh control for different split dimensions over the whole part.

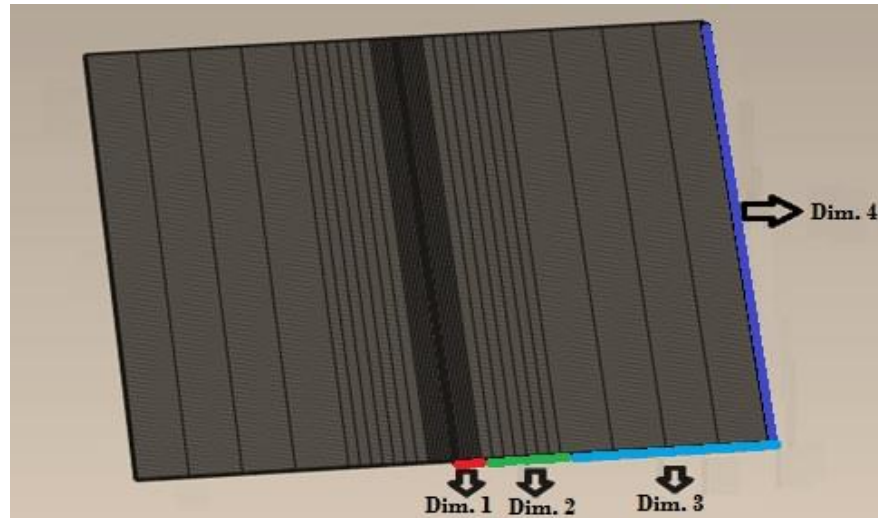


Figure 9-11 Mesh preciseness decision to have a independent mesh

Six different mesh preciseness have considered for selected dimensions and the most appropriate one has considered respect to the time and software limitations. The temporal mesh has considered 0.1[s] which is almost equal to experimental one to prevent any possible aliasing phenomenon.

It is important to notice in this step random values for $h_{\text{convective}}$ and emissivity and absorption coefficient has considered and the model have not calibrated yet. Figures 9-12, 9-13 depicts the study duration and maximum temperature at the centerline respect to the number of elements considered.

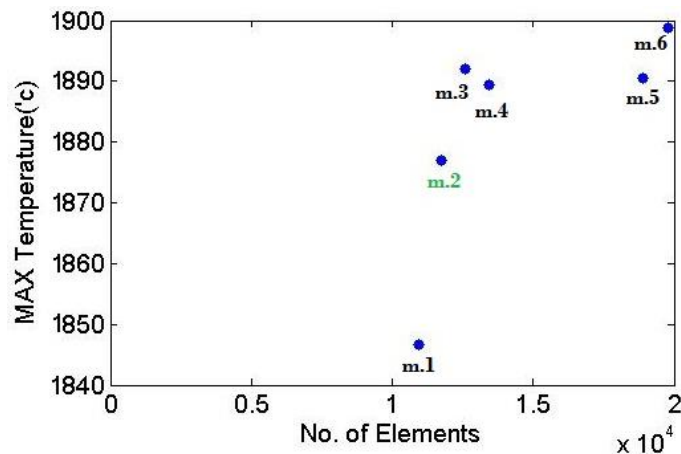


Figure 9-12 maximum temperature at centerline and no. of element for each mesh decision

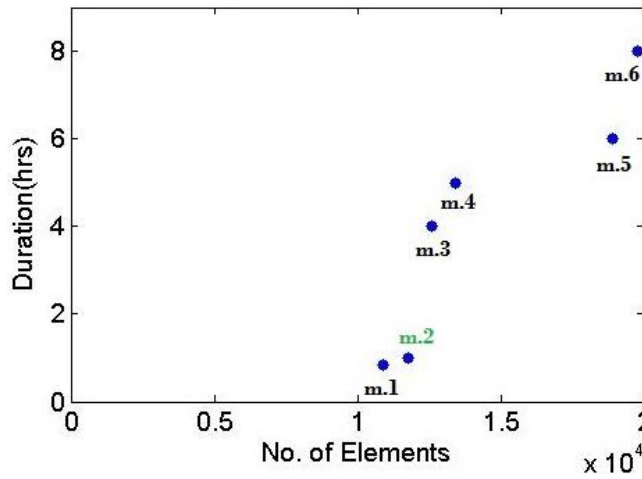


Figure 9-13 duration of simulation and no. of element for each mesh decision

Mesh Number 2 have selected due to having a good indication of maximum temperature in the most critical area respect to time consumption. Table 9-1 shows the detailed information for the selected mesh.

Selected mesh	Dim.1	Dim.2	Dim.3	Dim.4	Thickness	No. of elements	No. of nodes
No.6	10	7	4	140	2	11760	23496

Table 9-1 Number of divisions, elements and nodes for the selected mesh

Figure 9-14 shows the mesh for all the parts specially the centerline which has a the most criticality.

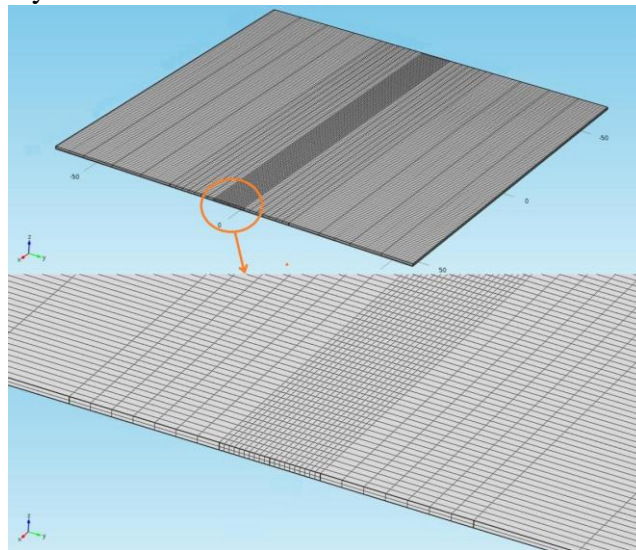


Figure 9-14 Part mesh

9.2 Processing

In this phase, after equations filling out, thermal field description is solved numerically.

Summary of all the salient features that characterize model are reported in Table 9.2.

Parameters	
Node number	23496
Element number	11760
Simulation time[min]	43

Table 9-2 Processing parameters

These parameters are appropriately lead to temperature convergence, and the time consumption for each simulation is acceptable while the number of elements are enough to describe the problem correctly.

9.3 Post Processing:

The model have built and it is not calibrated yet. According to calibration strategy the preliminary step is to understand the effects of calibration parameters.

9.3.1 Calibration parameters effect

A logical guess in order to apply values for the calibration parameters is the start of investigation. The guess has considered according to the typical values reported in literature for calibration parameters .Table 9-3

Calibration Parameter	Range
1-Emissivity	0-1
2-Absorption	0-1
3- $h_{convective}$	0-30 [$\frac{W}{m^2K}$]

Table 9-3 Calibration parameter range

Figures 9-15, 9-16, 9-17 depicts the effect of each process parameter for the farthest distance from centerline.

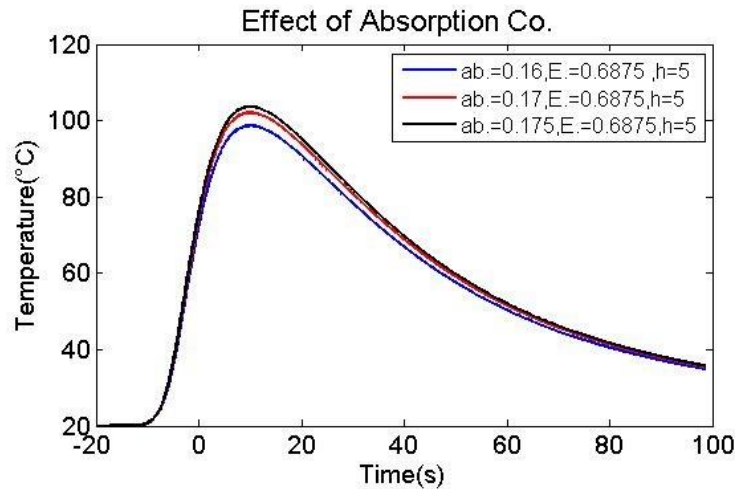


Figure 9-15 Effect of absorption coefficient

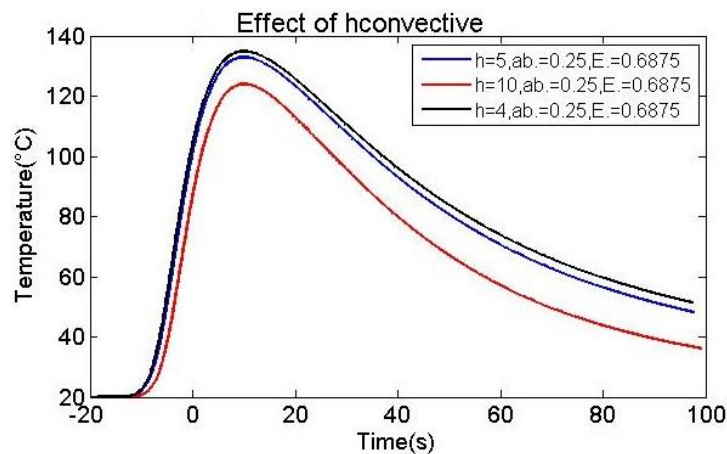
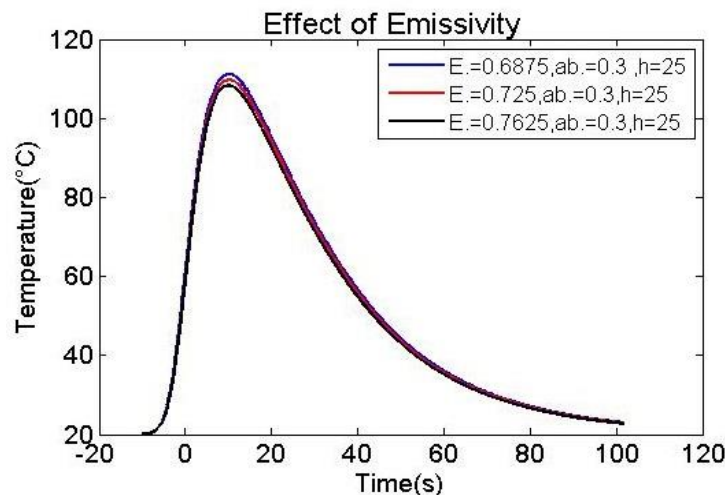
Figure 9-16 Effect of $h_{convective}$ 

Figure 9-17 Effect of emissivity

As it seen from the graphs, the effect of parameters have explained briefly:

- Absorption coefficient has a high effect on the maximum temperature but the effect on the cooling area is not so much, the absorption coefficient does not change the trend of Temperature profile so much.
- The $h_{convective}$ has a low effect on maximum temperature and a considerable effect on cooling area, while this coefficient has a high effect on the trend of temperature profile.
- The emissivity coefficient has a slight effect on maximum temperature and the cooling area, it does not change the trend of temperature profile so much.

Chapter 10 Comparison

Considering the effects, rough estimation of calibration parameters have guessed, then a more precise search around the rough selected calibration parameters is investigated. The way to get close to the parameters is to consider a range of parameter investigation and then make this range smaller and smaller by comparing the temperature profiles and calibration parameters effects to obtain an acceptable process parameters (Figure 10-1).

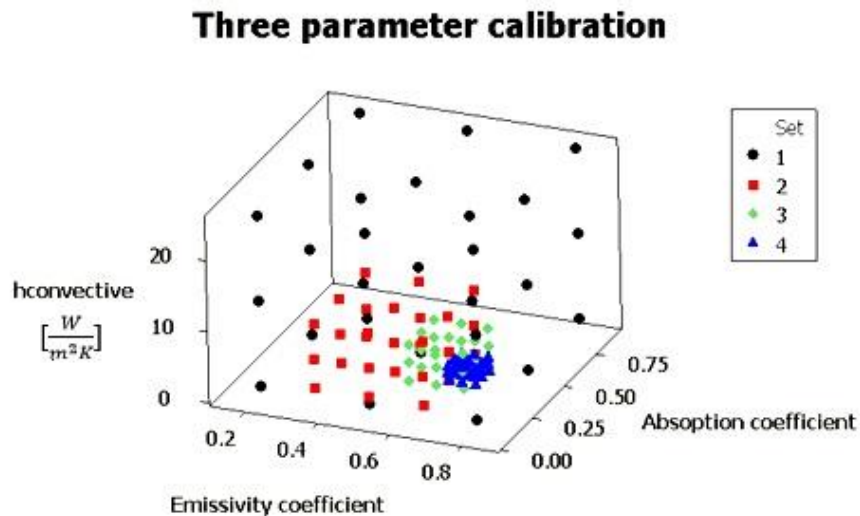


Figure 10-1 getting close to the correct parameters

10.1 Experimental average and numerical comparison

Comparison of the temperature profiles for all combination of calibration parameters with the average experimental temperature profiles for each special distance from the centerline, results in proposing the calibration parameters.

Table 10-1 presents the proposed calibration parameters.

Calibration Parameters	Calibrated value
1-Emissivity	0.6875
2-Absorption	0.295
3- $h_{convective}$	$5[\frac{W}{m^2K}]$

Table 10-1 process parameters

Figures 10-2, 10-3, 10-4, 10-5, 10-6 show the comparison of calibrated temperature profiles with the average experimental temperature profiles in each special distance from the centerline for the selected parameters.

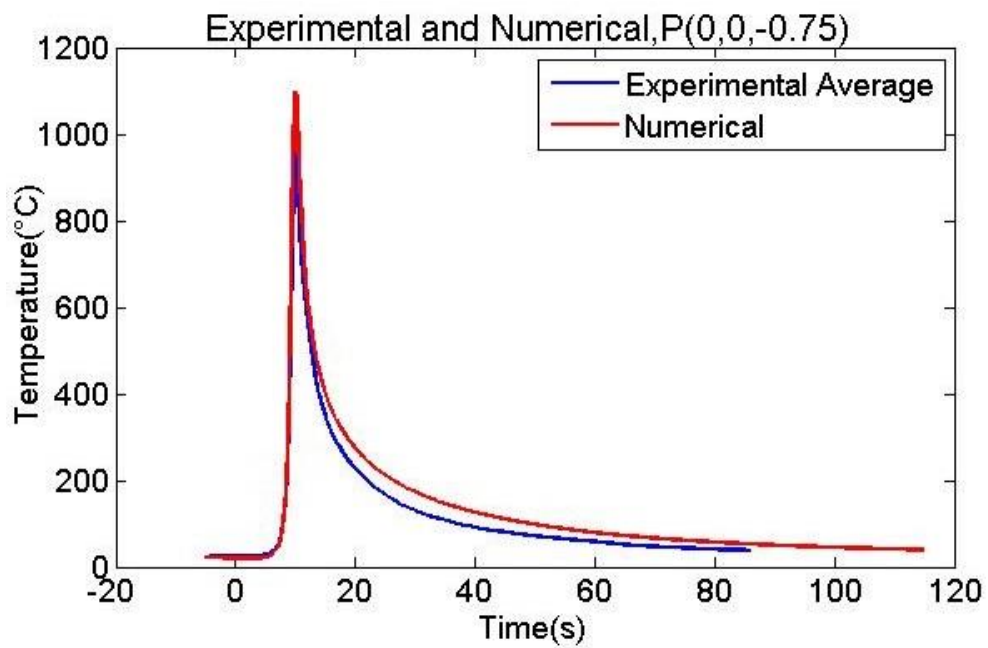


Figure 10-2 Experimental and numerical comparison at centerline

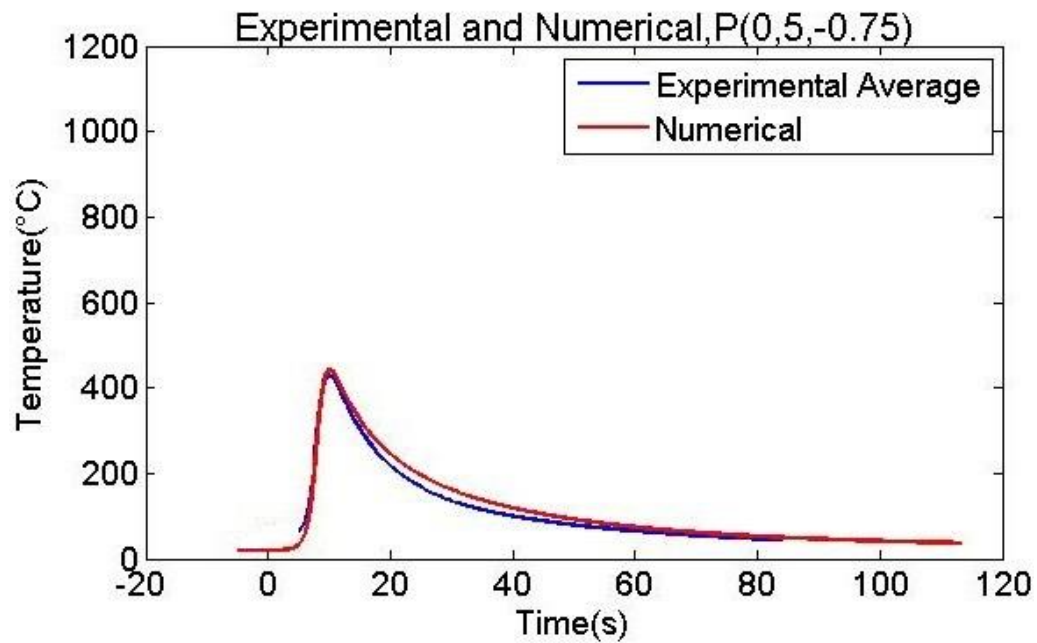


Figure 10-3 Experimental and numerical comparison at 5[mm] far from centerline

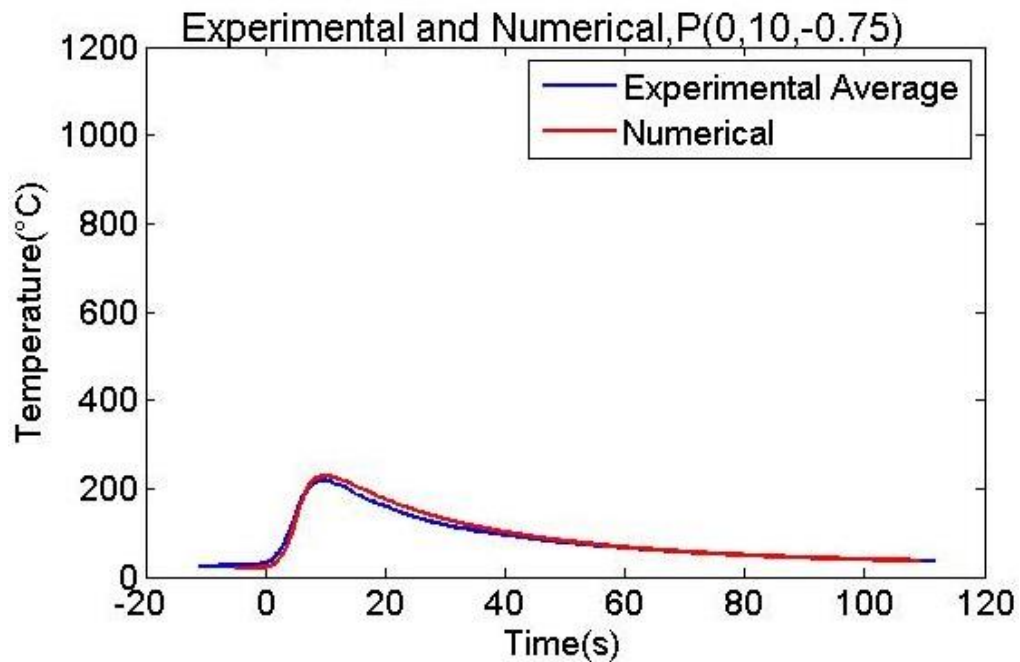


Figure 10-4 Experimental and numerical comparison at 10[mm] far from centerline

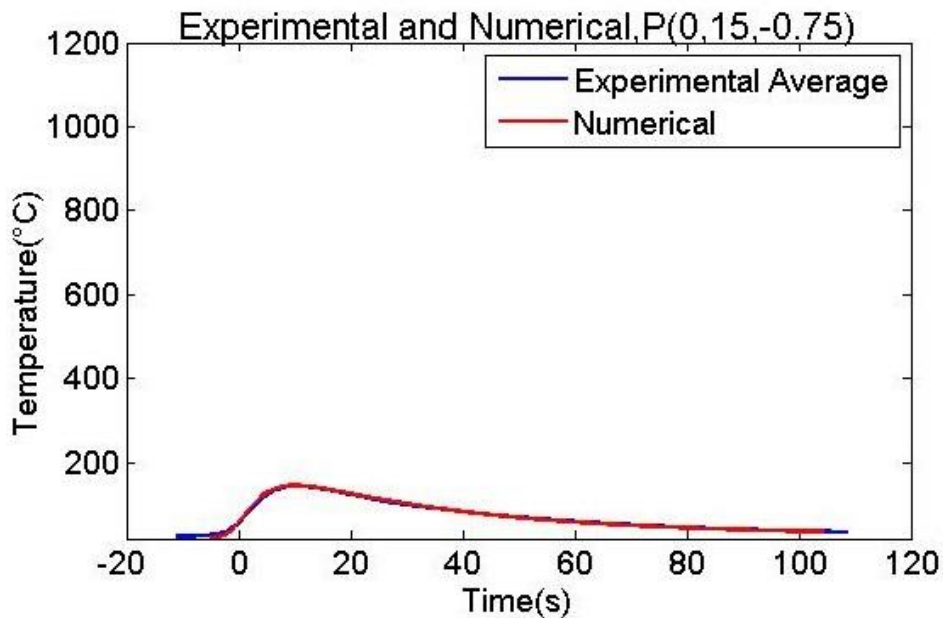


Figure 10-5 Experimental and numerical comparison at 15[mm] far from centerline

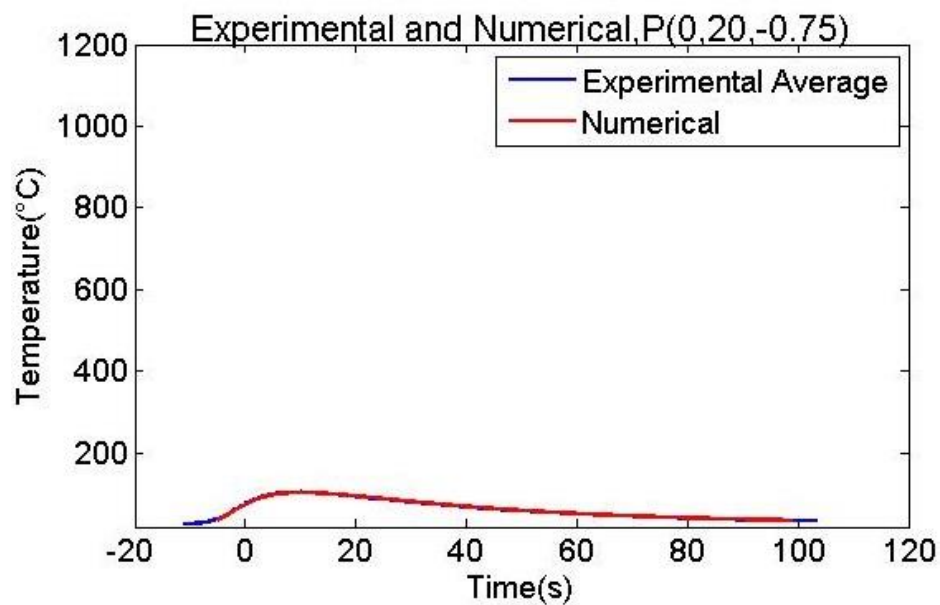


Figure 10-6 Experimental and numerical comparison at 20[mm] far from centerline

Maximum temperature obtained is the most important aspect of modeling because it affects the metallurgical characteristics a lot, so comparison of the maximum temperature obtained in experimental and simulation have performed and presented in Figure 10-7

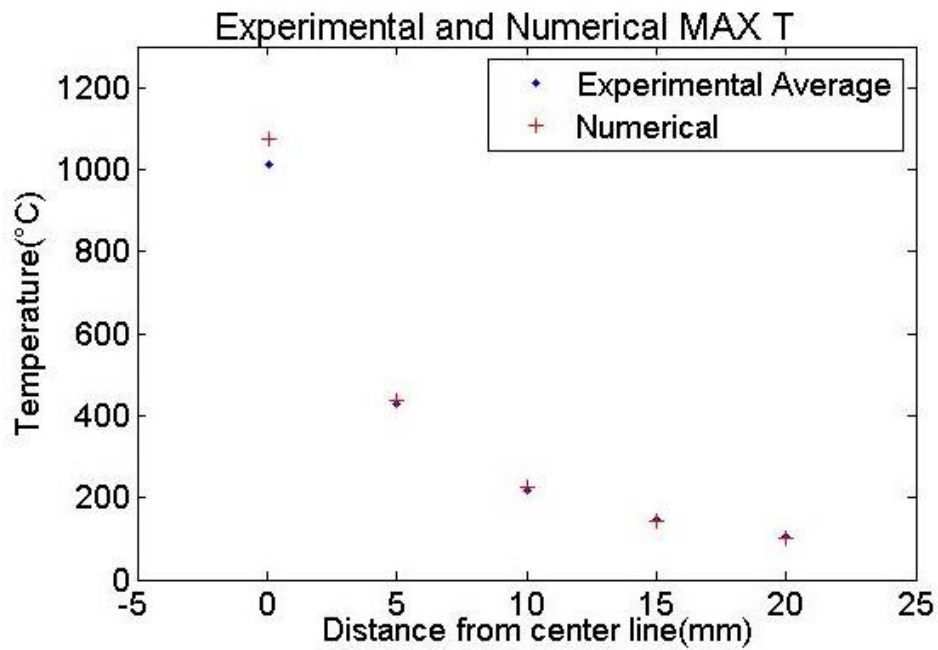


Figure 10-7 Experimental and numerical maximum temperature comparison

As it can be seen in this Figure 10-7 the maximum temperature difference at centerline is more than the other distances, the reason can be explained by small a error that can happen in locating thermocouple at the exact position. Since the temperature gradient at centerline is very high a small disposition of thermocouples can lead to have a great difference of the maximum temperature obtained.

Chapter 11 Conclusion

A numerical model has considered for the laser annealing of the CP Ti1, shielding gas effect assumed as constant convective cooling.

The results show that emissivity and absorption affect the maximum temperature significantly, while a lower effect for the cooling part.

$h_{\text{convective}}$ affects the maximum temperature and the cooling part and also the trend of temperature profile.

The numerical and experimental results have a very good agreement.

The obtained results give this opportunity to claim that the numerical model have built up well and it is reliable to use for favorite goals. As it mentioned the final aim of this work is to increase the productivity. Next chapters will discuss about optimizing productivity and the implemented approaches.

Part 4

One laser source productivity optimization

Chapter 12 One Laser Source Optimization

12.1 Productivity definition

Productivity is the final goal, the aim is to have an acceptable annealing first, then, having a larger area in the lower time.

The productivity measurement has applied for the cross section that there is almost a steady state condition (Figure 12-1).

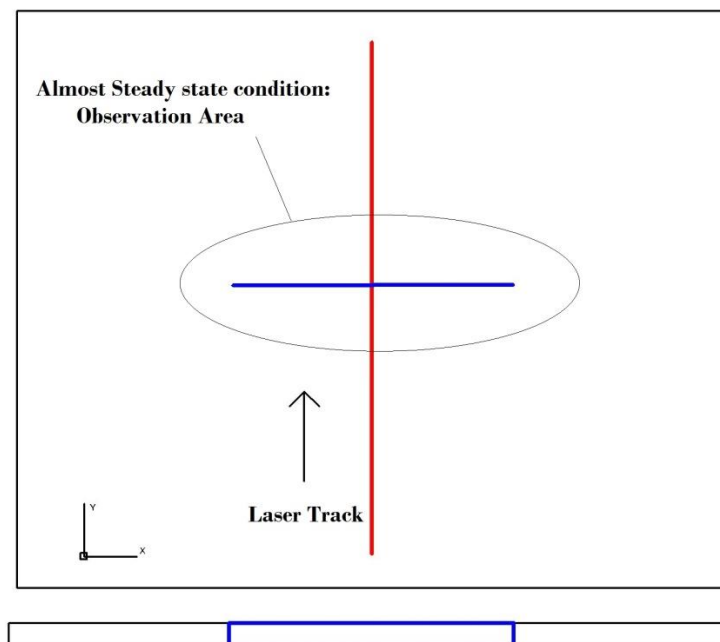


Figure 12-1 Studied cross section

Productivity generally is the rate of treating the volume (Figure 12-2).
Productivity can be defined as:

$$Productivity \left[\frac{mm^3}{s} \right] = \frac{Volume}{Time} = (L \times V) \times T$$

Where:

L: Annealed length [mm]

V: Laser track speed [mm/s]

T: Thickness [mm]

The thickness is constant and equal to 0.75[mm] according to section 5, So, the function of productivity for this thesis work can be defined as:

$$Prod. \left[\frac{mm^2}{s} \right] = L \times V$$

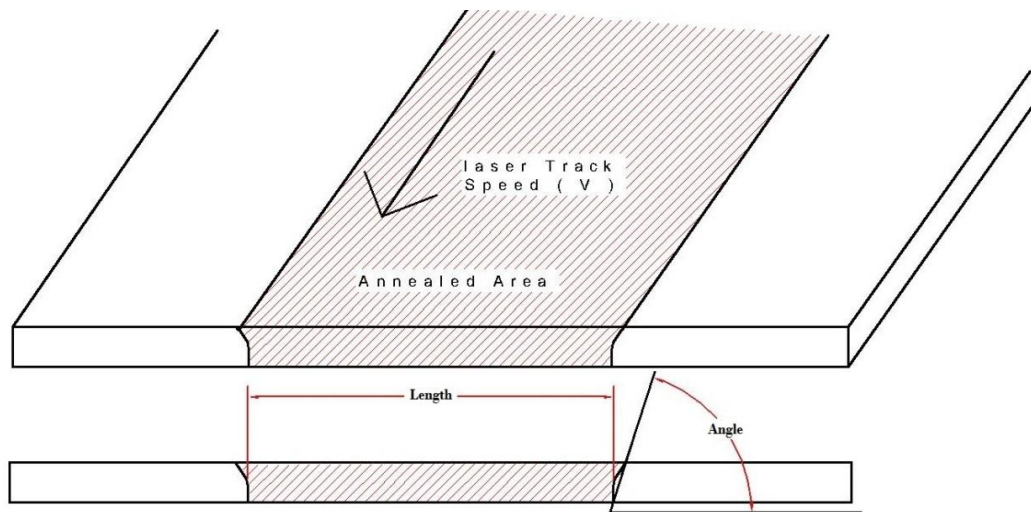


Figure 12-2 Length, Angle of annealed area

The productivity function can have a meaning when a successful annealing have done. Five status can happen when laser annealing happen:

1. Melted :

Laser power during the interaction time is too much leading to melting the workpeice. (Figure 12-3)

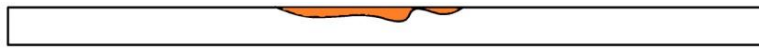


Figure 12-3 Melted

2. Not annealed

Laser power during the interaction time is not sufficient to obtain any grain enlargement. (Figure 12-4)



Figure 12-4 Not annealed

3. Not fully penetrated annealing:

Laser power during the interaction time is not sufficient to obtain grain enlargement for all the thickness. (Figure 12-5)



Figure 12-5 Not fully penetrated

4. Low angle annealing

Laser power during the interaction time is not sufficient to have a uniform annealing. (Figure 12-6)



Figure 12-6 Low angel annealing

5. Acceptable annealing

Laser power during the interaction time is sufficient to have a uniform annealing. Minimum accepted angle considered 70° . (Figure 12-7)



Figure 12-7 Accepted annealing

Angle is a criterion to define the uniformity of the annealing, angle near 90° is acceptable, since the annealed area is uniformed and there is no over power effect. The limit for angle is considered 70° , so having annealing boundary higher than 70° is acceptable. Length and angle of annealed area are shown in Figure 12-2. The melting temperature for CP Ti1 is about 1670°C [52]. In this thesis work the melting temperature have considered about 1500°C , since the CP Ti1 has rolled about 50% and some cold work and energy have put to the material, furthermore, some disturbances during the experiments may affect the material and considering a lower melting temperature to ensure the acceptability of study is a proper idea.

12.2 One source optimizing method

The dependence of mechanical properties on annealing temperature is one of the interesting phenomena of deformation behavior of bulk nano-structured materials (NSM). For instance, an increase in hardness of NSM as an effect of subsequent annealing was already reported in earlier works, and subsequently verified by a number of other investigations. Interestingly, this increase in hardness is apparently not associated with the method of nano-material fabrication. It was observed in metallic NSM obtained by inert gas condensation, compaction and also in those produced by severe plastic deformation. This phenomenon may be of special interest for researchers addressing recent questions pertaining to high strength and ductility in nano-materials raised in the scientific literature.

Since much of such data are limited to microhardness measurements, the confirmation of the effects of the annealing process on material strength through the use of tensile testing is important in order to confirm the observation [70].

There are several studies that report different annealing temperatures(The reported temperature are related to any kind of annealing) :

[71, 72] reported that Nucleation and growth of recrystallized nuclei occur as a result of annealing after rolling or swaging of pure titanium at $400\text{--}600^\circ\text{C}$ [73]. mentioned that under severe plastic deformation conditions, such as torsional straining, the recrystallization temperature of pure titanium is reduced to about 300°C . Also during annealing, grain growth in the HPT processed Ti starts at temperature 350°C and higher.

Khaled M. Ibrahim, Mansour Mhaede and Lothar Wagner evaluate the influence of hot swaging (SW) and annealing treatment on microstructure and mechanical properties of commercially pure titanium produced by investment casting. During SW at 700°C , the diameter of the cast titanium bars was reduced from 25 to 8.5 mm in 14 steps. After SW, material was annealed for 1 hour at 500, 700, or 870°C . Annealing at 500°C did not significantly change this microstructure, while annealing at both 700 and 870°C led to recrystallization and formation of

equiaxed microstructures. The cast bars exhibited a typical hard α -layer in near-surface regions with maximum depth and maximum hardness of 720 μm and 660 HV0.5, respectively. Due to SW, the tensile strength of the as-cast material drastically increased from 605 to 895 MPa. Annealing at 500 °C decreased this tensile strength slightly from 895 to 865 MPa while annealing at 700 °C led to a further pronounced drop in tensile strength from 865 to 710 MPa. No additional decrease in tensile strength was observed by increasing the annealing temperature from 700 to 870 °C. The tensile ductility of the as-cast and hot swaged samples was approximately the same in the range of 0.05 to 0.11, while the annealed samples showed values in the range of 0.25 to 0.53. In addition, the as-cast and hot swaged samples revealed a brittle cleavage fracture surfaces [74].

Also there are other different values reported in literature: [3] reports that temperatures as high as 593°C for stress relieving and 788°C for annealing of titanium are not uncommon, [5] says that the temperature for annealing CP titanium is about 595-705 °C for 2 hours of soaking, [75] mentioned that the titanium annealing happen about 700 °C for about 1 hour of soaking and [76] declares that most titanium grades are typically stress-relieved at about 538°C for 45 minutes and annealed at 704°C for two hours. A slightly higher stress relief temperature (593°C, 2 hours.) and annealing temperature (788°C, 4 hours.) are appropriate for the Grade 5 alloy. Air cooling is generally acceptable.

Table 12-1 shows the reported annealing temperatures:

Material	Annealing temperature	Condition	Reference
Pure titanium	400-600 °C		[71, 72]
Pure titanium	300_350°C		[73]
CP titanium	500_870°C	1 Hour soaking	[74]
Titanium	788°C		[3]
CP titanium	595-705 °C	2 Hours soaking	[5]
Titanium	700 °C	1 Hour soaking	[75]
Most titanium grades	704 °C	2 Hours soaking	[76]
Titanium Grade 5	788°C	4 Hours soaking	[76]

12-1 Reported annealing temperatures for titanium and its alloys

It can be seen that there is a range for the annealing temperature and it also depends on the soaking temperature and the specific titanium alloy.

12.2.1 Optimization Strategy

The strategy is to use the temperature annealing of CP Ti1 as a link between experimental and numerical. Some variable process parameters will be considered. The experimental tests will be done with variable process parameters while the calibrated numerical model is also running with the same variable process parameters simultaneously.

Microstructure observation of experimental samples will be done in the cross section where there is almost a steady state condition. (Figure 12-8)
The acceptability of process has evaluated and the productivity will be measured according to prod. Function (section 12.1).

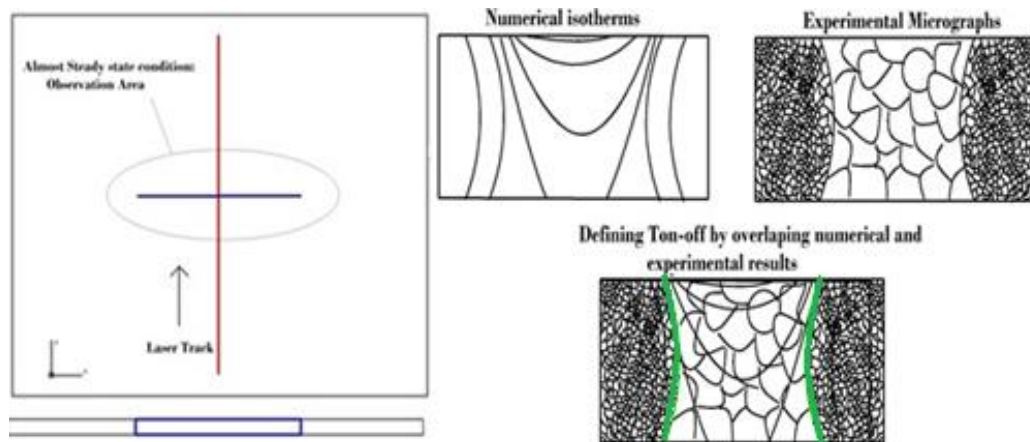


Figure 12-8 Study area, skim of numerical and experimental overlapping

The numerical results also will be gathered in the cross section where almost steady state condition is dominating and the isotherms in this cross section will be published.

Overlapping numerical isotherms with the experimental micrographs in the mentioned cross section gives this opportunity to define the annealing temperature (T_{on-off}).

Defining T_{on-off} gives this merit to expand the area of the investigation by running the simulation for bigger range of the variable process parameters and productivity calculation for them. Moreover, it is possible to announce which variable process parameters do not lead to a successful annealing. Finally, the optimized process parameters will be proposed.

12.2.2 Assumption

The numerical model selected to achieve the results, is the calibrated one (section 9, 10). The calibration parameters which are the absorption coefficient, emissivity coefficient and $h_{convective}$ assumed to be constant and same as the calibrated ones mentioned in Table 12.2.

Calibration parameters	Value	Assumption
Absorption coefficient	0.295	Constant – No Temperature effect
Emissivity coefficient	0.6875	Constant – No Temperature effect
$h_{convective}$	$5 \left[\frac{W}{m^2 K} \right]$	Constant – No Temperature effect

Table 12-2 Parameters behavior Assumption

12.3 Annealing temperature identification

Following the optimization strategy the experimental and numerical parts are handled. Here the goal is to overlap the experimental and numerical parts to gain the annealing temperature (T on-off).

12.3.1 Experimental Analysis

Experimental parts have done in order to have more sets of variable parameters and check the possible annealing status that can happen, be able to compare the results with numerical one.

12.3.1.1 Experimental design

The fixed parameters are exactly the same with what explained in section 8.1.1, just 4 sets of parameters have considered for laser track speed (V) and the laser power (P) according to [69]. Each combination coded with a certain number as it seen in Figure12-9.

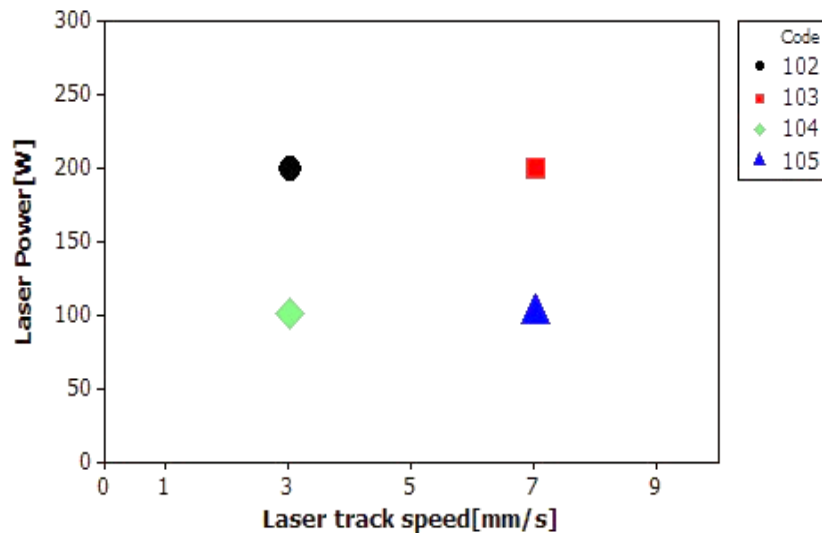


Figure 12-9 Variable Process Parameters

12.3.1.2 Experimental execution

The experimental execution is the same as what explained in section 4 With the same configuration and parameters.

In this section after laser annealing the microstructure observation will be done according to the section 4.2 for the favorite cross section explained in optimization strategy (section 12.2.1).

12.3.1.3 Experimental results

The annealed area in transversal cross section in the middle of the workpiece, which almost steady state condition dominating there the has observed and the length of annealed area and the angle of boundaries have measured for all sets of parameters (section 12.1), finally in the cases that the annealed is accepted the productivity has calculated.

One example of micrographs for each process parameter combination is presented in Table 12-3.

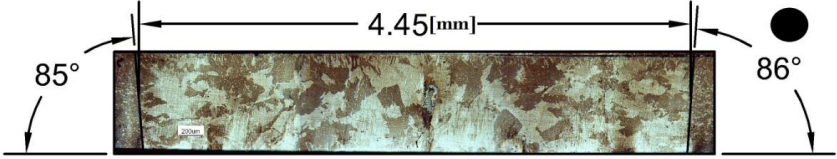
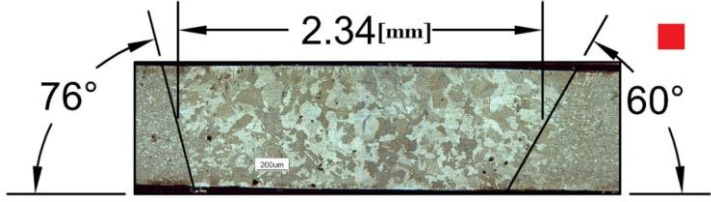

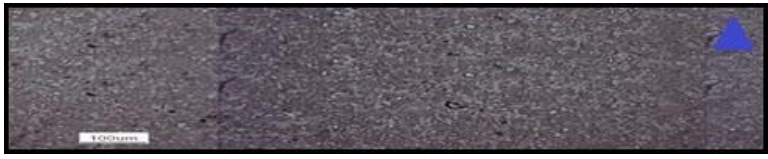
Process Parameters	Micrographs
P=200 [W] V=3 [mm/s]	
P=200 [W] V=3 [mm/s]	
P=100 [W] V=3 [mm/s]	
P=100 [W] V=7 [mm/s]	

Table 12-3 A sample of micrographs for each process parameter combination

For each parameters combination 6 experimental replications have done, the total number of 24 experiments have considered in this section, and the length, angle and the productivity have measured for all of them. Since there are two angles for each of experiment the average is considered. Detailed measurement results are presented in Table 12-4.

Sample Code	Total No. of Experiments	Annealing Status	Length Average [mm]	Standard Deviation	Angle Average	Standard Deviation	Productivity [mm ² /s]
102 P=200[W] V=3[mm/s]	6	Annealed	4.016	0.26	83°	2.63	12.05
103 P=200[W] V=7[mm/s]	6	Annealed with low angle	1.975	0.22	61°	2.34	13.82
104 P=100[W] V=3[mm/s]	6	Not Fully Penetrated	0		0		0
105 P=100[W] V=7[mm/s]	6	Not annealed	0		0		0

Table 12-4 Detailed summary of measurement for variable process parameters

12.3.2 Numerical analysis

The model have used is the calibrated model described in part 3 with the assumption of constant calibration parameters described in section 10.1.

12.3.2.1 Preprocessing

The numerical model used in order to study isotherms for the favorite cross section is the calibrated model and all the physical parameters comprised the geometry, material, mesh, heat source, boundary conditions are the same.

12.3.2.2 Processing

The model features have described in section 9.1. The parameters are appropriately lead to temperature convergence, and the time consumption for each simulation is acceptable while the number of elements are enough to describe the problem for all the defined variable process parameters presented in 12.3.1.1.

12.3.2.3 Post processing

The isotherms graphs related to the favorite cross section have gathered, for each set of the parameters. The isotherm graphs have presented in Table 12-5.

Process Parameters	Numerical isotherms
P=200 [W] V=3 [mm/s]	
P=200 [W] V=3 [mm/s]	
P=100 [W] V=3 [mm/s]	
P=100 [W] V=7 [mm/s]	

Table 12-5 Numerical isotherms for each process parameter combination

12.3.3 Results

In order to obtain the annealing temperature (Ton-off) the experimental micrographs are overlapped with the numerical isotherms for all experimental tests. For the samples number 105 no overlapping have done since these samples are not annealed as it shown in Table 12-3. The total overlapping graphs are 18 for the samples 102, 103, 104. Table 12-6 shows an example of overlapping experimental and numerical results for each sets of parameters.

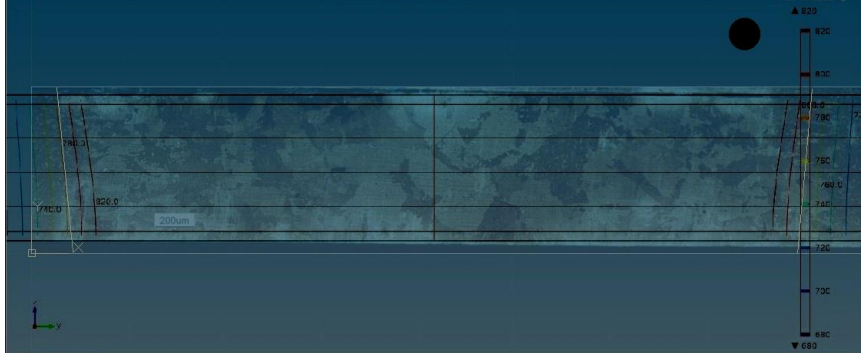
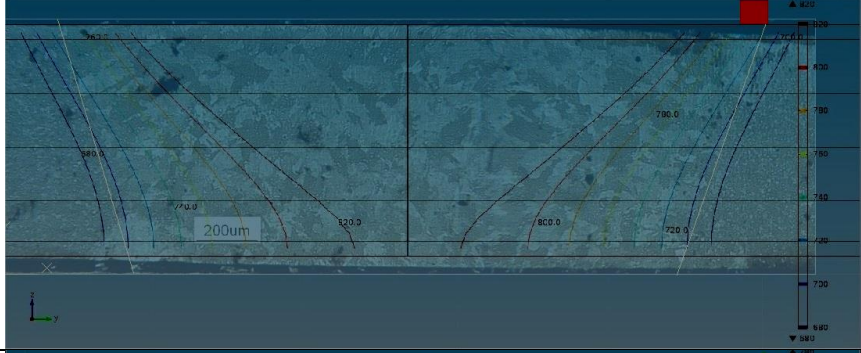
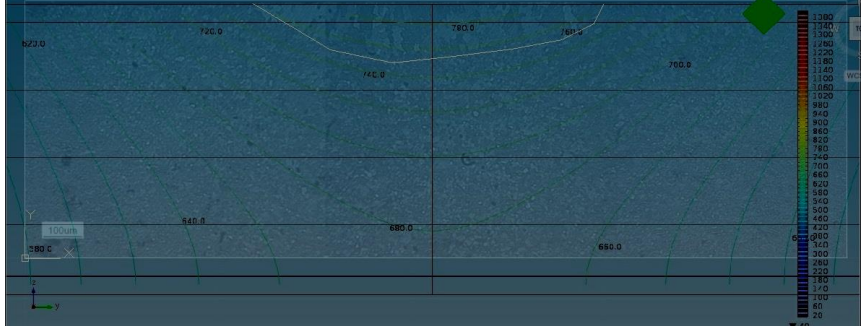
Process Parameters	Overlapping micrographs and isotherms
P=200 [W] V=3 [mm/s]	
P=200 [W] V=3 [mm/s]	
P=100 [W] V=3 [mm/s]	

Table 12-6 An example of numerical isotherms and experimental micrographs overlapping

Ton-off have measured for all 18 samples, and the interval plot have published in Figure 12-10.

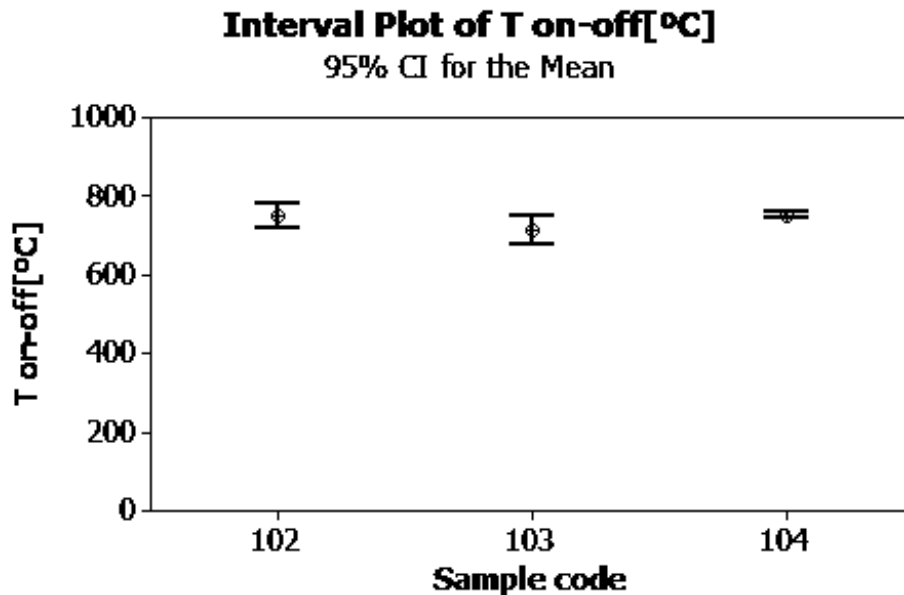


Figure 12-10 Ton-off interval plot

The total average for all samples, and the decided Ton-off value are presented in Table 12-7. The decided Ton-off value is about 10 °C in order to ensure the annealing process. The decided Ton-off is higher than 75% of all Ton-off collected.

T on-off Average	Decided Ton-off
739 °C	750 °C

Table 12-7 Ton-off decision

12.3.4 Conclusion

The numerical isotherms are overlapped with experimental micrographs for a range of parameters presented in Figure 12-11, and a certain temperatures have decided for the start of annealing (Ton-off).

12.3.4.1 Assumption

In order to expand the area of investigation by the simulation it is assumed that the Ton-off is constant for process parameters outside the range that used to define the Ton-off according to Figure 12-11.

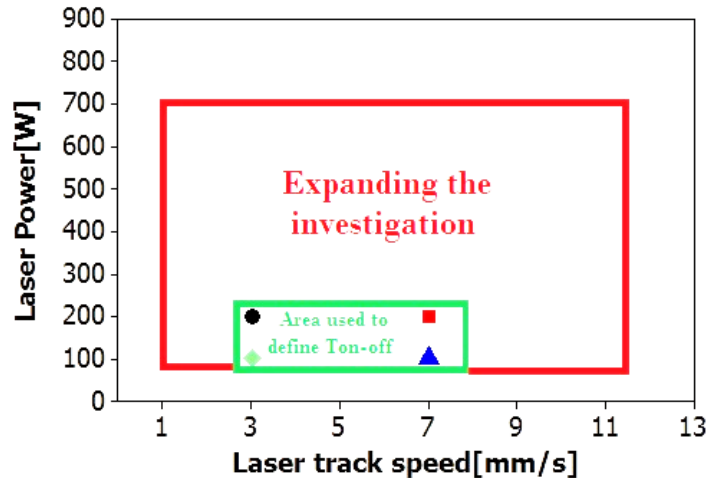


Figure 12-11 Area used to define process parameters and the expansion area

12.4 Optimized solution

Defining a certain Ton-off gives this opportunity to run the simulation and expand the studied area.

Measuring the productivity, according to the numerical isotherms for wider range of variable process parameters.

12.4.1 Study design

The approach in order to design the area of study is to run the simulation with random process parameters and selection the most appropriate process parameters by checking the results through isotherms, this loop can happen several time in order to increase the nodes of investigation. Two iterations have considered with this approach and the preliminary and the final study area have considered as it shown in Figures 12-12, 12-13.

The maximum speed studied is 13[mm/s] because more than that the annealing results were unacceptable (melting or low angle annealing) and the maximum power decided 700[W], since more than that the annealing results were unacceptable according to the maximum range of speed.

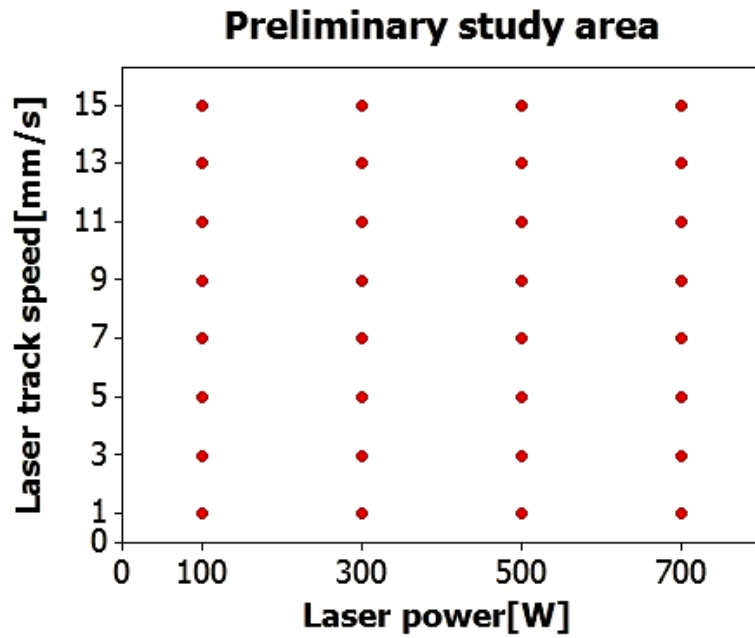


Figure 12-12 First iteration in order to define the study area

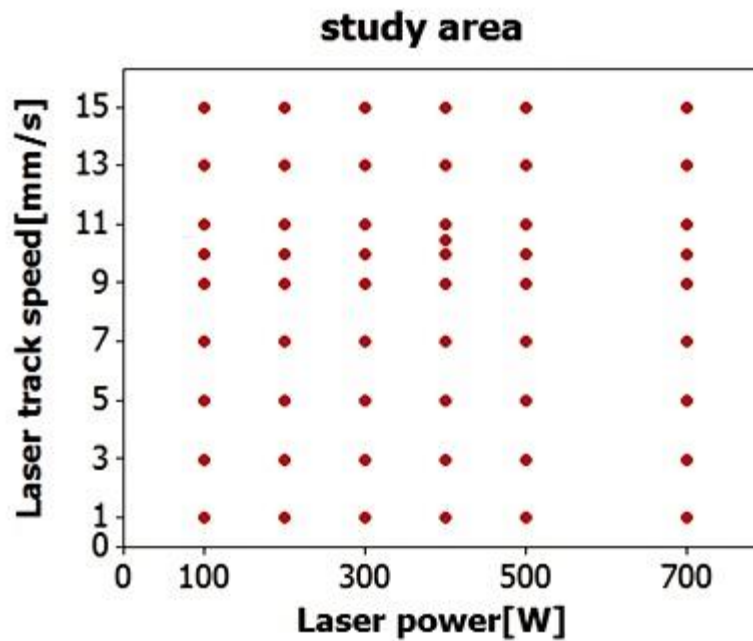


Figure 12-13 Study area

12.4.2 Isotherms productivity measurements

The isotherms gathered from simulation can describe in five status as it explained in section 12.1:

1. Melted
When there is an isotherm having temperature more than 1500°C .
2. Not annealed
When there is not any isotherm having the temperature more than 750°C .
3. Not full penetrated
When the isotherm having the temperature 750°C is not fully penetrated through the thickness of the workpiece.
4. Low angle
When the isotherm having the temperature 750°C is fully penetrated through the thickness of the workpiece but the angle is less than 70° .
5. Accepted isotherm
When the isotherm having the temperature 750°C is fully penetrated through the thickness of the workpiece and the angle is over 70° .

Figure 12-14 depicts a typical acceptable isotherm and the measurement method used in order to calculate the angle and the length. The measurement of length is done in the middle of the workpiece and the measurement of angle is done through connecting the start and end of the isotherm.

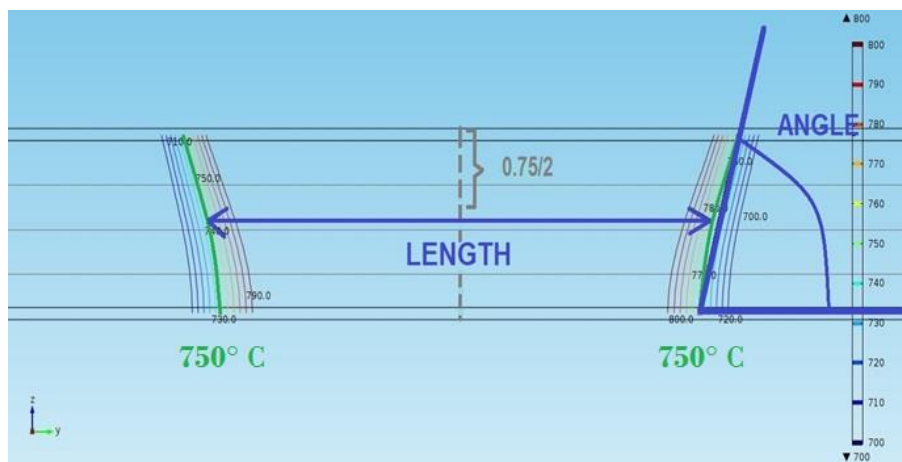


Figure 12-14 Productivity measurement for accepted annealing

12.4.3 Results

The isotherms for each set of variable process parameters have collected. First the status of the annealing have checked Figure 12-15. Then, the length, the angle and the productivity have measured for the accepted ones and presented in Figure 12-16, 12-17 and Table 12.8.

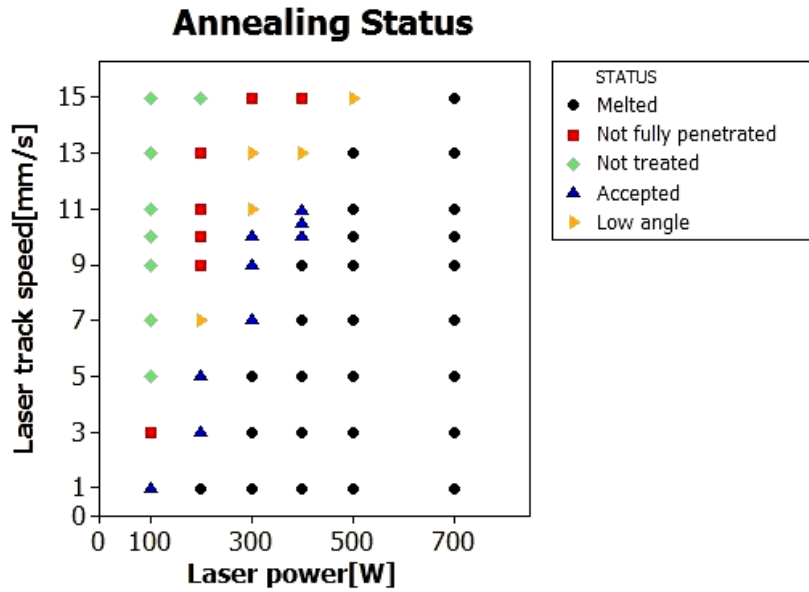


Figure 12-15 Annealing status according to the numerical isotherms

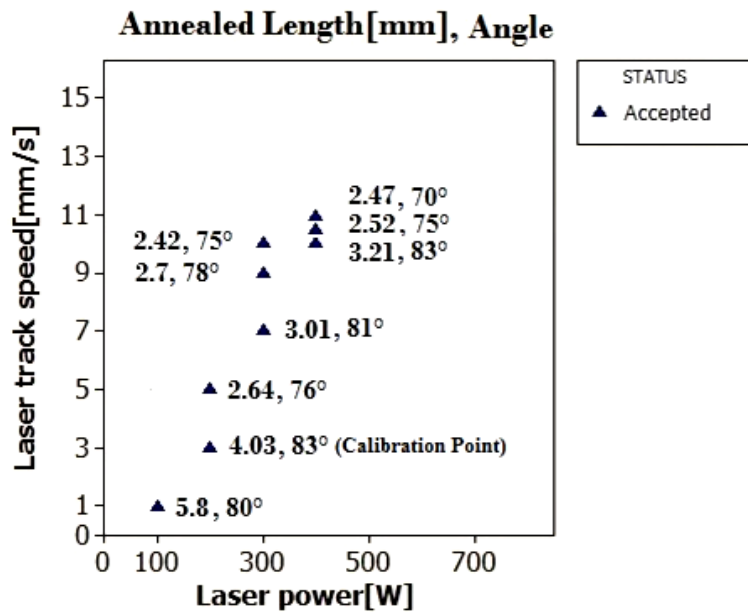


Figure 12-16 Length and Angle measurement of numerical isotherms

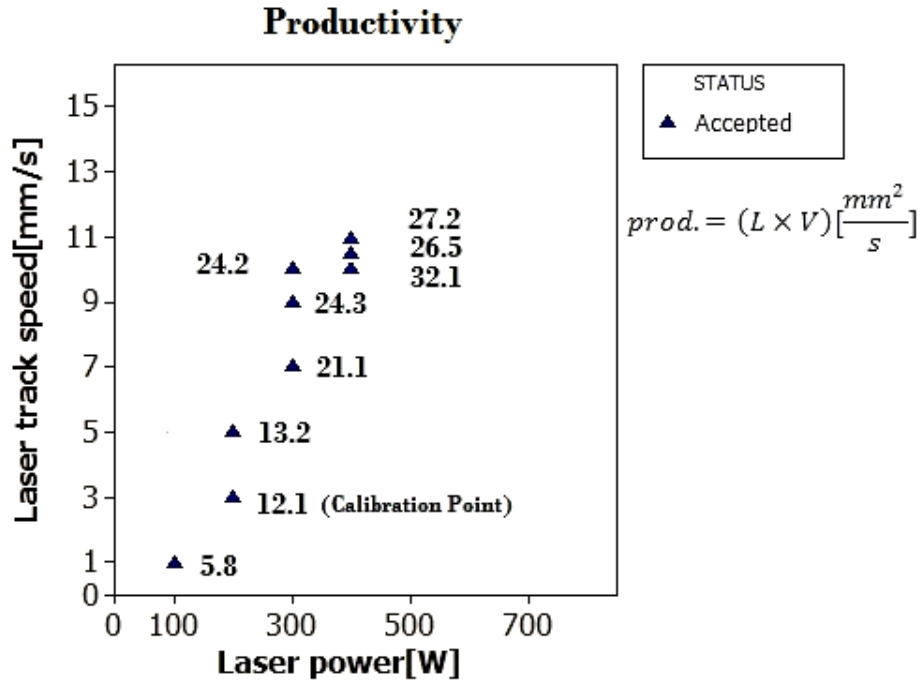


Figure 12-17 Prod. Calculation for accepted numerical isotherms

Acceptable process parameters		Length[mm]	Angle	Prod. [$\frac{mm^2}{s}$]
100	1	5.8	80°	5.8
200	3	4.03	83°	12.1
200	5	2.64	76°	13.2
300	7	3.01	81°	21.1
300	9	2.7	78°	24.3
300	11	2.42	75°	24.2
400	10	3.21	83°	32.1
400	10.5	2.52	75°	26.5
400	11	2.47	70°	27.2

Table 12-8 Length Angle and Prod. For accepted numerical isotherms

12.4.4 Proposed Parameters

The experimental and numerical results linked, with the annealing temperature. The numerical simulations give this opportunity to expand the process parameter investigation.

According to the results of numerical part the proposed variable process parameters to have the optimized productivity are presented in Table12-9.

Process Parameters		Prod.
Laser Power[W]	Laser track speed[mm/s]	$L \times V \left[\frac{mm^2}{s} \right]$
400	10	32.1

Table 12-9 Proposed process parameters

According to the numerical results the proposed parameters have the highest productivity, while the feasibility of the process is guaranteed and the angle ensure a very acceptable uniformity.

12.5 Experimental validation

Experimental validation always is necessary to check the reliability of the numerically proposed parameters. Validation is important because always there are some errors in modeling and numerical analysis.

12.5.1 Design of experimental validation

The emphasis of the experimental validation is on the proposed and critical accepted parameters, while two experiments have designed in order to check the melting and low angle annealing status. Two replication of experiments have decided (only due to the criticality of one process parameter five replication have decided for that specific one). Figure 12-18 and Table 12-10 depict the chosen process parameters for experimental validation.

Sample Code	Variable Process Parameters		Status	No. of replication
	Laser Power [w]	Laser track speed [mm/s]		
1	500	13	Melted	2
2	400	13	Low Angel	2
3	400	11	Accepted	5
4	400	10.5	Accepted	2
5	400	10	Accepted-Proposed	2
6	300	7	Accepted	2

Table 12-10 Chosen process parameters in order to experimental validation

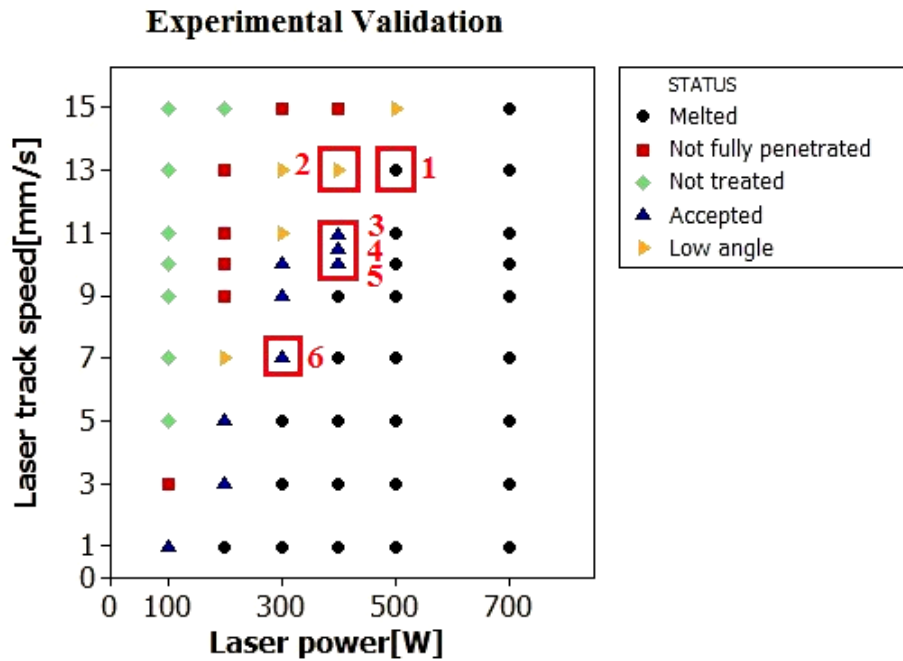


Figure 12-18 Chosen process parameters in order to experimental validation

12.5.2 Execution of experimental validation

The experimental execution is exactly the same as section, the experiment with the same setup and approach have performed for all the new variable parameters. Since the goal is to compare the experimental micrographs in the favorite cross section with almost steady state condition the microscopic observation have done according to section 4.2.

12.5.3 Results

Here the micrographs and the hardness tests as a second validation criterion are presented in Tables 12-11, 12-12, 12-13, 12-14, 12-15, 12-16 for selected parameters. Summary of Measurements of length, angle and the productivity are presented in Table 12-17 .

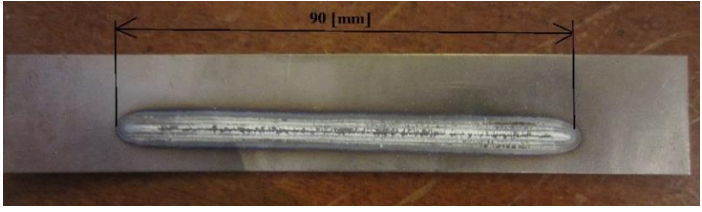
Sample 1	
Process parameters	Result
<p>P=500[w]</p> <p>V=13[mm/s]</p>	

Table 12-11 Sample 1 macro observation (melting status)

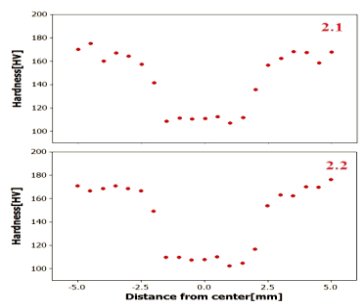
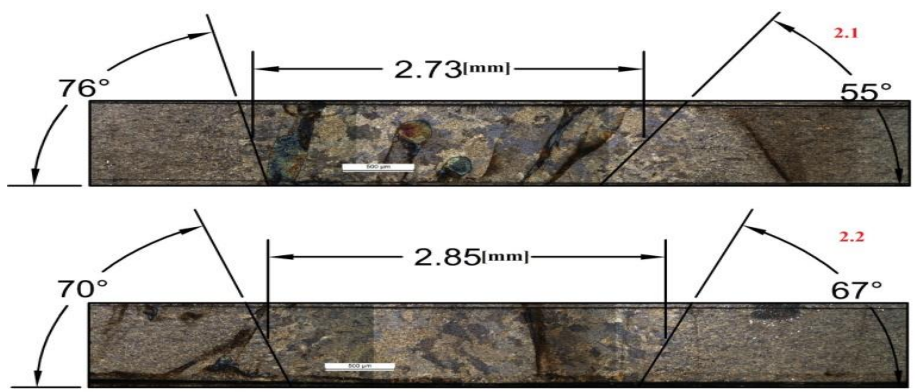
Sample 2	
Process parameters	Hardness test
<p>P=400[w]</p> <p>V=13[mm/s]</p>	
Isotherms observation	
	

Table 12-12 Sample 2 hardness test and micro observation (low angle status)

Sample 3	
Process parameters	Hardness test
<p>P=400[w] V=11[mm/s]</p>	
Isotherms observation	

Table 12-13 Sample 3 hardness tests and micro observation (Accepted annealing)

Sample 4	
Process parameters	Hardness test
<p>P=400[w] V=10.5[mm/s]</p>	
Isotherms observation	

Table 12-14 Sample 4 hardness tests and micro observation (Accepted annealing)

Sample 5	
Process parameters	Hardness test
<p>P=400[w] V=10[mm/s]</p>	
Isotherms observation	

Table 12-15 Sample 5 hardness tests and micro observation (Accepted annealing)

Sample 6	
Process parameters	Hardness test
<p>P=300[w] V=7[mm/s]</p>	
Isotherms observation	

Table 12-16 Sample 6 hardness tests and micro observation (Accepted annealing)

Sample code	No. of repeat	Variable process parameters		Status	Length [mm]	Angle	Prod. [$\frac{mm^2}{s}$]
		Laser Power [w]	Laser track speed [mm/s]				
1	2	500	13	Melted	---	---	---
		500	13	Melted	---	---	---
2	2	400	13	Low angle	---	65.5°	---
		400	13	Low angle	---	68.5°	---
3	5	400	11	Accepted	3.23	75.5°	35.53
		400	11	Accepted	3.15	74.5°	34.65
		400	11	Accepted	3.51	70.5°	38.61
		400	11	Melted	---	---	---
		400	11	Melted	---	---	---
4	2	400	10.5	Accepted	2.91	72.5°	30.55
		400	10.5	Accepted	3.53	79°	37.06
5	2	400	10	Accepted	3.25	80.5°	32.5
		400	10	Accepted	4.49	84°	44.9
6	2	300	7	Accepted	4.24	77.5	29.68
		300	7	Accepted	3.58	81.5	25.06

Table 12-17 Length Angle and Prod. for experimental validation

12.6 Comparison

The comparison between numerical and experimental validation have done. The value considered for the experimental lengths and the angles for each sample is the average of all replications for that specific sample. Figures 12-19, 12-20, 12-21 present the comparison for length, angle and productivity.

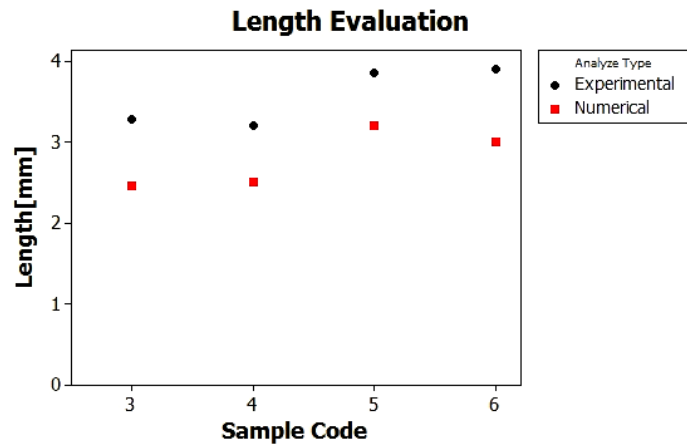


Figure 12-19 Length Comparison

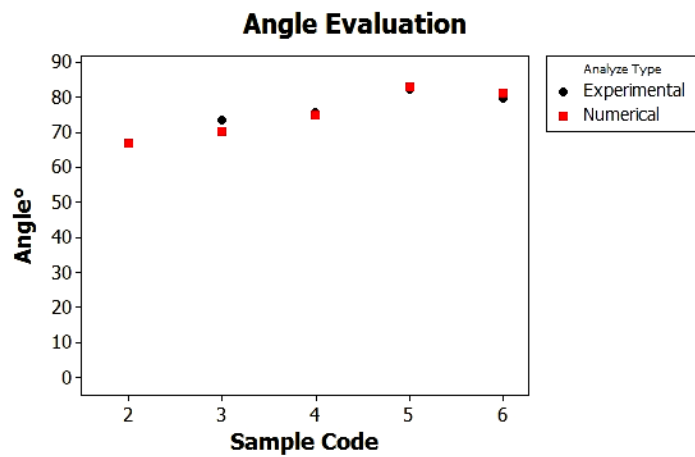


Figure 12-20 Angle Comparison

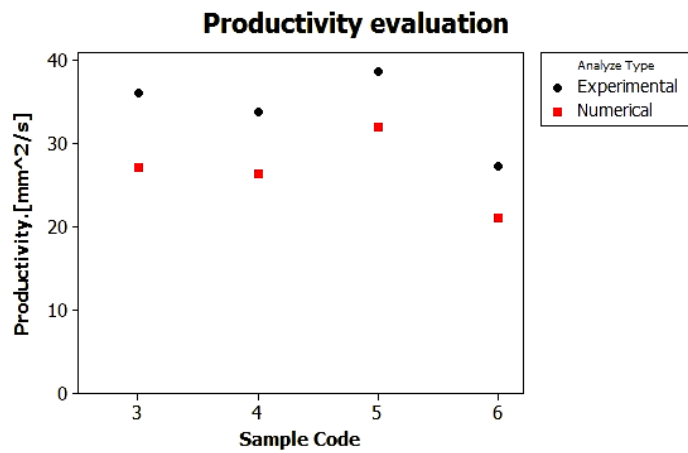


Figure 12-21 Productivity Comparison

In order to evaluate the difference between numerical and experimental validation the percentage error for length, productivity and the angle calculated like below and presented in Figures 12-22, 12-23.

$$\text{Length Percentage error}[\%] = \frac{(L_{\text{Experimental}} - L_{\text{Simulation}})}{L_{\text{Simulation}}}$$

$$\text{Angle Percentage error}[\%] = \frac{|A_{\text{Experimental}} - A_{\text{Simulation}}|}{A_{\text{Simulation}}}$$

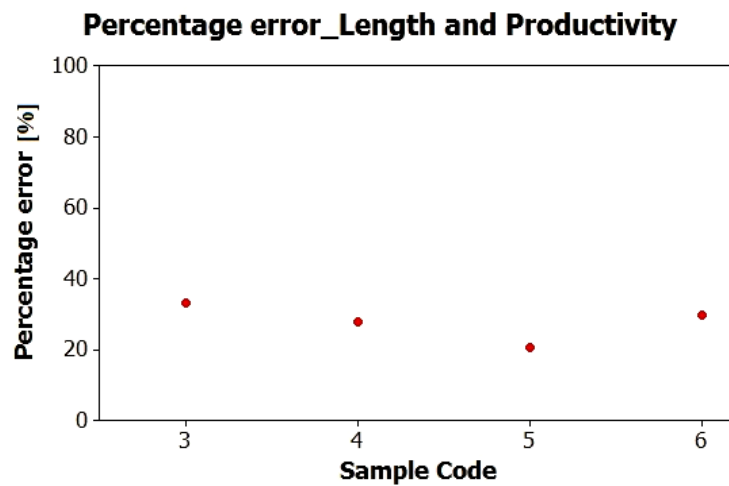


Figure 12-22 Percentage error, Length and Productivity

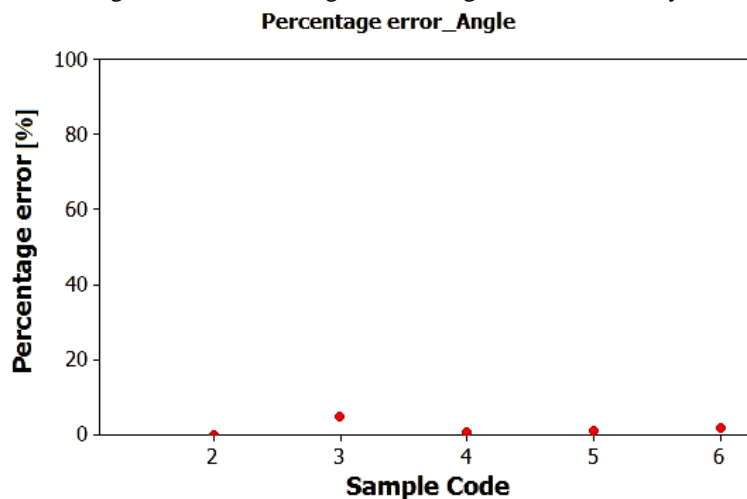


Figure 12-23 Percentage error, Angle

12.7 Conclusion

According to the validation results, the two experimental validations related to the melting and low angle status were successful.

- The length (productivity) is higher about 20-30% experimentally for the accepted process parameters and the angle difference is about 0-5%.
- The amount of error is almost equal for all process parameters
- The model underestimate the productivity (which is positive from safety point of view), this can be explained by the assumption of constant calibration parameters specially the absorption coefficient and constant Ton-off for all process parameters Figure 12-24.
- According to the available laser source and focusing system the maximum productivity obtained with single source laser for the CP Ti1 is $38.7 \left[\frac{mm^2}{s} \right]$.

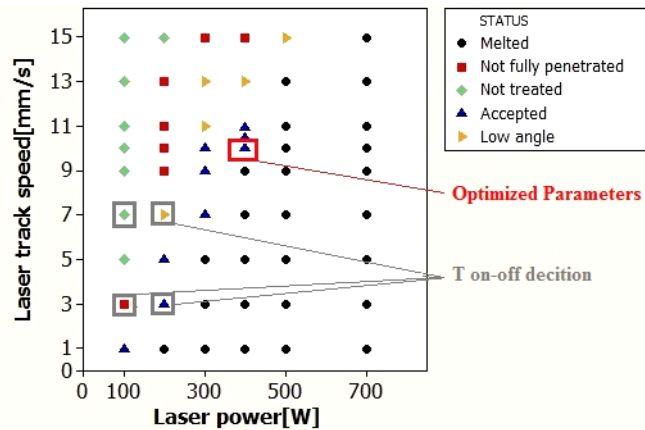


Figure 12-24 Ton-off decision and the optimized parameters

The optimized process parameters are validated and presented in Table 12-18.

Process Parameters		Prod. $\left[\frac{mm^2}{s} \right]$	
Laser Power[W]	Laser track speed[mm/s]	Simulation	Experimental
400	10	32.1	38.7

Table 12-18 Optimized and validated process parameters

Part 5

Dual side by side laser sources
productivity optimization

Chapter 13 Two laser sources

In order to gain the goal determinedly, and optimized the productivity as much as possible it is a good idea to investigate the idea of two side by side laser sources. In this part the concept of two laser sources and the optimum distance between two laser sources and study the productivity numerically will discussed.

13.1 Two sources concept

The main idea is to superimpose two laser gaussian density profiles by having two side by side laser sources and obtain an almost uniform rectangular density profile on the surface of substrate.

There are two gaussian density profiles that start to interact and overlap in their interface (Figure 13-1), varying the process parameters (laser track speed, laser power) and specially the distance between two sources can give any shape to the temperature profile over the surface of substrate.

The design of distance between two laser sources should be in a way to guarantee almost rectangular temperature profile for a wide range of laser track speed and laser power.

The modification of laser intensity profile previously have done in several studies as it mentioned in the state of the art.

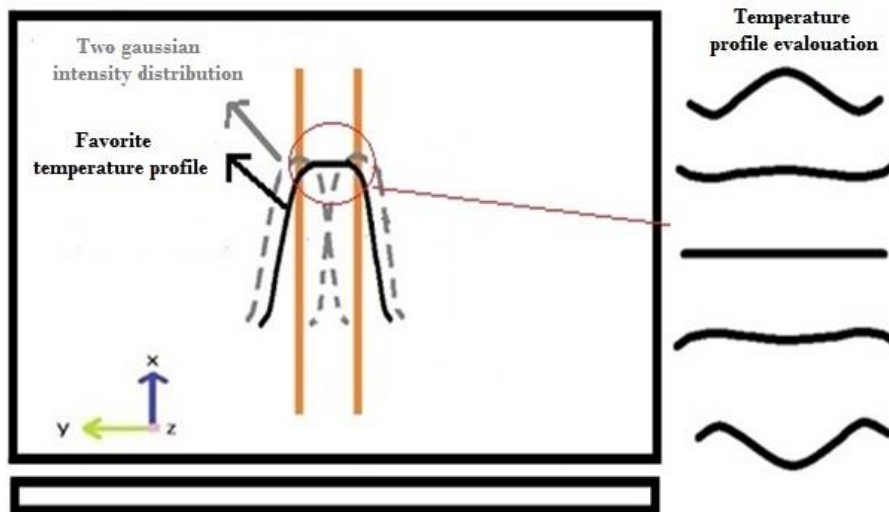


Figure 13-1 Favorite density profile and possible evolution

13.2 Optimization strategy

The strategy in order to optimize the productivity with two laser sources is to define a specific range of distance between two sources which guarantee the rectangular temperature profile where there is the feasibility of annealing varying variable process parameters.

To start the distance definition, it is important to know the effect of the variable process parameters and the distance on the temperature profile.

Temperature profile analysis area is present in Figure 13-2. Almost steady state condition is dominating in the analysis area while it located in the most critical area with highest temperature gradient.

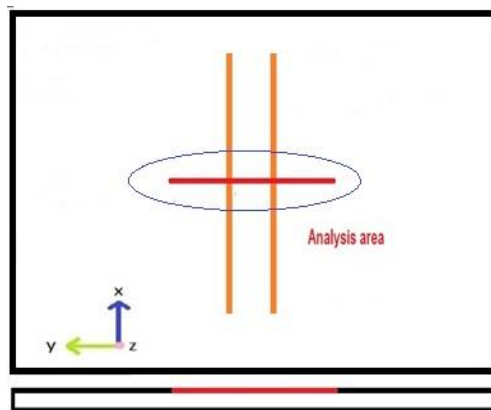


Figure 13-2 Analysis area, parameters effect investigation

An optimized range of distance will take to the consideration after the process parameters effect investigation. Figure 13-3 shows the distance definition between two sources.

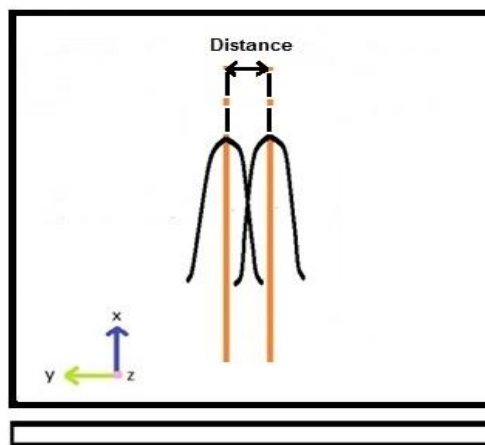


Figure 13-3 Distance definition between two sources

Then the numerical model will run for the different variable process parameters with the defined distances, the annealing status, the length, productivity and the angle will be measured.

13.3 Boundary limit of process parameters

The numerical model has built up as it explained in section 9, the only difference is that there are two side by side laser sources instead of one source.

The effect of laser track speed, laser power and the distance between two sources have studied according to some trial simulations. It is possible to see that the effect of distance is significant on the temperature profile in the studied area, while the laser power and the laser track velocity do not affect the density profile so much. According to the results in previous section and the feasibility process parameters proposed for the single source the distance range for two laser sources in order to have almost rectangular temperature profile in the analysis area is decided and presented in Table 13-1.

Distance/2 [mm] range
1.08_1.32

Table 13-1 distance range

In order to study the productivity the distance range divide into five fixed distances according to Table 13-2.

Division	Distance/2 [mm]
1	1.08
2	1.14
3	1.20
4	1.26
5	1.32

Table 13-2 distance division

13.4 Productivity evaluation

In order to evaluate the productivity the numerical model used with the same preprocessing and processing configurations (section 9.1) with two laser sources. To start the evaluation the process parameters will be define.

13.4.1 Laser track speed and laser power definition

According to the different distances as a boundary that guarantee the rectangular temperature profile over the surface, laser power and laser track speed are also considered and presented in Table 13-3.

The laser power in Table 13-3 represents the total power for two sources, while for each source it is half of presented value.

Study area		
Distance/2 [mm]	Laser power [W]	Laser track speed [mm/s]
1.08	100	1
1.14	300	3
1.20	500	5
1.26	700	7
1.32	---	9
---	---	11
---	---	13

Table 13-3 Study area

13.4.2 Results

The isotherms have collected and the length, angle and the productivity have measured for the acceptable process parameters.

Figures 13-4, 13-5, 13-6, 13-7, 13-8 depicts the annealing status and the productivity for accepted process parameters for each division of distances.

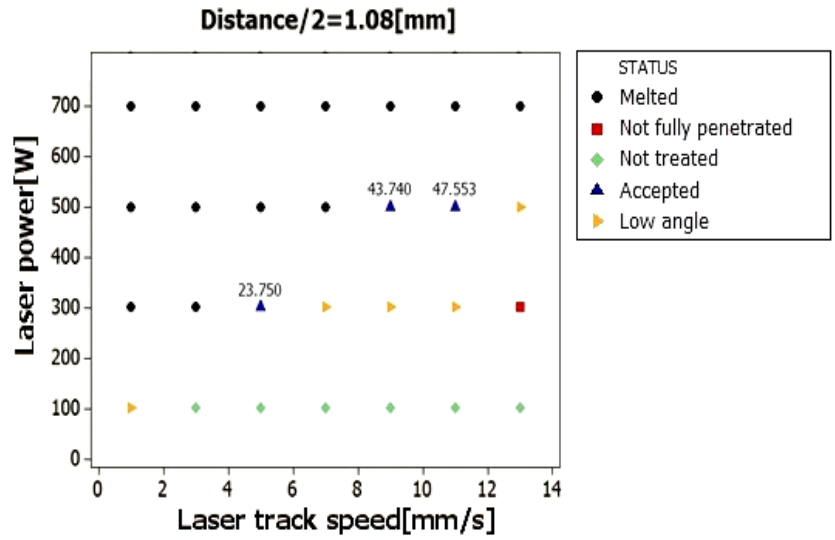


Figure 13-4 Annealing status and productivity for distance=2.16[mm]

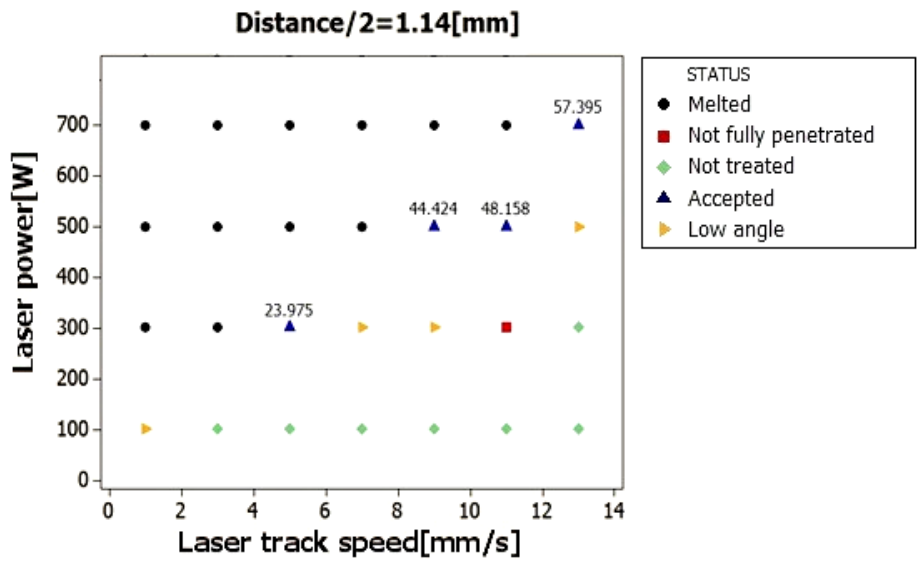


Figure 13-5 Annealing status and productivity for distance=2.28[mm]

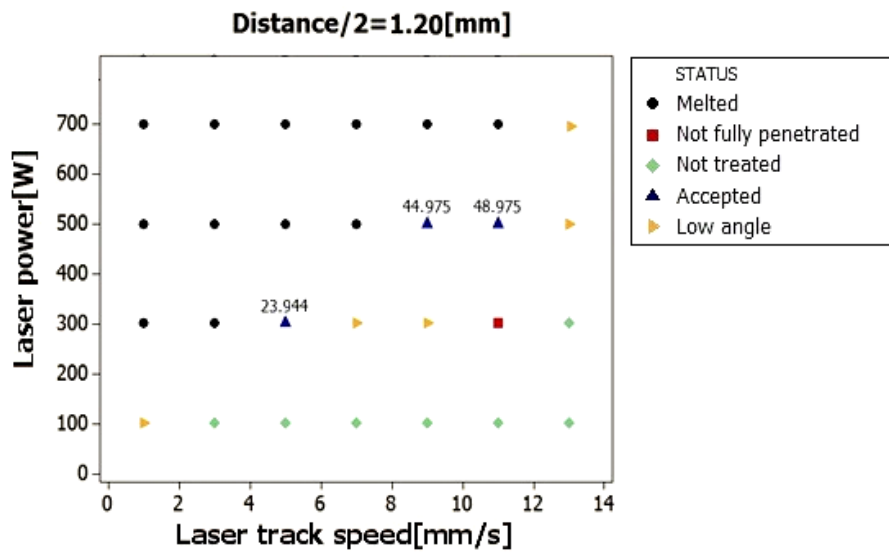


Figure 13-6 Annealing status and productivity for distance=2.40[mm]

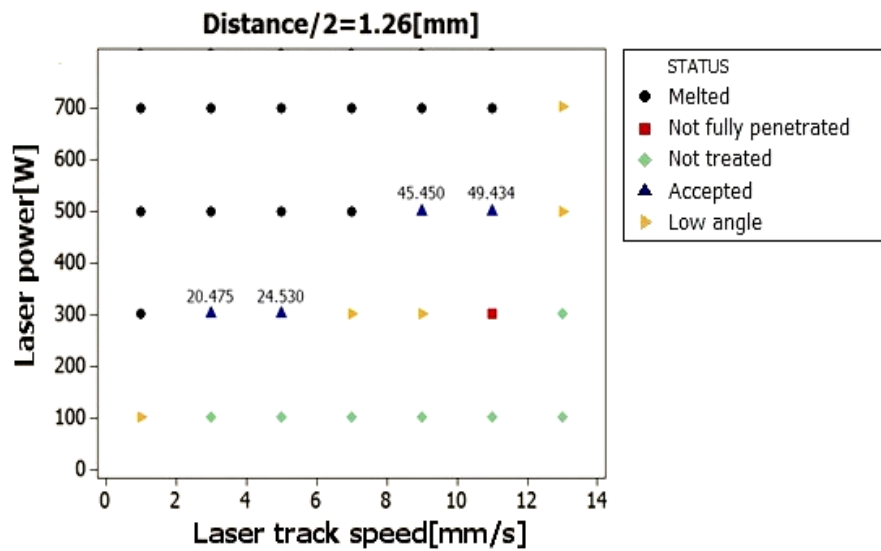


Figure 13-7 Annealing status and productivity for distance=2.52[mm]

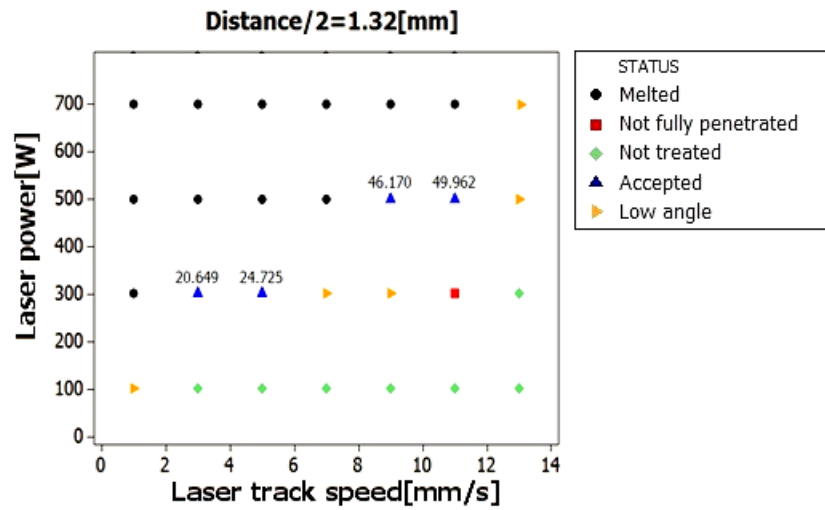


Figure 13-8 Annealing status and productivity for distance=2.64[mm]

13.5 Conclusion

According to the numerical results for two laser sources, it is possible to propose the distance and process parameters in order to have the optimum productivity. The proposed distance and process parameters are presented in Table 13-4.

Two sources optimal distance and variable process parameters		
Total Laser power [W]	Laser track velocity [mm/s]	Two sources Distance[mm]
700	13	2.28

Table 13-4 Optimum distance and process parameters

The optimum productivity according to the numerical results presented in Table13-5.

Simulation optimum productivity
$\left[\frac{mm^2}{s}\right]$
57.39

Table 13-5 Two laser sources optimum productivity

Part 6

Single source and dual laser
sources productivity comparison

Chapter 14 Single and dual sources comparison

Two criterion have defined in order to compare the single source and dual laser sources productivity.

First is to consider the equal process parameters which guarantee an acceptable annealing both for single and dual laser sources and compare the productivity.

Second way is to compare the optimum productivity that can reach in single or dual laser sources. Here both criterions are investigate.

All productivities reported in this part are the values reported by simulation.

14.1 Comparison with Equal process parameters

Since in the studied area there is not any equal process parameter to give an acceptable annealing for both one source and dual source annealing, a process parameter have considered that gives an acceptable annealing in single laser source and an almost acceptable annealing(with small angle degrees lower that limit) in all distances of dual laser sources.

Having laser power equal to 300[w] and laser track speed equal to 7[mm/s] guarantee an almost acceptable annealing for both single and dual laser sources according to section 12.3.3 and section 13.4.2.

The productivities related to single and different distances of two sources for the selected process parameter are presented in Table 14-1.

Equal process parameter comparison		Productivity $\left[\frac{mm^2}{s}\right]$
Single source		21.1
Dual laser sources	Distance	
Distance 1	2*1.08	24.71
Distance 2	2*1.14	25.09
Distance 3	2*1.20	25.31
Distance 4	2*1.26	25.62
Distance 5	2*1.32	25.95

Table 14-1 productivity comparison single and dual laser sources (P=300, V=7[mm/s])

The productivity for dual laser sources with different distances is 15_18% more than the productivity in single sources.

14.2 Optimal process parameters comparison

The optimal process parameters and the optimized productivity proposed for single and dual laser sources according to sections 12.7 and 13.5 are presented in Table 14-2.

Optimized Productivity [$\frac{mm^2}{s}$]			
Single laser source		Dual laser sources	
32.1		57.39	
Optimal Variable process parameters			
Single laser source		Dual laser source	
Laser power[W]	Laser track velocity[mm/s]	Laser power[W]	Laser track velocity[mm/s]
400	10	700	13

Table 14-2 Optimized productivity and process parameters for single and dual sources

As it seen the optimal productivity for dual laser sources is almost two times more, Which means that the process time consumption decreases about two times.

14.3 Conclusion

From optimal process parameters or same process parameters productivity comparison for single and dual laser sources it is concluded that dual laser sources productivity have higher productivity.

- Having same variable process parameters (laser power and laser track speed) for single and dual laser source, dual laser sources shows at least 15% more productivity.
- The optimal productivity of dual sources is almost two times more than single source.

Future Development

The future research activities can expand the current investigation in several issues. Some possible investigation areas have proposed below:

- Investigation of multiple laser sources with different arrangements in order to obtain favorite temperature profile over the substrate to optimize annealing or other industrial applications.
- Investigation of the laser annealing soaking time and its effects on the process.
- Investigation on possible ways to apply laser beam intensity modification and find out suitable beam shapes for laser annealing or other industrial applications.
- Investigation on the absorption and emissivity dependency to the temperature or other parameters for CP Ti or other material and proposing the trend.

Appendix A

Trajectory of heat source MATLAB code:

```
clc
close all
clear all

n=input('Inserisci il numero di tratti: ');
fprintf('\n\n\n')
clc

for ii=1:n

    %inserimento coordinate punto iniziale tratti i-esimo
    fprintf('Inserisci coordinata x del punto di partenza del
tratto [mm]%d: \n',ii)
    x_if(ii+(ii-1))=input(' ');
    fprintf('Inserisci coordinata y del punto di partenza del
tratto [mm]%d: \n',ii)
    y_if(ii+(ii-1))=input(' ');
    fprintf('\n\n\n')

    %inserimento coordinate punto finale tratti i-esimo
    fprintf('Inserisci coordinata x del punto finale del tratto
[mm]%d: \n',ii)
    x_if(ii+(ii-1)+1)=input(' ');
    fprintf('Inserisci coordinata y del punto finale del tratto
[mm]%d: \n',ii)
    y_if(ii+(ii-1)+1)=input(' ');
    clc
end

%conversione coordinate mm-> m

x_if=x_if./10^3;
y_if=y_if./10^3;

% caratterizzazione delle velocità d'andata
for ii=1:n
    fprintf('Inserisci la velocità dell tratto %d [mm/s]:\n',ii)
    v_i(ii)=input(' ');
```



```
fprintf('Inserisci la direzione del vettore velocità x: inserire
1 se concorde -1 se discorde',ii)
v_xi(ii)=input(' ');
fprintf('Inserisci la direzione del vettore velocità y: inserire
1 se concorde -1 se discorde',ii)
v_yi(ii)=input(' ');
clc
end

%conversione coordinate mm/s-> m/s

v_i=v_i./10^3;

for ii=1:n
fprintf('Inserisci la velocità dell tratto di ritorno %d
[mm/s]:\ninserire 0 se non presente',ii)
v_b(ii)=input(' ');
clc
end

% composizione matrice B

B=zeros(max(size(y_if)));

for ii=1:n
temp=zeros(2);
temp(:,1)=x_if(2*(ii-1)+1:2*(ii-1)+2);
temp(:,2)=diag(ones(2));
B(2*(ii-1)+1:2*(ii-1)+2,2*(ii-1)+1:2*(ii-1)+2)=temp;
end

ab=B\y_if';

for ii=1:max(size(ab))/2
coeff_a(ii)=ab(1+(ii-1)*2)
coeff_b(ii)=ab(ii*2)
end

for ii=1:max(size(y_if))/2
x_start(ii)=x_if(1+(ii-1)*2);
y_start(ii)=y_if(1+(ii-1)*2);
x_stop(ii)=x_if(2+(ii-1)*2);
y_stop(ii)=y_if(2+(ii-1)*2);
d(ii)=sqrt((x_stop(ii)-x_start(ii))^2+(y_stop(ii)-
y_start(ii))^2);
t_on(ii)=d(ii)/abs(v_i(ii))
end
```

```

for ii=1:n
clear scritta
figure (1)
plot([x_start(ii):(x_stop(ii)-
x_start(ii))/100:x_stop(ii)], [y_start(ii):(y_stop(ii)-
y_start(ii))/100:y_stop(ii)], 'LineWidth',2);
hold on
text(x_start(ii),y_start(ii), '\leftarrow
start', 'HorizontalAlignment', 'left')
hold on
text(x_stop(ii),y_stop(ii), '\leftarrow
stop', 'HorizontalAlignment', 'left')
hold on
scritta='\leftarrow Track_';
scritta(max(size(scritta))+1)=num2str(ii);
text((x_stop(ii)+x_start(ii))/2, (y_stop(ii)+y_start(ii))/2, scritt
a, 'HorizontalAlignment', 'left')
hold on
xlabel('X [mm]')
ylabel('Y [mm]')
title('Track position')
end

    if n>1

        for ii=1:n-1
            d_off(ii)=sqrt((x_start(ii+1)-
x_stop(ii))^2+(y_start(ii+1)-y_stop(ii))^2)
            t_off(ii)=d_off(ii)/v_b(ii);
        end
    end

t(1)=t_on(1);

if n>1
    for ii=1:n-1
        t(max(size(t))+1)=t_off(ii);
        t(max(size(t))+1)=t_on(ii+1);
    end
end

if n>1

    for ii=1:max(size(t))
        h(ii+1)=sum(t(1:ii));
    end
end

```

```

        end
    else
        h(1)=t(1)
    end

    for ii=1:max(size(coeff_a))
        vx(ii)=v_xi(ii)*abs(v_i(ii)*cos(atan( (y_stop(ii)-
        y_start(ii)) / (x_stop(ii)-x_start(ii)) ) ));
        vy(ii)=v_yi(ii)*abs(v_i(ii)*sin(atan( (y_stop(ii)-
        y_start(ii)) / (x_stop(ii)-x_start(ii)) ) ));
    end

    u=h(2:max(size(h)));

    nome_vx='traj_vx';
    nome_vy='traj_vy';

    nome_vx(max(size(nome_vx))+1)='.';
    nome_vx(max(size(nome_vx))+1)='m';
    nome_vy(max(size(nome_vy))+1)='.';
    nome_vy(max(size(nome_vy))+1)='m';

    %% scrittura file traj_x

    fid=fopen(nome_vx,'w')
    fprintf(fid, 'function tr_vx=traj_x(t)\n tr_vx=')

    if n>1
        for jj=1:n-1
            fprintf(fid, '(%f+%f.*(t-%d)).*(t>%d &
t<%d)',x_start(jj) ,vx(jj),h(1+(jj-1)*2),h(1+(jj-1)*2),h(2+(jj-
1)*2));
            fprintf(fid, '+(%f).*(t>%d &
t<%d)+',x_start(jj+1),h(2+(jj-1)*2),h(3+(jj-1)*2));
        end

        fprintf(fid, '+(%f+%f.*(t-%d)).*(t>%d &
t<%d)',x_start(jj+1) ,vx(jj+1),h(max(size(h))-1),h(max(size(h))-
1),h(max(size(h))));
        fprintf(fid, '\nend');
        fclose(fid);

    else
        jj=1;
    end

```

```

        fprintf(fid, '(%f+%f.*(t-%d)).*(t>%d & t<%d)',x_start(jj)
, vx(jj),0,0,h(max(size(h)))));
        fprintf(fid, '\nend');
        fclose(fid);
    end

    %% scrittura file traj_y

    fid=fopen(nome_vy,'w')
    fprintf(fid, 'function tr_vy=traj_y(t)\n tr_vy=')

    if n>1
        for jj=1:n-1
            fprintf(fid, '(%f+%f.*(t-%d)).*(t>%d &
t<%d)',y_start(jj) ,vy(jj),h(1+(jj-1)*2),h(1+(jj-1)*2),h(2+(jj-
1)*2));
            fprintf(fid, '+(%f).*(t>%d &
t<%d)',y_start(jj+1),h(2+(jj-1)*2),h(3+(jj-1)*2));
        end

        fprintf(fid, '+(%f+%f.*(t-%d)).*(t>%d &
t<%d)',y_start(jj+1) ,vy(jj+1),h(max(size(h))-1),h(max(size(h))-
1),h(max(size(h)))));
        fprintf(fid, '\nend');
        fclose(fid);

    else
        jj=1;
        fprintf(fid, '(%f+%f.*(t-%d)).*(t>%d & t<%d)',y_start(jj)
,vy(jj),0,0,h(max(size(h)))));
        fprintf(fid, '\nend');
        fclose(fid);
    end

    %% scrittura file accensione e spegnimento laser

    for ii=1:max(size(t))
        if mod(ii,2)~=0
            on_off(ii)=1;
        else
            on_off(ii)=0;
        end
    end

    fid=fopen('laser_on_off.m','w')
    fprintf(fid, 'function Laser_on=laser_on_off(t)\n Laser_on=')

```

```
if n>1
    for jj=1:n-1
        fprintf(fid, '(%d).*(t>%d & t<%d)',on_off(1+(jj-
1)*2),h(1+(jj-1)*2),h(2+(jj-1)*2));
        fprintf(fid, '+(%f).*(t>%d & t<%d)+',on_off(2+(jj-
1)*2),h(2+(jj-1)*2),h(3+(jj-1)*2));
    end

    fprintf(fid, '(%d).*(t>%d &
t<%d)',on_off(max(size(on_off))),h(max(size(h))-
1),h(max(size(h))));
    fprintf(fid, '\nend');
    fclose(fid);

else
    jj=1;
    fprintf(fid, '(1).*(t>%d & t<%d)',0,h(max(size(h))));
    fprintf(fid, '\nend');
    fclose(fid);
end
```

Appendix B

Heat source generation MATLAB code

```
clc
close all
clear all

df0= 50; %um
fr= 100; %mm
ff= 200; %mm
M2= 5.14; %mm
lam= 1064; %nm
def= -50; %mm DEFOCALIZZAZIONE
alpha=10; %° sessagesimali
z=[-120:0.1:120]; %mm
w = 0.865 %portion of gaussian distribution
%% conversione unità di misura
df0=df0*1e-6;
fr=fr*1e-3;
ff=ff*1e-3;
lam=lam*1e-9;
alpha=90-alpha;
alpha=alpha*2*pi/360;
def=def*1e-3;
z=z*1e-3;
kg=4/pi;
k=kg.*M2;

%%

dg=ff/fr*df0;
teta=((k*lam)/dg);
r=sqrt(dg^2+(z).^2.*teta.^2)/2;
rp=sqrt(dg^2+(def).^2.*teta.^2)/2;
r01=rp/sqrt(2) ;

y=alpha.*(z-def);

plot(z,r,z,-r,z,y)
xlabel('distanza dal punto di fuoco [m]')
ylabel('W fascio[m]')
```

```
[x_inter,y_inter]=polyxpoly(z,r,z,y);
rdef=abs(y_inter/sin(alpha))
area_ellisse=pi*rdef*rp;
disp('m^2')
r02=rdef/sqrt(2);

fid=fopen('distr.m','w');
fprintf(fid,'function distr=distr(x,y)\n distr=');
fprintf(fid,'exp(-x.^2./(%d).^2-y.^2./(%d).^2)\n',r01,r02);
fprintf(fid,'end') ;
fclose(fid);

Q=input('Inserisci la potenza in [W]: ');
Ass=input('Inserisci valore assorbimento: ');
q02_mean=Q/area_ellisse;
q02 = abs(q02_mean*(log(1/1-w))/w);

fid=fopen('dati.txt','w');
fprintf(fid,'Q\t%d[W]\n',Q);
fprintf(fid,'Ass\t%d\n',Ass);
fprintf(fid,'r01\t%d[m]\n',r01);
fprintf(fid,'r02\t%d[m]\n',r02);
fprintf(fid,'rp\t%d[m]\n',rp);
fprintf(fid,'rdef\t%d[m]\n',rdef);
fprintf(fid,'Area\tpi*rp*rdef\n');
fprintf(fid,'q02\t%d[W/m^2]\n',q02);
fclose(fid);

x=[-5:0.1:5]*1e-3;
y=[-5:0.1:5]*1e-3;

[X,Y]=meshgrid(x,y);
figure(2)
surf(X,Y,exp(-X.^2./(r01).^2-Y.^2./(r02).^2))
```

References

1. A. Poulon-Quintin, A., et al., *Microstructure and mechanical properties of surface treated cast titanium with Nd:YAG laser*. Dent Mater, 2012. **28**(9): p. 945-51.
2. A. Poulon-Quintin, E.W., C. Bertrand, I. Watanabe, *Microstructure and mechanical properties of surface treated cast titanium with Nd:YAG laser*. Dental Materials, 28(9), pp.945-951; 201, 2012.
3. <http://www.wisegeek.com/what-is-titanium-heat-treating.htm>.
4. <http://www.keytometals.com/Article97.htm>
5. <http://cartech.ides.com/datasheet.aspx>.
6. Tian, Y.S., et al., *Research progress on laser surface modification of titanium alloys*. Applied Surface Science, 2005. **242**(1-2): p. 177-184.
7. S. McElroy, D.Y., G. Reddy, *Laser Processing of Titanium Aluminides*. Journal of Materials Engineering and Performance, 2000.
8. Bertrand, C. and A. Poulon-Quintin, *Proposals for optimization of laser welding in prosthetic dentistry*. J Prosthodont, 2010. **19**(1): p. 69-76.
9. György, E., et al., *Influence of the ambient gas in laser structuring of the titanium surface*. Surface and Coatings Technology, 2004. **187**(2-3): p. 245-249.
10. Otto, A. and M. Schmidt, *Towards a universal numerical simulation model for laser material processing*. Physics Procedia, 2010. **5**: p. 35-46.
11. Yilbas, B.S. and N. Al-Aqeeli, *Analytical investigation into laser pulse heating and thermal stresses*. Optics & Laser Technology, 2009. **41**(2): p. 132-139.
12. Ready, J.F., *Effects Due to Absorption of Laser Radiation*. Journal of Applied Physics, 1965. **36**(2): p. 462.

13. M. K. EL-ADAWI, M.A.A.-N., and S. A. SHALABY, *Laser heating of a two-layer system with constant surface absorption: an exact solution*. Int. J. Heat Mass Transfer. Vol. 38, No. 5, pp. 947-952, 1994.
14. YILBAS, B.S., *ANALYTICAL SOLUTION FOR TIME UNSTEADY LASER PULSE HEATING OF SEMI-INFINITE SOLID*. Int. J. Mech. Sci. Vol. 39, No. 6, pp. 671-682, 199, 1996.
15. Yilbas, B.S., *A closed form solution for temperature rise inside solid substrate due to time exponentially varying pulse*. International Journal of Heat and Mass Transfer 45 (2002) 1993–2000, 2001.
16. Yilbas, B.S., S.Z.S., *Heat transfer analysis of laser heated surfaces - conduction limited case* Applied Surface Science 108 (1997) 167-175 1996.
17. Yilbas, B.S., M.K., *Repetitive laser pulse heating with a convective boundary condition at the surface*. J. Phys. D: Appl. Phys. 34 (2001) 222–231.
18. K. Lit, P.S., *PLANE STRESS MODEL FOR FRACTURE OF CERAMICS DURING LASER CUTTING* Int. J. Mach. Tools Manuf. Vol. 35. No. II. pp. 1493-1506. 1995, 1994.
19. H.G. Wang, Y.H.G., T.L. Chen, IT. Zhang, *A study of thermal stresses during laser quenching*. Journal of Materials Processing Technology 63 (1997) 550-553, 1997.
20. Yilbas, B.S., et al., *Laser-shock processing of steel*. Journal of Materials Processing Technology, 2003. **135**(1): p. 6-17.
21. Laazizi, A., et al., *Applied multi-pulsed laser in surface treatment and numerical–experimental analysis*. Optics & Laser Technology, 2011. **43**(7): p. 1257-1263.
22. Chande, T. and J. Mazumder, *Two-dimensional, transient model for mass transport in laser surface alloying*. Journal of Applied Physics, 1985. **57**(6): p. 2226.
23. V V Semak, J.A.H., M H McCay and T D McCay *Melt pool dynamics during laser welding* J. Phys. D: Appl. Phys. 28 (1995) 2443-2450, 1995.

24. C. R. HEIPLE, J.R.R., R. T. STAGNER AND R. J. ADEN *Surface Active Element Effects on the Shape of GTA, Laser, and Electron Beam Welds* WELDING RESEARCH SUPPLEMENT, 1983.
25. B. Courant, J.-J.H., S Benayoun and J-P L'Huillier, *Melting and solidification processes in a moving graphite-covered titanium surface subjected to multi-pulse laser irradiation*. J. Phys. D: Appl. Phys. 34 (2001) 1437–1446 2000.
26. M. A. Anjos , R.V., R. Li , M. G. Ferreira , W. M. Steen and K. Watkins *Fe-Cr-Ni-Mo-C alloys produced by laser surface alloying* Surface and Coatings Technology, 70 (1995) 235 242 1996.
27. ASHBY, H.R.S.a.M.F., *The Prediction of Case Depth in Laser Transformation Hardening* METALLURGICAL TRANSACTIONS 1990.
28. Hill, M.C., *METHODS AND GUIDELINES FOR EFFECTIVE MODEL CALIBRATION*. U.S. GEOLOGICAL SURVEY WATER-RESOURCES INVESTIGATIONS REPORT 98-4005, 1998.
29. De, A., *A smart model to estimate effective thermal conductivity and viscosity in the weld pool*. Journal of Applied Physics, 2004. **95**(9): p. 5230.
30. Rouquette, S., J. Guo, and P. Le Masson, *Estimation of the parameters of a Gaussian heat source by the Levenberg–Marquardt method: Application to the electron beam welding*. International Journal of Thermal Sciences, 2007. **46**(2): p. 128-138.
31. S. Pereyra, G.A.L., G. Frontini, S.A. Urquiza, *Sensitivity Analysis and Parameter Estimation of Heat Transfer and Material Flow Models in Friction Stir Welding*. Materials Research, 2013.
32. Zhiqiang Fan, K.P.a.F.L., *Sensitivity Analysis of Process Parameters in Laser Deposition*. Mechanical and Aerospace Engineering, 2005.
33. M. PICASSO, C.F.M., J.-D. WAGNIIB.RE, A. FRENK, and M. RAPPAZ, *A Simple but Realistic Model for Laser Cladding*. METALLURGICAL AND MATERIALS TRANSACTIONS, 1992.

34. Ming-Hsi Hsu, A.Y.K., Jan-Tai Kuo and Wen-Cheng Liu, *PROCEDURE TO CALIBRATE AND VERIFY NUMERICAL MODELS OF ESTUARINE HYDRODYNAMICS*. JOURNAL OF HYDRAULIC ENGINEERING 1999.
35. Chau, K.W., *Intelligent manipulation of calibration parameters in numerical modeling*. Advances in Environmental Research, 2004. **8**(3-4): p. 467-476.
36. E. Esterhuizen, C.M., M. Murphy, *Numerical Model Calibration for Simulating Coal Pillars, Gob and Overburden Response*.
37. Cappon, H. and K.J. Keesman, *Numerical modeling, calibration, and validation of an ultrasonic separator*. IEEE Trans Ultrason Ferroelectr Freq Control, 2013. **60**(3): p. 614-21.
38. Ding, C., et al., *Cosine-Gaussian correlated Schell-model pulsed beams*. Opt Express, 2014. **22**(1): p. 931-42.
39. Ponomarenko, S.A., *A class of partially coherent beams carrying optical vortices*. Optical Society of America, 2001.
40. H. Lajunen, T.S., *Propagation characteristics of partially coherent beams with spatially varying correlations*. Optical Society of America, 2011.
41. S. Sahin, O.K., *Light sources generating far fields with tunable flat profiles*. Optical Society of America, 2012.
42. S. Sahin, O.K., *Light sources generating far fields with tunable flat profiles*. Optical Society of America, 2012.
43. Zhang, Y. and D. Zhao, *Scattering of multi-Gaussian Schell-model beams on a random medium*. Opt Express, 2013. **21**(21): p. 24781-92.
44. Reddy, S.G., et al., *Experimental generation of ring-shaped beams with random sources*. Opt Lett, 2013. **38**(21): p. 4441-4.
45. Mei, Z. and O. Korotkova, *Cosine-Gaussian Schell-model sources*. Opt Lett, 2013. **38**(14): p. 2578-80.
46. Alieva, T., et al., *Partially coherent stable and spiral beams*. J Opt Soc Am A Opt Image Sci Vis, 2013. **30**(11): p. 2237-43.

47. Korotkova, O. and E. Shchepakina, *Rectangular Multi-Gaussian Schell-Model beams in atmospheric turbulence*. Journal of Optics, 2014. **16**(4): p. 045704.
48. XIE, J., *An experiment in which a high-power CO₂ laser beam was split into two equal- power beams that were then used as a welding heat source indicated the dual- beam laser could significantly improve weld quality*. WELDING JOURNAL, 1999.
49. XIE, J., *Weld Morphology and Thermal Modeling in Dual-Beam Laser Welding* WELDING JOURNAL, 1999.
50. *ASTM E235 Standard Specification for Type K and Type N Mineral-Insulated, Metal-Sheathed Thermocouples for Nuclear or for Other High-Reliability Applications*. 2012.
51. E. Capello, B.P., *Enhancing dual phase steel formability by diode laser heat treatment*. JOURNAL OF LASER APPLICATIONS 2009.
52. Company, R.T., *TITANIUM ALLOY GUIDE*. An RTI International Metals, Inc. Company, 2000.
53. Xuanyong Liu, P.K.C., Chuanxian Ding, *Surface modification of titanium, titanium alloys and related materials for biomedical applications*. Materials Science and Engineering R 47 2005.
54. HARPUR, N.F., *Applications of Titanium*. AIRCRAFT ENGINEERING, 1979.
55. D. Buckley, T.K., R. Johnson *INFLUENCE OF CRYSTAL STRUCTURE ON THE FRICTION AND WEAR OF TITANIUM AND TITANIUM ALLOYS IN VACUUM*. NATIONAL AERONAUTICS AND SPACE ADMINISTRATION_WASHINGTON, D. C, 1965.
56. Imam, M.A., *The 12th World Conference on Ti-ti and countries*. www.tms.org/jom.html, 2011.
57. Williams, J.C., *Titanium Alloys: Processing, Properties, and Applications*. 2010.
58. <http://www.titaniumart.com/titanium-info-cp.html>.

59. *Unalloyed Commercially Pure Titanium*. fwmetals.com.
60. M. Hayashi, H.Y., M. Ishii, H, Harada, *Recrystallization Behavior of Commercially Pure Titanium During Hot Rolling* NIPPON STEEL TECHNICAL REPORT No. 62 1994.
61. W. steen, J.m., *Laser material processing*. Intelligent Manufacturing, 2010.
62. www.tct.it E-mail: info@tct.it. TITANIUM CONSULTING & TRADING.
63. <http://www.vegasfastener.com/Titanium.php>
64. http://www.engineeringtoolbox.com/emissivity-coefficients-d_447.html
65. <http://www.omega.com/literature/transactions/volume1/emissivityb>.
66. Company, B.S., *Thermal Loading Study of the TAD Waste Package*. 2008.
67. *Properties and Selection of non ferrous alloys and special purpose materials*. METAL HANDBOOK TENTH EDITION.
68. <http://www.npl.co.uk/reference/faqs/>
69. ISFAHAN, R.Sharif.H., *LOCAL ANNEALING OF TITANIUM USING FIBER LASER TO IMPROVE FORMABILITY*. 2014.
70. R.Z. Valiev, A.V.S., A.K. Mukherjee, *The effect of annealing on tensile deformation behavior of nanostructured SPD titanium*. Scripta Materialia 49 (2003) 669–674, 2003.
71. K.Y. Zhu, A.V., F. Brisset, K.Lu, J.L, *Nanostructure formation mechanism of alpha-titanium using SMAT*. Acta Materialia 52 (2004) 4101–4110, 2004.
72. U. ANDRADE, M.A.M., K. S. VECCHIO, A. H. CHOKSHI, *DYNAMIC RECRYSTALLIZATION IN HIGH-STRAIN, HIGH-STRAIN-RATE PLASTIC DEFORMATION OF COPPER* Acta metall, mater. Vol. 42, No. 9, 1993.

73. A. Hasnaoui, H.V.S., P.M. Derlet, *On non-equilibrium grain boundaries and their effect on thermal and mechanical behaviour: a molecular dynamics Abstract computer simulation*. Acta Materialia 50 (2002) 3927–3939, 2002.
74. Kh. M. Ibrahim, M.M., L. Wagner, *Effect of Annealing Temperature on Microstructure and Mechanical Properties of Hot Swaged cp-Ti Produced by Investment Casting*. Journal of Materials Engineering and Performance, 2010.
75. <http://avstop.com/ac/apgeneral/heattreatmentoftitanium.html>.
76. <http://www.azom.com/article.aspx?ArticleID=1245>.

